

New Designs for Bioinspired Microstructures with Adhesion to Rough Surfaces

Dissertation

zur Erlangung des Grades

des **Doktors der Ingenieurwissenschaften**

der Naturwissenschaftlich-Technischen Fakultät

der Universität des Saarlandes

von

Sarah Christine Lidwina Fischer



Saarbrücken, November 2017

Tag des Kolloquiums:	29. August 2018
Dekan:	Prof. Dr. G. Jung
Berichterstatter:	Prof. Dr. E. Arzt
	Prof. Dr.-Ing. S. Diebels
	Prof. Dr. C. Creton
Vorsitz:	Prof. Dr.-Ing. D. Bähre
Akad. Mitarbeiter:	Dr.-Ing. F. Aubertin

Abstract

Adhesion to substrates with surface roughness is a research field with many unsolved questions. A more thorough understanding of the underlying principles is important to develop new technologies with potential implications for instance in robotics, industrial automatization and wearable interfaces. Nature is a vast source of inspiration as animals have mastered climbing on various surfaces at high speed with several attachment and detachment events in a short time.

In this work, new designs for dry adhesives inspired by natural blueprints are presented. Different strategies were explored to understand and tune adhesion on a range of substrates from smooth glass to polymers with skin-like roughness. Both the material properties and the geometry of the dry adhesives were utilized to improve adhesion strength. Three concepts are presented in this work: (i) composite structures with tunable interface, (ii) soft pressure sensitive adhesive layers, and (iii) funnel-shaped microstructures. This thesis aims for better understanding of the adhesion behavior as a function of several important factors including hold time, substrate material and roughness.

The new concepts for bioinspired structures investigated in the present thesis will contribute to the development of performant, reversible adhesives for a variety of applications where surface roughness is involved.

Kurzzusammenfassung

Adhäsion an rauen Oberflächen stellt immer noch ein Forschungsfeld mit vielen ungelösten Problemen dar. Um neue Technologien mit Bedeutung für beispielsweise die Robotik, industrielle Automatisierung und körpernahe Sensorik zu entwickeln, bedarf es eines tieferen Verständnisses der zugrunde liegenden Prinzipien. Hier stellt die Natur eine vielfältige Inspirationsquelle dar, da bestimmte Lebewesen in der Lage sind, auf unterschiedlichsten Untergründen zu haften.

Im Rahmen dieser Arbeit werden der Natur nachempfundene Modelle und Lösungen zur Haftung vorgestellt. Zum Verständnis der Haftungsmechanismen und zur Optimierung der Hafteigenschaften auf einer Bandbreite von Substraten, von glattem Glas bis hin zu rauen, hautähnlichen Polymeroberflächen, wurden unterschiedliche Herangehensweisen untersucht. Zur Erhöhung der Haftkraft kamen sowohl Variationen in den verwendeten Materialien, als auch in der Geometrie der Haftstrukturen zum Einsatz. Drei Konzepte werden in dieser Arbeit vorgestellt: (i) Kompositstrukturen mit variablen Grenzflächen; (ii) weiche, drucksensitive Schichten und (iii) trichterförmige Mikrostrukturen. Es wird ein besseres Verständnis des Adhäsionsverhaltens in direktem Zusammenhang mit verschiedenen Struktur-, Substrat- und Messparametern angestrebt.

Die in dieser Arbeit vorgestellten, neuen Konzepte für bioinspirierte Strukturen sollen zur Entwicklung performanterer, reversibler Haftverbindungen für einen breiten Anwendungsbereich auf rauen Oberflächen beitragen.

Résumé

L'adhésion sur des surfaces rugueuses offre beaucoup de questions ouvertes aux chercheurs. Pour développer des technologies pionnières dans les domaines comme la robotique, automatisation industrielle et les capteurs portables, une connaissance plus détaillée des mécanismes gouvernant ce phénomène est nécessaire. La nature est une source d'inspiration vaste avec une multitude d'animaux possédant la capacité d'escalader diverses surfaces à grande vitesse.

Cette thèse présente de nouveaux designs d'adhésifs secs inspirés par la nature. Différentes stratégies ont été explorées afin de comprendre et modifier l'adhésion sur des surfaces variées comme le verre poli ou des polymères avec une texture de surface ressemblant celle de la peau. Les propriétés des matériaux et la géométrie des structures ont été utilisées comme paramètres pour maximiser l'adhésion. Cette thèse comprend trois parties : (i) des structures composites avec interface variable, (ii) des films mous sensibles à la pression, et (iii) des structures en forme d'entonnoir. Les paramètres étudiés englobent entre autre le temps d'attente, le matériau du substrat et sa rugosité. Tous les concepts peuvent être raffinés et optimisés envers certaines applications.

Les nouveaux concepts de structures inspirés par la nature présentés ci-dessus ont pour but de contribuer au développement d'adhésifs performants et réversibles pour une variété d'applications pour lesquelles la rugosité joue un important rôle.

*>> Today you are You,
that is truer than true.
There is no one alive,
That is Youer than You! <<*

Dr. Seuss

Acknowledgements

The research for this thesis was conducted at the INM – Leibniz Institute for New Materials in the Functional Microstructures Group between 2014 and 2017 under the scientific guidance of Prof. Eduard Arzt.

I would like to thank all the people who accompanied me through this journey and supported me, scientifically and personally, to accomplish this important step.

Foremost, I would like to thank my Doktorvater Prof. Eduard Arzt for giving me the opportunity to pursue my Ph.D. within his research group and constructive discussions during our meetings.

Additionally I cordially thank Prof. Stefan Diebels for the motivating discussions and for taking over the second report of my thesis.

For his supervision from the very beginning of my thesis on, I would like to thank Dr. René Hensel. During discussions he contributed new ideas to advance my research projects. Additionally I would like to thank Dr. Klaus Kruttwig for the mentorship during the second half of my Ph.D. I had the pleasure to work with him on the skin adhesive projects, never short of new ideas and approaches to advance the projects in our various productive meetings.

A special thanks goes to Katja Groß, a master student that I had the pleasure to oversee, who impressed me with her structured planning and execution of her experiments on the funnel-shaped microstructures. Additionally I would like to acknowledge Silviya Boyadzhieva, Martin Danner and Angela Rutz for the constructive discussions, their conscientious scientific work, the well-needed distractions and the endless list of memorable moments during the past year. Additionally, I would like to thank the other students who I had the pleasure to work with and supervise during the past years and who helped me perform experiments for my thesis: Lukas Engel, Selina Neuhaus, Julian Weiß, Euiyoung Park.

Additionally, I would like to thank my office colleagues during my Ph.D. thesis from the bottom of my heart. Everyone one of them was extremely supportive and encouraging. Ein herzliches Dankeschön gilt Dr. Henrike Peuschel, Jonas Heppe, Jessica Kaiser, Jona Engel und Melanie Groh für eure Unterstützung und die gemeinsamen Spieleabende. Merci beaucoup aussi à Emmanuel Terriac et Luiza Stankevics pour votre soutien et les fous rires. Trotz der wechselnden Büronachbarn wurde eine wichtige Tradition, ein reichhaltiger Vorrat an Süßigkeiten zur Motivation im Büro, stets aufrechterhalten.

Furthermore I would like to thank the team of the Mechanical Workshop of our institute for their help in planning and fabricating complex molds and devices according to our needs. In general, I would like to thank all former and current members of the Functional Microstructures Group and the Leibniz Institute for New Materials for the pleasant working atmosphere, especially Verena Tinnemann, Viktoriia Barreau, Jamie Booth, Susanne Selzer, Lisa Sold, Vera Bandmann and Isabella Reichert.

Finally I would like to thank my friends and family for their support and encouragement. I would like to thank Dr. Cécile Helfen for thorough proof-reading and discussions of my thesis. I would also like to say “Tack så mycket!” to Manuel Bastuck for proof-reading, continuous motivation and motivating me

to learn the beautiful Swedish language. Thank you to Michael Becker for fantastic discussions over the past years, never being short of ideas as well as encouraging words and cheering me up when I needed it most. I would also like to acknowledge Henrik Ollmann for his support and patience over the past years while accepting occasional late working hours.

Ultimately, I would like to thank my parents for their unconditional support.

Abbreviations and symbols

Materials and material properties:

PEGdma	P oly(e thylene g lycol) d imethacrylate
PEGdma 600	P oly(e thylene g lycol) d imethacrylate with an average molecular weight of $600 \text{ g} \cdot \text{mol}^{-1}$
PDMS	P oly d imethylsiloxane
SSA	S oft s kin a dhesive
PSA	P ressure s ensitive a dhesive
PU	P olyurethane
PBS	P hosphate b uffered s olution
BSA	B ovine s erum a lbumin
L929	Murine mouse fibroblasts cell line
EDTA	E thylen d iaminetetraacetic a cid
FITC	F luorescein i sothi c yanate
LDH	L actate d ehydrogenase enzyme
IP-L	Photoresist IP-L 780
GS	Glass substrate
ES	Epoxy substrate
VS	VitroSkin substrate
UV-light	Ultraviolet light
E	Young's modulus (MPa)
E_1, E_2	Young's modulus of the tip (E_2) and stem (E_1) of composite structures (MPa)
G'	Storage modulus (MPa)
G''	Loss modulus (MPa)
G^*	Complex modulus (MPa)
ν	Poisson's ratio
$\tan \delta$	Damping factor
G_c	Critical energy release rate (mJ/m^2)
p_{atm}	Atmospheric pressure $p_{atm} \approx 100 \text{ kPa}$
σ_{suc}	Adhesive stress induced by suction (kPa)
θ	Water contact angle ($^\circ$)
σ_{cap}	Adhesive stress induced by capillarity (kPa)
L	Length of three-phase contact line (μm)
γ	Surface tension of water (N/m)
R	Radius of fluid meniscus (μm)
h	Thickness of the fluid film (μm)

Methods:

SEM	Scanning electron microscope
ESEM	Environmental scanning electron microscope
FIB	Focussed ion beam microscope
AFM	Atomic force microscope

Roughness parameters:

R_a	Arithmetical mean roughness (μm)
R_z	Mean peak-to-valley distance (μm)
RMS	Root-mean-square roughness (μm)
S_m	Mean distance between successive points as they cross the mean line (μm)
S	Mean spacing of adjacent peaks (μm)
PSD	Power spectral density, or roughness power spectrum
$C(\mathbf{q})$	Power spectral density
\mathbf{q}	Wave vector
\mathbf{p}	Point on the surface with coordinates (x, y)
$z=h(\mathbf{p})$	Height distribution
δ_c	Material-defined length scale (μm)
$R_{z,crit}$	Critical roughness threshold determining whether the substrate roughness influences adhesion experiments (μm)

Adhesion parameters:

C	Machine compliance ($\mu\text{m}/\text{mN}$)
h_{film} or t	Initial film thickness (μm)
F	Force (N)
F_p	Maximum force necessary for detachment (pull-off force) (mN)
A	Apparent contact area (mm^2)
σ	(Engineering) stress $\sigma = F/A$; positive stress is defined as tension, negative stress is compression (kPa)
σ_{max} or σ_p	Maximum stress (pull-off stress) (kPa)
S or Δ	Displacement (μm)
s_0	Displacement at which the force became zero and tensile deformation started (μm)
s_{end}	Displacement at which detachment occurs (μm)
$s_{pull-off}$	Displacement at which pull-off stress is reached (μm)
ε	Relative displacement $\varepsilon = (s - s_0)/h_{film}$
ε_{max}	Maximum relative displacement; displacement at which detachment occurs
W_{sep}	Work of separation $W_{sep} = \int_{s_0}^{s_{end}} \sigma ds$ (J/m^2)
t_{hold} or τ	Hold time (s)
R_{min}	Minimum radius of curvature of a film with thickness t (μm)
A_p	Area of a pillar (μm^2)

A_t	Area of the tip (μm^2)
δ	Displacement/elongation of the pillars necessary to form conformal contact (μm)
γ	Adhesion energy (J/m^2)
γ_t	Adhesion energy per pillar (J/m^2)
h_{min}	Minimum height of the pillars necessary for adaptation to roughness (μm)

Characterization of pull-off stress as function of hold time (Chapter 3):

τ	Hold time (s)
σ_0	Initial pull-off stress at 0 s hold time (kPa)
σ_∞	Pull-off stress at high hold time (kPa)
$\Delta\sigma$	Difference between the initial pull-off stress and the equilibrium pull-off stress at very high hold time $\Delta\sigma = \sigma_\infty - \sigma_0$ (kPa)
τ_0	Characteristic relaxation time (s)

Stress relaxation parameters (Chapter 6):

t	Hold time (s)
τ_i, τ_1 and τ_2	Characteristic relaxation times (s)
σ_i, σ_1 and σ_2	Relaxation stress constants (kPa)
σ_∞	Stress at infinite hold time $t \rightarrow \infty$ (kPa)

Numerical simulations (Chapter 2):

σ_{22}/σ_a	Normal stress divided by the applied normal stress
D	Diameter of the fibril (μm)
D_f	Diameter of the mushroom tip (μm)
h	Height of the mushroom tip (μm)

Structure parameters of funnel-shaped structures (Chapter 7):

D	Funnel-structure diameter (μm)
d	Funnel-structure flap thickness (μm)
θ	Funnel-structure opening angle ($^\circ$)
r	Contact radius of funnel-structure (μm)

Contributions of Co-Authors

Details of the contributions of all co-authors to the individual chapters are acknowledged in the following. Chapter 4, 5 and 7 have been published in peer-reviewed journals.¹⁻³

The research leading to these results has received funding from the European Research Council under the European Union's Seventh Framework Programme (FP/2007-2013) / ERC Grant Agreement n. 340929 awarded to Eduard Arzt and by the German Research Foundation (Deutsche Forschungsgemeinschaft) through the grant n. HE 7498/1-1 awarded to René Hensel.

Published chapters

Chapter 4

Fischer, S. C., Arzt, E., & Hensel, R. (2016). Composite pillars with a tunable interface for adhesion to rough substrates. *ACS applied materials & interfaces*, 9(1), 1036-1044.

The publication is an open access article published under an ACS AuthorChoice License, which permits copying and redistribution of the article or any adaptations for non-commercial purposes. The article is available under: <http://pubs.acs.org/doi/abs/10.1021%2Facsami.6b11642> .

Enquiries about the permissions related to the content of the publications should be directed to ACS.

All authors contributed to the conceptual design of the work. Sarah Fischer manufactured the composite samples, performed adhesion experiments as well as simulations and carried out analysis of data. Research was directed by René Hensel and Eduard Arzt. Sarah Fischer wrote the manuscript with contributions from René Hensel and Eduard Arzt.

The authors acknowledge Prof. Robert M. McMeeking (UC Santa Barbara, USA), Prof. Attila Kossa (Budapest University of Technology and Economics, Hungary) and RamGopal Balijepalli for helpful discussions on the contact mechanics of composite pillars. The authors further thank Martin Schmitz, Susanne Selzer and Lukas Engel for their technical support. Sarah Fischer would like to thank Michael M. Becker (Fraunhofer Institute for Nondestructive Testing, Saarbrücken) for computing time on the Comsol server.

Chapter 5

Fischer, S. C., Kruttwig, K., Bandmann, V., Hensel, R., & Arzt, E. (2017). Adhesion and Cellular Compatibility of Silicone-Based Skin Adhesives. *Macromolecular Materials and Engineering*, 302(5).

The publication is an open access article published under a CC BY-NC-ND 4.0 licence, which permits copying and redistribution of the article or any adaptations for non-commercial purposes. The article is available under: <http://onlinelibrary.wiley.com/doi/10.1002/mame.201600526/full> .

Copyright Wiley-VCH Verlag GmbH & Co. KGaA. Reproduced with permission.

Sarah Fischer and Klaus Kruttwig contributed equally to this work. All authors contributed to the conceptual design of the work. Sarah Fischer performed adhesion measurements with help of Klaus Kruttwig. Sarah Fischer analyzed the adhesion measurements. Klaus Kruttwig performed cell experiments and their analysis. Sarah Fischer and Klaus Kruttwig wrote the manuscript with help from Vera Bandmann, René Hensel and Eduard Arzt.

The authors would like to acknowledge Angela Rutz for her assistance in performing the biological experiments. Katja Groß, Lukas Engel, Henrik Ollmann and Joachim Blau are acknowledged for their help in setting up and performing the adhesion experiments. The authors would like to thank Biesterfeld Spezialchemie GmbH (Hamburg, Germany), especially Robert Radsziwill, for continuous support and discussions.

Chapter 7

Fischer, S. C., Groß, K., Torrents Abad, O., Becker, M. M., Park, E., Hensel, R., & Arzt, E. (2017). Funnel-Shaped Microstructures for Strong Reversible Adhesion. *Advanced Materials Interfaces*.

The publication is an open access article published under a CC BY 4.0 licence, which permits copying and redistribution of the article or any adaptations. The article is available under: <http://onlinelibrary.wiley.com/doi/10.1002/admi.201700292/full> .

Copyright Wiley-VCH Verlag GmbH & Co. KGaA. Reproduced with permission.

All authors contributed to the conceptual design of the work. Katja Groß, Oscar Torrents Abad and Sarah Fischer performed the adhesion experiments and carried out analysis of data. Michael Becker carried out the simulations and analyzed the simulations with help of Sarah Fischer. Sarah Fischer wrote the manuscript with help of Michael Becker, Oscar Torrents Abad, Katja Groß, René Hensel and Eduard Arzt.

The authors acknowledge Robert M. McMeeking (UCSB) for helpful discussions and Birgit Heiland for performing the FIB cross-sections.

Additional publication not included as chapter

Balijepalli, R. G., Fischer, S. C., Hensel, R., McMeeking, R. M., & Arzt, E. (2017). Numerical study of adhesion enhancement by composite fibrils with soft tip layers. *Journal of the Mechanics and Physics of Solids*, 99, 357-378.

The publication is an open access article published under a CC BY-NC-ND 4.0 licence, which permits copying and redistribution of the article or any adaptations for non-commercial use. The article is available under: <http://www.sciencedirect.com/science/article/pii/S0022509616306548?via%3Dihub>

All authors contributed to the conceptual design of the work. RamGopal Balijepalli designed, performed and analysed the simulations. Sarah Fischer manufactured the samples, performed and analysed experiments. RamGopal Balijepalli and Sarah Fischer discussed results and wrote the manuscript with contributions from Robert McMeeking, René Hensel and Eduard Arzt.

S.C.L.F. would like to acknowledge the technical support by Martin Schmitz and Susanne Selzer. Furthermore, Lukas Engel is acknowledged for his help in manufacturing composite fibrils.

Submitted manuscript

Chapter 8

Fischer, S. C., Boyadzhieva, S., Hensel, R., Kruttwig, K., & Arzt, E. Adhesion and relaxation of a soft elastomer on surfaces with skin like roughness

All authors contributed to the conceptual design of the work. Silviya Boyadzhieva performed adhesion measurements with help of Sarah Fischer and Klaus Kruttwig. Sarah Fischer performed analysis of adhesion experiments with help from Silviya Boyadzhieva. Sarah Fischer wrote the manuscript with contributions from René Hensel, Klaus Kruttwig and Eduard Arzt.

The authors thank Costantino Créton (ESPCI Paris, France) and Martin Müser (Saarland University, Germany) for helpful discussions. Furthermore Martin Danner and Angela Rutz are acknowledged for their assistance in preparing samples. The authors would like to thank Biesterfeld Spezialchemie GmbH (Hamburg, Germany), especially Robert Radsziwill for continuous support and discussions.

Contents

Abstract	III
Kurzzusammenfassung.....	IV
Résumé.....	V
Acknowledgements	IX
Abbreviations and symbols	XI
Contributions of Co-Authors	XV
1 Introduction.....	3
2 Literature background.....	5
2.1 Attachment in nature	5
2.2 Synthetic adhesives	7
2.2.1 Learning from the gecko: Variation of the tip shape of fibrillar adhesives.....	8
2.2.2 Learning from the ladybug: Gradients and multi-material structures	9
2.2.3 Learning from the octopus: Adhesion using suction.....	10
2.3 Roughness	11
2.3.1 Characterization of roughness	12
2.4 Adhesion.....	15
2.4.1 Normal tack test	15
2.4.2 Detachment mechanisms and stress distributions	17
2.4.3 Roughness and adhesion.....	18
2.4.4 Adhesion on skin	19
2.4.5 Tympanoplasty	22
3 Scope of this work	25
4 Composite Pillars with Tunable Interface for Adhesion to Rough Substrates *	29
4.1 Abstract	29
4.2 Introduction.....	30
4.3 Material and methods.....	31
4.3.1 Fabrication of composite pillars	31
4.3.2 Adhesion experiments.....	32
4.4 Results	33
4.5 Discussion	39
4.6 Conclusion	41
4.7 Supporting information.....	42
4.7.1 Parameters obtained from fit equation	42

4.7.2	Numerical simulations.....	43
5	Adhesion and Cellular Compatibility of Silicone-Based Skin Adhesives *	47
5.1	Abstract	47
5.2	Introduction.....	48
5.3	Materials and Methods	49
5.3.1	Preparation of polymer samples	49
5.3.2	Adhesion measurements.....	49
5.3.3	Materials characterization.....	51
5.3.4	Contact angle goniometry.....	51
5.3.5	Cell culture experiments.	51
5.3.6	Immunofluorescence analysis.	51
5.3.7	Protein adsorption test.	52
5.4	Results and Discussion	52
5.4.1	Mechanical and adhesion properties	52
5.4.2	Biological properties.....	55
5.4.3	Comparison between smooth and rough substrates.....	58
5.5	Conclusions.....	60
5.6	Supplemental information	61
6	Adhesion and relaxation of a soft elastomer on surfaces with skin like roughness	63
6.1	Abstract	63
6.2	Introduction.....	64
6.3	Materials and Methods	65
6.3.1	Manufacturing of adhesive film samples	65
6.3.2	Adhesion measurements and analysis	65
6.3.3	Substrate manufacturing.....	65
6.3.4	Substrate characterisation	66
6.4	Results	66
6.4.1	Substrate surfaces	66
6.4.2	Influence of film thickness and roughness	68
6.4.3	Influence of hold time and material relaxation.....	70
6.5	Discussion	73
6.6	Conclusions.....	74
6.7	Supplemental information	75
6.7.1	Adhesion measurements on master substrates compared to epoxy replicas	75
6.7.2	Fitting parameters for compressive stress relaxation.....	77

7	Funnel-shaped Microstructures for Strong Reversible Adhesion *	81
7.1	Abstract	81
7.2	Introduction	82
7.3	Materials and methods	83
7.3.1	Microstructure fabrication	83
7.3.2	Adhesion measurements	85
7.3.3	SEM imaging	85
7.3.4	Numerical simulations	85
7.4	Results and discussion	86
7.5	Conclusion	92
7.6	Supplemental information	93
7.6.1	Indentation depth dependent adhesion of mushroom structures	93
7.6.2	In-situ compression of funnel-shaped structures	93
8	Discussion	97
8.1	Discussion and Outlook	99
8.2	Summary and Conclusions	104
9	List of figures	109
10	List of tables	112
11	List of publications	113
12	References	115

Introduction and Literature Background

1 Introduction

Adhesion is omnipresent in our everyday life, for instance in sticky notes, scotch tape, super glue and band aids. However, adhesion plays a role in many more situations, even if they are less obvious: small molecules adhere to counter surfaces and play a crucial role in biophysical processes in our body; components of the blood adhere to vessel walls, agglomerate to form clumps and ensure that wounds are closed. These are a few among countless examples where adhesion plays an important role, showcasing how vast this research field is. Scientists aim to extend the understanding of the interactions of different surfaces in order to ultimately be able to control them.

Artificial adhesives have been investigated for a long time, and a multitude of options exist to bond two surfaces in the long term. For this purpose, the adhesion between substrate and adhesive should be so strong that failure occurs in the adherent, i.e. a cohesive failure, governed by the material strength. Especially since technology is moving at a fast pace towards flexible and smaller devices, adhesives will more and more replace screws. Here the challenge of new generations of adhesives arises. The desire to additionally recycle products or generate reversible attachment, for instance for devices interfacing the human body, is growing. Adhesives for this purpose have to be strong and at the same time able to be detached without damaging the substrates. These two attributes are difficult to balance: The interfacial adhesion must be extremely powerful to make the bond functional, but in order to be reversible, detachment needs to occur through this same interface. This requires establishing extended understanding of the physical processes at the interface using knowledge about surface roughness, mechanical properties, stress distributions, and, more generally, contact mechanics.

Nature is a vast source of inspiration for new developments in this field, with animals like geckos and spiders being able to climb various surfaces, supporting their body weight together with the ability to attach and detach in very short time with no damage to the fibrillary adhesive pads consisting of many setae on their toes. To balance performance and reversibility of the adhesive structures with the ability to attach to various materials, nature builds a functional hierarchy. Single seta attach to the substrate using van der Waals forces, i.e. weak and short ranged forces compatible with all materials. This forms the base for universal and reversible adhesion. The overall performance of the system results from the high number of fibrils, leading to considerable adhesion strength. Shear additionally modulates the adhesive strength of the adhesive system. The gecko's adhesive system is optimized to establish a balance of reversibility, performance and adhesion to a multitude of substrates, supported by the muscular action of the animal. For artificial systems, one of the challenges is to establish this balance in order to integrate reversibility while retaining sufficient adhesion strength on the targeted substrates. This will require adhesives to become more and more tailored to applications in order to fulfil the exigent specifications. Biomimetic design is one approach to master these requirements. It consists in reducing the complexity of the natural models rather than replicating exactly the structures found in nature with their intricate design and materials. Bioinspired adhesives are based on an interplay of structure and material. They need to fulfil the key functionality of the natural model while at the same time being artificially manufactured.

One of the challenges for synthetic adhesives is the topography of the counter surface. Mushroom-shaped structures made out of one single material are the current gold standard for adhesion to

smooth substrates, and can at present be manufactured beyond laboratory scale. Extension of their use to applications involving rough surfaces has been limited, for instance, by the geometry of the tips and the material selection. Using multi-material structures enables new ways of combining very different mechanical properties. However, the interaction of complex multi-material structures with rough surfaces are not yet sufficiently understood. To develop the next generation of adhesives, an interdisciplinary approach is necessary to gain fundamental knowledge about interfacial phenomena, how to control them and ultimately use them as tools to improve artificial adhesives.

In this work, new concepts in the field of bioinspired dry adhesives are explored to contribute to this development. Both material properties and tip shape are used to tune adhesion on various substrates, from smooth glass to epoxy substrates with skin-like topography. The work starts with a literature survey covering the topics relevant for this work followed by an overview of the work. Thereafter, the thesis will be divided into three main parts, each focusing on a different aspect: The first part focusses on adhesion of multi-material macrostructures with a tunable interface geometry between both materials. The second part focuses on elastomers for medical applications characterized systematically in terms of film thickness, mixing ratio, surface roughness, and contact time for instance. The third part presents a novel tip shape concept for high adhesion to smooth surfaces strengthened by numerical investigations. Finally, all parts will be summarized and connected to other research efforts in the field.

2 Literature background

This section provides an insight into the state of the art in the field of bioinspired adhesives and adhesion to rough surfaces. First, attachment strategies found in nature will be discussed with an emphasis on attachment to rough surfaces. In the second part, dry adhesive designs derived from natural role models will be presented focusing on concepts based on tip shape variation and material variation. Thereafter, general concepts on surface roughness and its characterization will be introduced to prelude the theory of adhesion on complex surfaces at the end of this section.

2.1 Attachment in nature

Many animals need the ability to attach to surfaces in order to survive in their habitat. The strategies for attachment depend on the function required, but also on the environment (humidity, temperature,...)⁴ and physical characteristics of the animals (weight, size,...).⁵⁻⁷ A selection of important strategies is shown in **Figure 2.1** together with examples of animals utilizing this principle. There are many more animals and plants using these phenomena, many of them capable of using several strategies in combination. More details about biological attachment devices can be found here.⁸⁻¹¹

Fibrillar adhesives are found on many climbing animals like geckos, spiders and beetles.^{7,12-15} The hairy structures are compliant due to their high aspect ratio, and can be combined with hierarchy¹² or a material gradient^{16,17}. In fibrillar adhesives, the contact area is split into many individual contacts, gaining adhesion energy through a size effect, sometimes referred to as contact splitting.¹⁸⁻²⁰ Fibrillar adhesives enable animals to attach and detach quickly to walk or flee from predators. The structure of the fibrils and area of coverage strongly depend on the species and weight of the animal.^{7,14}

Smooth adhesive pads are found on mussels²¹, spiders or climbing plants like English Ivy²², thus in terrestrial as well as aquatic species. They have a terminal layer consisting of a very soft coating²³ or liquid secretions and can be reversible, for instance in spiders and beetles, or irreversible, for example in mussels. This attachment mechanism is especially well suited for adhesion to rough surfaces as the terminal layer can conform to the substrate, fill cavities to result in high contact area to almost all surface profiles.

Mechanical interlocking is a principle present in limpets, porcupines²⁴ or parasite worms²⁵. Attachment is secured by creating undercuts, either with hooks or by inflating body parts. This can be used for attachment or for defense against predators.

Frictional adhesives provide probabilistic attachment and consist of two counter surfaces with protrusions causing attachment upon normal or shearing contact.²⁶ They are important for beetles, catfish, sticklebacks and dragon flies.^{8,27} These systems serve as temporary attachment, to immobilize certain body parts or attach to another animal.²⁸

Clamping is used by a variety of animals and the body parts are scaled up with animal size. Clamps in the range of several cm (crabs) down to several μm (spiders, lice²⁶) exist. Clamping always involves muscular forces and serves as temporary attachment to grab prey or for self-defense.

Suction is based on generating a pressure difference between the environment and inside a cavity. It is most effective under water due to incompressibility of this medium and therefore found in various aquatic animals (octopus²⁹), but sometimes also on semiaquatic animals (leeches). Establishing as well as releasing the adhesion requires muscular actuation.



Figure 2.1. Concepts for attachment in nature. Fibrillar adhesives, wet/soft adhesives, mechanical interlocking, friction, clamping and suction. Associated with each schematic is an example from nature where these concepts are implemented. Photos are licensed under the Creative Commons License CC0.³⁰

For adhesion to rough surfaces, adaptability is crucial. In nature, two distinct strategies are used to yield high contact areas: extremely soft, smooth adhesive pads, and fibrillar adhesives (**Figure 2.2**).⁷ Both solutions result in a structure with a low effective elastic modulus, which is key to the adaptability.

Soft adhesive pads of animals and also commercial pressure sensitive adhesives have a storage modulus lower than 100 kPa. This is in line with the Dahlquist Criterion³¹, which predicts this to be the limit below which high tack is reached without much force applied. Fibrillar structures such as the

structures on gecko feet have a similar effective elastic modulus while the material they are made of, beta-keratin³², has an elastic modulus in the GPa range.³³ As described by Jeong and Suh³⁴ and later by Pattantyus-Abraham et al.³³, there are several geometrical criteria favorable for **effective modulus reduction**: high aspect ratio features, angled and tilted structures, multiple length scale hierarchical features as well as tip shape modifications. All these characteristics are important factors to tune artificial dry adhesives.

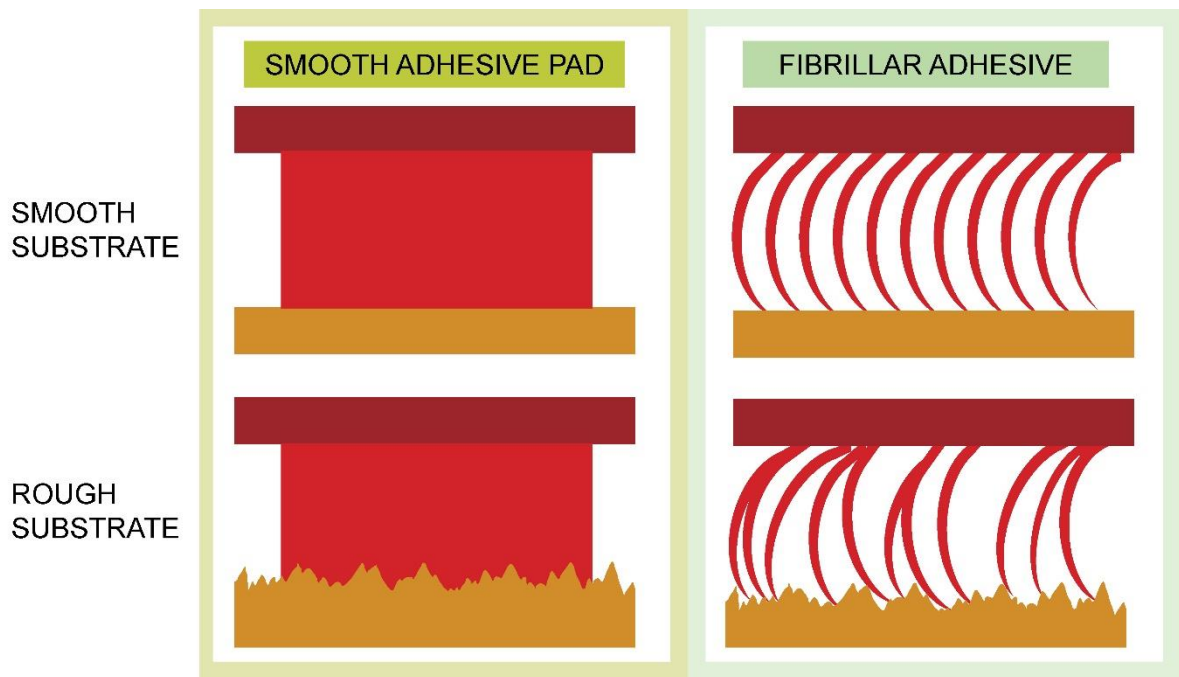


Figure 2.2. Adhesion to rough surfaces in nature: smooth adhesive pads and fibrillary adhesives. Figure adapted from Gorb and Scherge.²⁶

A variety of different strategies are found in nature to realize attachment through structure, material properties, muscle force or combinations. Rather than trying to copy these intricate systems, the biomimetic approach consists of identifying the central characteristics of natural models and distilling them to a minimum.

2.2 Synthetic adhesives

The development of versatile synthetic adhesives is central for new technologies such as novel gripping systems^{35,36} and wall climbing robots.³⁷ In the following section, the three most relevant strategies to mimic natural adhesive systems for the present work will be introduced. **Figure 2.3** features schematic representations of different design concepts. There are many more fascinating bioinspired technologies for attachment, including artificial mussel proteins^{38,39} or mechanically interlocking structures for biomedical applications^{25,40}, which will not be discussed in detail in the present document.

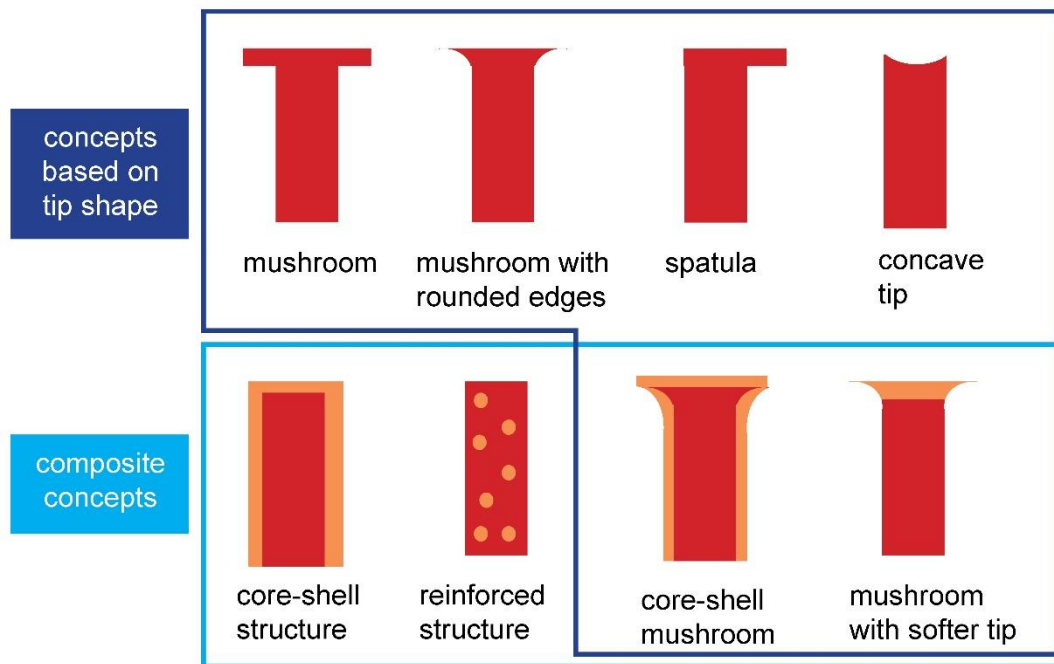


Figure 2.3. Biomimetic concepts to increase adhesion by varying tip shape or material properties. Tip shape concepts: mushroom structures⁴¹, mushroom structures with rounded edges^{42–44}, spatula⁴⁵, concave tip⁴⁶; Composite concepts: core-shell structure⁴⁷, reinforced structures⁴⁰; Combination of tip shape and composite concept: core-shell mushroom^{48,49}, mushroom with softer tip⁵⁰.

2.2.1 Learning from the gecko: Variation of the tip shape of fibrillar adhesives

The toe pads of **geckos** exhibit a fibrillar structure with several hierarchical levels, with each stalk splicing into successively finer fibrils and, finally, spatula-shaped terminal elements.¹² Several groups have mimicked such **hierarchically** assembled structures in artificial designs^{51–55} but many unsolved questions remain. For instance, introduction of hierarchy generally reduces the available contact area in synthetic adhesives and increases the propensity to elastic buckling.^{56,57} In addition, it is very difficult to manufacture the hierarchical structures as precisely and down to the size found in nature.

A common strategy to mimic the gecko’s attachment system is the **variation of the tip shape** of cylindrical structures. The so-called mushroom tips consist of a gradual broadening of the contact area which influences the stress distribution and leads to a considerable increase in adhesion compared to a cylindrical fibril as shown by many experimental^{45,58} and theoretical^{41,59} studies. In practice, different techniques exist to generate mushroom structures, including anisotropic etching and modification of previously made pillar structures with inking.^{52,60–62} In addition to this, various other concepts for geometrical tip modification exist, aiming to introduce an asymmetry with potential implications in the field of directional or switchable adhesives including triangular⁶³, spatula-shaped^{14,51}, slanted tips^{64,65} or tips defects⁶⁶.

Variation of the tip shape influences the stress distribution between structure and substrate, which influences the adhesion. A conventional cylindrical pillar exhibits a stress concentration at the edges, which will lead to detachment. For mushroom shaped structures for example, mechanical modelling studies predict that large, thin flaps yield the highest adhesion^{41,59} as they reduce the intensity of the edge singularity, increase the stress in the center of the contact and thereby reduce the propensity for

edge crack formation. In addition, it has been shown that rounded edges at the transition from stem to tip have advantages over sharp corners as they further reduce stress concentrations.⁴¹

With a different approach of tip modification, Gao and Yao⁴⁶ predicted an optimal stress distribution for structures with small diameter and a tip with a small dimple. In this case, their simulations indicate high adhesion strength without any applied preload, yielding an “optimal shape” for certain combinations of size, dimple depth and mechanical properties.

2.2.2 Learning from the ladybug: Gradients and multi-material structures

The **ladybug** provides another blueprint for the design of fibrillar adhesives. In contrast to the gecko, its adhesive pad consists of fibrils without hierarchy exhibiting an **axial gradient of Young’s modulus** in each fibril. Experiments using nanoindentation have demonstrated that the Young’s modulus decreases by three orders of magnitude from stalk to tip.¹⁶ A numerical study revealed that such a material gradient can also prevent clustering of an array of fibrils, especially for fibrils with high aspect ratio coming into contact with rough substrates.¹⁷ Similar effects were observed in smooth adhesive pads of other insects.⁶⁷

In order to mimic this gradient in artificial structures, materials with different mechanical properties can be combined to create a transition from high to low elastic modulus. Recently, Minsky et al.⁴⁷ showed experimental and numerical studies of fibrils with axial variations of the Young’s modulus adhering to smooth surfaces. They designed composite structures consisting of a stiff cylindrical core embedded in a soft shell, realizing a switchability through shear load. It was found that very thin soft tip layers promise the best adhesion enhancements for smooth substrates. This is in line with previous studies covering tack tests of thin, elastic films. Webber et al.⁶⁸ demonstrated that the stress distribution is influenced by material properties, confinement ratio, and other parameters yielding variations in adhesion strength and detachment mechanisms. In general, their material choice was not steered towards optimal structures for rough surfaces as the soft material was Sylgard 184. After demonstrating the feasibility of the structures at the macroscale⁴⁷, they were able to adapt the manufacturing process at the micro-scale using a combination of photolithography and replication to make pillars with a diameter in the range of 200 μm ⁶⁹. They demonstrated the ability to use those structures towards the handling of silicon membranes in micro-transfer-printing. A major limitation in their approach is the manual assembling of the structures, which will necessitate adaptation when targeting non laboratory scale arrays of the structures.

Combinations of both principles, with both modified shape and material, exist as well. Bae et al.⁴⁸ demonstrated that clustering could be minimized while normal and shear adhesion to a smooth substrate were enhanced with core-shell microstructures. Polyurethane acrylate pillars were manufactured and subsequently uniformly coated with Sylgard 184. In another work, Bae *et al.*⁴⁹ demonstrated that mushroom structures with a softer mushroom cap manufactured with Sylgard 184 in an off-ratio composition with lower curing agent concentration were best for improving adhesion to skin, i.e. a compliant and rough surface, in the evaluated range of materials. However, the Young’s modulus of the soft material chosen was still in the MPa range. For even softer materials, gravity might cause the flaps to fold down and adhere to the sides of the structures.

2.2.3 Learning from the octopus: Adhesion using suction

While the two natural blueprints presented before are based on fibrillar adhesives, the octopus uses suction cups to adhere. They comprise two main parts, the infundibulum, which is the lower part in contact with the substrate, and the acetabulum which, serves to seal the suction cup or release pressure.^{29,70} This enables control of the pressure under the attachment organ, and thereby the strength and release of the contact.

In general, the stress generated by suction cups, σ_{suc} , is based on the pressure difference generated:

$$\sigma_{suc} = \frac{F_{suc}}{A} = p \cdot \left(\frac{V_0 - V_{min}}{V_0} \right), \quad (2.1)$$

where F_{suc} is the suction force, A is the contact area with diameter D , p is the pressure of the surrounding medium, V_{min} is the volume of the suction cavity in the compressed state and V_0 the maximum volume of the suction cavity (**Figure 2.4**). In air, this suction pressure can, thus, not exceed the atmospheric pressure of 100 kPa.

Suction cups are widely used in robotics or industrial pick-and-place applications.^{71–73} However, they require vacuum generation, which is costly and noisy.^{74–77} Some approaches exist to create passive suction cups which do not necessitate external stimuli to maintain adhesion.^{78,79} Kawasaki et al.⁷⁸ and Yoshida et al.⁷⁹ proposed wall-climbing robots with flexible polymer suction cups where detachment is realized by mechanical construction through which the structures are peeled off at one edge and air is released inside the cavities during the forward movement. Recently, Baik et al.⁸⁰ demonstrated a method to fabricate microstructures very closely mimicking the morphology of octopus suction cups, and demonstrated wet-tolerant normal adhesion of their structures. They achieved adhesion strength of about 15 kPa under dry conditions, 40 kPa under water and up to about 160 kPa submerged in oil. However, they did not use the structure to switch adhesion. Another study by Chen et al.⁸¹ demonstrated adhesive microstructures formed by self-assembly, so called nanosuckers, which consist of pillars with a concave tips. They demonstrated the adhesion strength of a 1 cm² patch of structures made of Sylgard 184 to reach between 30 and 70 kPa on smooth glass substrates in air depending on the structures' geometry. Under water, values of about 30 kPa were reported on smooth glass. Additionally, the authors suggested that the structures also adhere to surfaces with small roughness due to the flexibility of the material.

A multitude of strategies exist to mimic dry adhesive systems found in nature. However, adhesion strengths reached are significantly lower than the theoretical limit of about 20 MPa as estimated by Gao et al.⁴⁶ Especially with the introduction of roughness, artificial dry adhesives often lose much of their strength. Few concepts are at present able to secure adhesion on substrates with significant surface roughness. In our everyday life, the terms “smooth” and “rough” are often used to describe the tactile perception of a surface, many different surfaces being perceived as smooth (window glass, silk, plastic bottle) or rough (sandpaper, tree bark, paving). It is evident that this is not an accurate classification for substrates used to quantify adhesion. Therefore, in the next chapter, concepts to describe surface roughness will be introduced together with definitions of the terms smooth and rough in the frame of this work.

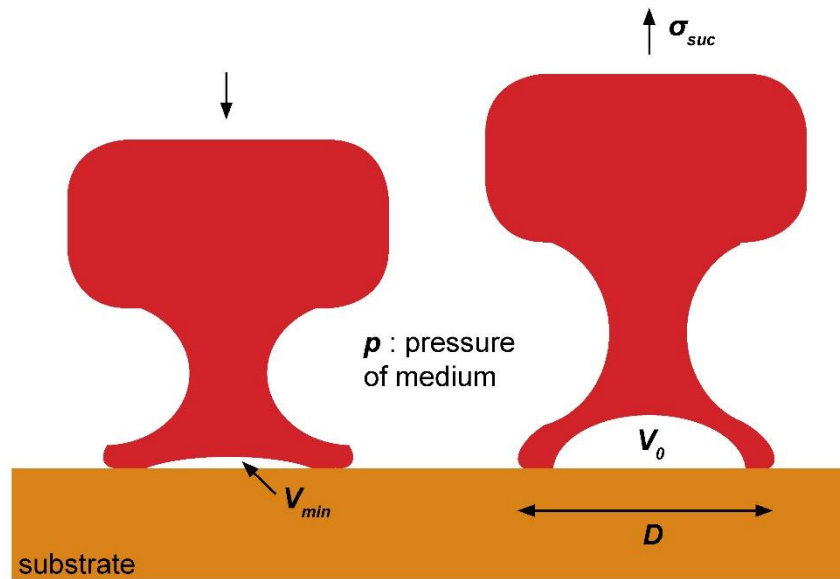


Figure 2.4. Representation of the origin of suction force. The volume under the suction cup in the compressed state, V_{min} , is expanded upon applying a tensile stress on the suction cup or by muscular action in animals. Based on V_{min} and the volume of the suction cup before detachment, V_0 , the maximum stress of a suction cup under a tensile stress, σ_{suc} , can be calculated for a medium with pressure p .

2.3 Roughness

Few technical surfaces are perfectly, atomically smooth due to the presence of defects and surface irregularities. “Smooth” in the context of this work means polished surfaces with nanoroughness, i.e. height differences in the range of 10^{-9} m or less such as exhibited by silicon wafers or polished glass. “Rough” denotes surfaces with larger height differences (**Figure 2.5**). Microroughness, i.e. roughness with height differences up to several micrometers, is typical for surfaces with topographies induced by light mechanical or electrochemical surface treatment for example, and already considerably reduces adhesion against most substrates.^{82–85} Human skin is an example of a surface with micro- to macroroughness with height differences in the sub-mm to mm range depending on several factors such as body part, age, life style, and humidity, for example.^{86–88} However, the roughness spectrum does not stop there. Asphalt for instance has a great technical relevance to study grip of tires to the roads and ensure traffic safety. Beyond this, geological structures such as rocks, meteorites and the earth itself can feature even larger asperities.

Even if this work will be limited to a small part of the immense roughness spectrum, it is important to characterize the surfaces and their profiles to ultimately compare results and generalize measurements beyond the exact surface that was used for testing.

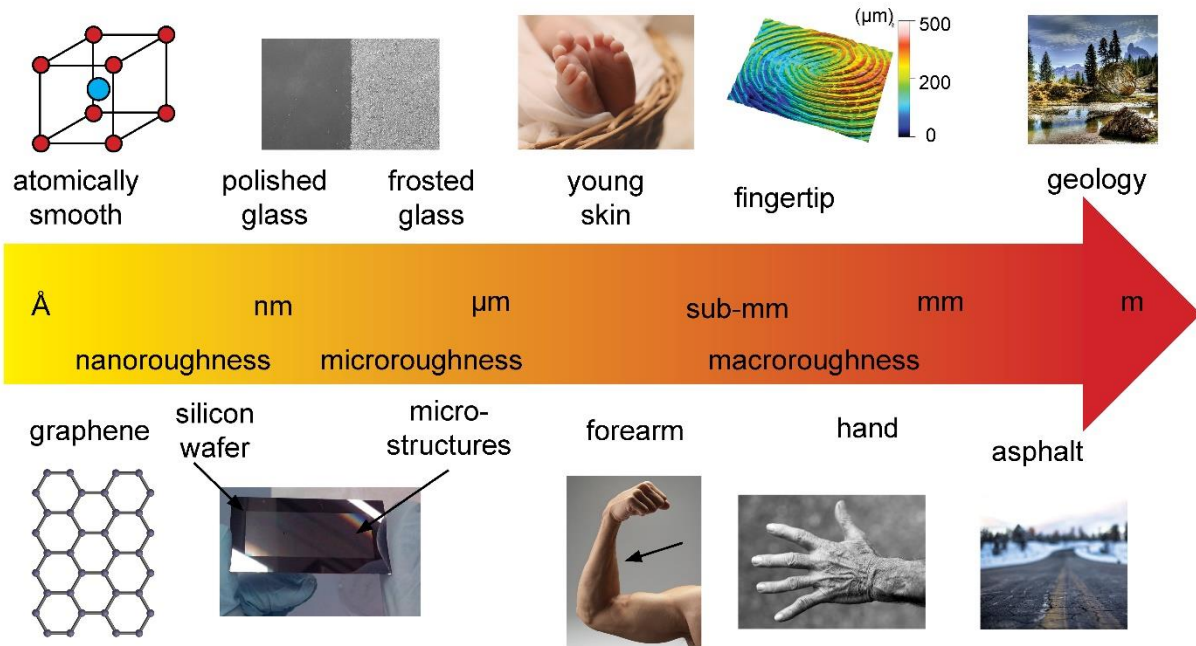


Figure 2.5. Wide span of the roughness “spectrum” from ideal atomically smooth surfaces to structures with asperities in the range of nm, μm , mm and beyond. Photos are licensed under the Creative Commons Licence CCO.³⁰

2.3.1 Characterization of roughness

Roughness can be characterized with several different techniques including atomic force microscopy (AFM), profilometry, white light interferometry (WLI) and laser scanning methods. However, it is important to keep in mind their limitations concerning the resolution limit but also the materials that can be measured to avoid artefacts. For very soft materials, contact methods can cause issues as the sample is deformed due to the force applied by the probe. In general, the probe geometry and size as well as the length of the sampling interval influence the measurement and need to be taken into account during data evaluation.

Many concepts exist to describe the roughness of a surface. In the following, a small selection of widely used parameters to quantify roughness will be introduced. A more extensive list of parameters can be found in several books or publications.^{26,89} Most parameters are based on two-dimensional roughness profiles $z(x)$ of length l and are expressed most frequently in the units nanometers or micrometers.

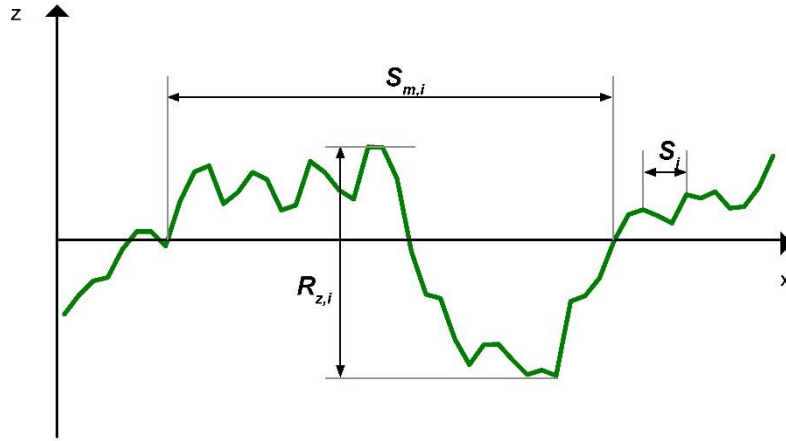


Figure 2.6. Schematic of a surface profile to illustrate the important factors to determine roughness parameters. Features of the roughness profile that can be used to compute roughness parameters include the peak-to-valley distance $R_{z,i}$, the mean distance between successive points as they cross the mean line, $S_{m,i}$, or the spacing of local, adjacent peaks, S_i .

The arithmetical mean roughness, R_a , is the arithmetic average of the absolute height $z(x)$ with respect to the base line over a length l :

$$R_a = \frac{1}{l} \int_{x=0}^{x=l} |z(x)| dx . \quad (2.2)$$

The root-mean-square roughness RMS is the square root of the standard deviation of R_a with \bar{z} being the mean value of $z(x)$:

$$RMS = \sqrt{\frac{1}{l} \int_{x=0}^{x=l} [\bar{z} - z(x)]^2 dx} . \quad (2.3)$$

The mean peak to valley distance, R_z , is defined as:

$$R_z = \frac{1}{k} \sum_{1}^k R_{z,i} . \quad (2.4)$$

In contrast to the previous parameters, which are vertical roughness parameters, i.e. they contain information about height differences, the next two concepts are lateral roughness parameters.

The mean distance between successive points as they cross the mean line, S_m , is given by:

$$S_m = \frac{1}{n} \sum_{1}^n S_{m,i} , \quad (2.5)$$

and the mean spacing of local, adjacent peaks, S , by:

$$S = \frac{1}{n} \sum_{i=1}^n S_i. \quad (2.6)$$

n refers to the total number of intervals i and k is the number of cut-off filters (i.e. number of windows the scans of length l are divided into).

It is not possible to reduce the roughness of a surface to one of these parameters without losing information. All parameters focus on certain aspects of the surface, but are not fully capable of capturing the surface properties. This becomes obvious when considering the three surfaces in **Figure 2.7**: Although the mean peak-to-valley distance, R_z , is identical, the surfaces clearly have different surface profiles.

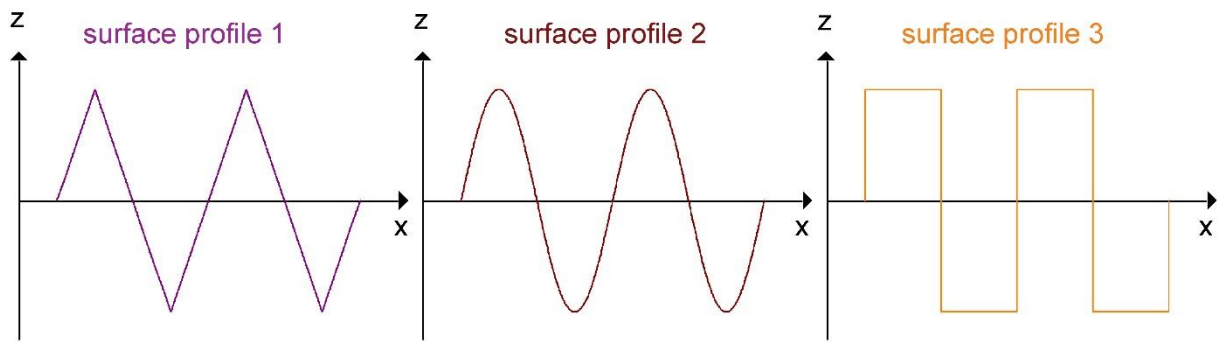


Figure 2.7. Comparison of three surfaces with same average peak-to-valley distance, R_z , but different topographies. Surface profile 1 is a triangle wave, surface profile 2 a sinusoidal wave and surface profile 3 a rectangular wave.

Therefore, descriptions have been developed to capture more surface properties. Pastewka and Robbins⁸³ suggest to combine both lateral and vertical roughness information into a scalar parameter. Other approaches include processing of three dimensional roughness profiles $z = f(x, y)$ as for example the **roughness spectrum** or **power spectral density** (PSD). The PSD is defined as the Fourier transform of the height-height correlation function and is mathematically described by:^{90,91}

$$C(\mathbf{q}) = \frac{1}{(2\pi)^2} \int \langle h(\mathbf{p}), h(\mathbf{0}) \rangle e^{-i\mathbf{q}\cdot\mathbf{p}} d^2\mathbf{p}, \quad (2.7)$$

where $z = h(\mathbf{p})$ is the height, \mathbf{p} is a point with coordinates (x, y) on the surface and \mathbf{q} is the wave vector. Bold letters designate two-dimensional vectors. Angular brackets $\langle \dots \rangle$ stand for ensemble averaging.

The foundation of this analysis is the fact that any surface roughness can be described as a superposition of sine waves with different wave lengths (Fourier's theorem). The roughness power spectrum reflects which wave vectors contribute to the powerspectrum. The usefulness of the calculated PSD depends on the characterization method and its resolution limit, i.e. most often the probe size. For surfaces like skin, it might be necessary to combine different techniques, for example profilometry and AFM measurements.⁸⁶

Assuming a surface with two superposed sine waves, the PSD of this surface would consist of two delta functions at the wavelength of the two sine waves. However, most surfaces contain components from various wavelengths and are self-affine fractal, which means that when magnified, the surface profile is scaled by the Hurst factor. In this case, the PSD is a continuous curve, increasing linearly from the small to large wave vector cut-off and then transitioning to a plateau until the roll-off wave vector.

Characterizing surface roughness is very complex. It is important to keep in mind that capturing surface properties of different substrates based on one term is not accurate, and therefore several factors, describing vertical as well as lateral features or better the PSD, need to be considered. To develop dry adhesives with better performance on surfaces with different topographies, it is important to understand what adhesion is, how it can be characterized and how it is influenced by roughness, which will be the scope of the following chapter.

2.4 Adhesion

Adhesion is a phenomenon that causes a finite detachment force between two surfaces. Cohesion, in contrast, designates the strength within one material. Many effects can cause adhesion: chemical bonds, including ionic or covalent bonds, mechanical effects, for example interlocking, as well as physical phenomena like magnetism, capillary forces, electrostatics, and intermolecular forces arising from asymmetric charge distribution (van-der-Waals forces).

Several methods exist to evaluate the strength and quality of adhesion, including normal tack test, peel test or lap shear tests. In the following chapter, the normal tack test will be introduced with a focus on the detachment process, followed by sections relating to the previous chapter, adhesion of bioinspired adhesives and their performance on substrates in the presence of surface roughness.

2.4.1 Normal tack test

The **normal tack test** is a standard procedure to evaluate adhesive strength of materials and is used in the present work. In contact with smooth substrates, the adhesion behavior of elastic solids is well explored, both experimentally and theoretically with many publications by Créton, Shull, Guduru and others.⁹²⁻⁹⁷ During a normal tack measurement, a specimen is pressed against a substrate until a certain compressive preload stress, σ_0 , is reached. After this, the position is held for a certain time, the hold time t_{hold} , until the probe is retracted until complete detachment. The displacement, s , is corrected with the machine compliance previously measured to compensate elastic deformation caused by the setup. In general, substrates can vary in geometry (planar, curved), roughness and material (glass, sapphire, epoxy resin,..) depending on the purpose of the measurement.

Based on the measured force-displacement and time-force profiles, many parameters can be analysed (**Figure 2.8**). The **stress**, σ , is calculated based on the force, F , divided by the apparent contact area, A , i.e. usually the area of the probe. The **pull-off stress**, σ_{max} , is defined as the maximum tensile stress. The **relative displacement**, ε , is a unitless parameter calculated based on the displacement, s ,

normalized by the film thickness, h_{film} , to be $\varepsilon = (s - s_0)/h_{\text{film}}$ where s_0 is the displacement at which the transition between compressive and tensile regime starts, i.e. the force becomes zero. This definition only applies to tack measurements on films, and will not be used for patterned substrates. The **maximum relative displacement**, ε_{max} , is the relative displacement corresponding to detachment. The **work of separation**, W_{sep} , is the area under the stress-displacement curve $W_{\text{sep}} = \int_{s_0}^{s_{\text{end}}} \sigma ds$, where s_{end} is the displacement at which detachment occurs. s_{end} does not have to correspond to the displacement at which the pull-off stress is reached, $s_{\text{pull-off}}$. In the case of very soft materials such as pressure sensitive adhesives, cavities form at the interface and the material is extended in fibrils, resulting in s_{end} being much larger than $s_{\text{pull-off}}$.

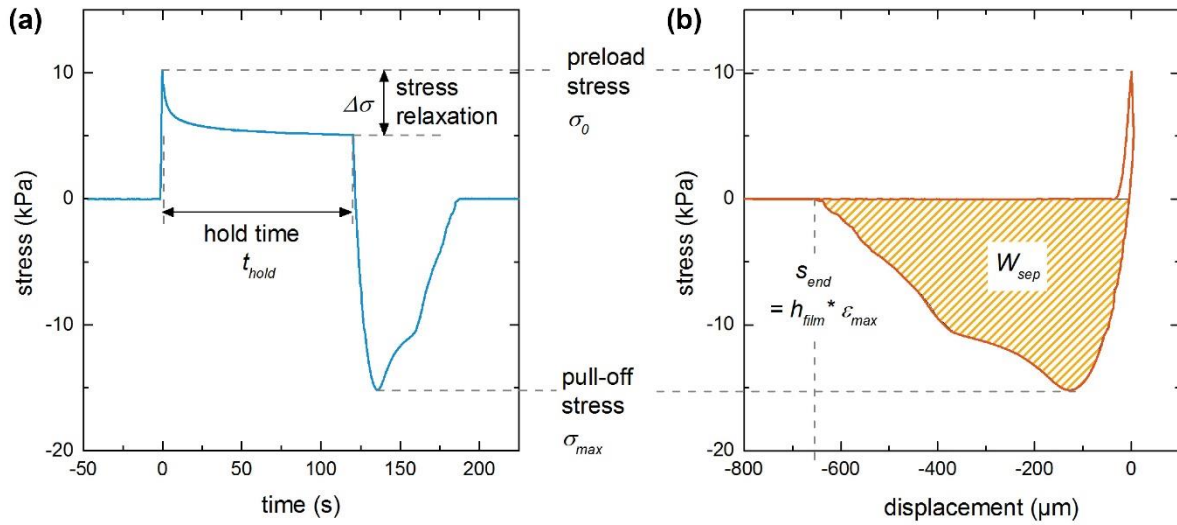


Figure 2.8. Normal tack test measurement data and their analysis. (a) Stress-time curve with time starting at 0 s when sample and substrate are first in contact. (b) Stress-displacement curve with displacement set to 0 when the tensile regime starts. Preload stress, pull-off stress, work of separation, hold time as well as stress relaxation are pictured in the figure. In both plots, tensile stresses are shown as negative and compressive stresses as positive values.

In addition to analyzing parameters from the tensile part of the adhesion measurement, the stress relaxation during the hold time contains information about the material behavior. When the preload stress is applied and the displacement held constant, the stress relaxes during the hold time as the material is not perfectly elastic. To describe the mechanical behavior of polymers, a linear elastic model, mechanically described by a spring, is not sufficient and material models comprising several springs and damping elements are necessary.^{98–100} The decrease of σ as a function of time, t , can be described as^{101,102}:

$$\sigma = \sigma_{\infty} + \sum_1^i \sigma_i \cdot \exp\left(-\frac{t}{\tau_i}\right), \quad (2.8)$$

where σ_{∞} is the equilibrium stress at very long hold times and σ_i and τ_i are the i -th pair of relaxation parameter and relaxation time. For soft elastomers, two or three time constants are usually taken into account.

2.4.2 Detachment mechanisms and stress distributions

The characterization and analysis of the detachment mechanisms is fundamental for understanding adhesion. Depending on material properties, confinement, i.e. ratio between film thickness and contact radius, and many other factors, the detachment can be very different, including detachment from a free edge, void formation, fibrillation, or combinations of phenomena.⁹⁶ Davis et al. showed that a variation of contact time in a very narrow range can lead to different detachment patterns depending on the hold time and the interfacial properties, describing a transition from defect-controlled to interface-controlled detachment due to the presence of entrapped air.¹⁰³

In fact, the detachment from a surface can be described by the formalism of fracture mechanics, as cracks have to be formed in order for delamination to take place. Therefore, many theoretical studies adapt fracture mechanics theory to describe problems in adhesion science, for example to predict adhesion strength based on the magnitude of the stress singularity at the edge of a fibril.^{41,59,104}

In a straight, cylindrical fibril, the stress distribution in the center region of the contact area is relatively homogeneous while stress singularities form at the edge of the contact (**Figure 2.9, left**) when interfacial friction is present. These stress concentrations initiate propagation of edge cracks which lead to detachment. Tip modification, such as mushroom-shaped tips, can influence the stress distribution, resulting in reduced local stresses under the mushroom flaps and reduced magnitude of the corner stress (**Figure 2.9, right**).⁴¹ To quantify the magnitude of the stress singularity, the value of the stress is often evaluated at a small distance from the edge, i.e. an assumed crack length. In some cases, this stress value can be lower than the stress underneath the stem, which will favor detachment other than the propagation of spontaneous edge cracks.^{41,105,106} In good agreement with these numerical simulations, it was experimentally observed that edge detachment can be suppressed and crack initiation occurred in the center of the contact area for mushroom structures, yielding significantly increased pull-off stresses compared to a straight fibril.^{107,108} In experiments, the adhesion strength of mushroom shaped fibrils has been shown to depend on defects on the structures, surface roughness and ambient pressure, but it is still unclear how these factors influence the detachment types in pillar arrays and especially to what extent suction plays a role for center crack detachment.^{36,108–110}

These observations can be used to predict geometrical design criteria to fabricate high-performance dry adhesive structures. Aksak et al. approached this problem using a cohesive zone model, incorporating the possibility for the crack to be initiated at the edge or the center of the pillar.⁴⁴ They found that the edge angle and the ratio of tip to stalk radius are important factors to tune adhesive performance. Similar results were found by Balijepalli et al. based on the analysis of the corner stress singularity, predicting highest adhesion for thin tips with large overhang.⁴¹

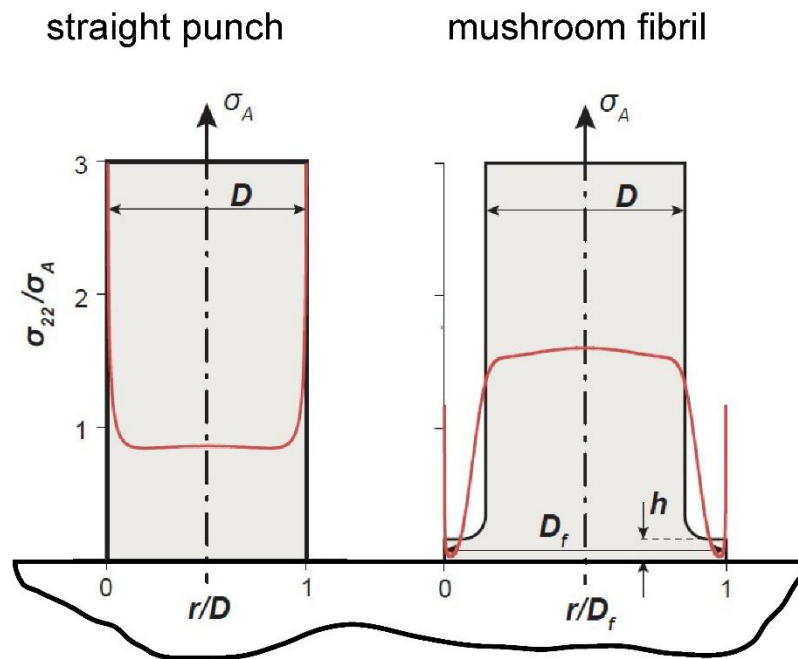


Figure 2.9. Normal stress distributions at the interface between fibril and substrate. The stress distribution is shown for (a) a flat punch and (b) a mushroom fibril in contact with a rigid half-space. Image courtesy of René Hensel with data published by Ram Gopal Balijepalli et al.⁴¹ D and D_f refer to the diameter of the fibril and the mushroom tip, h is the thickness of the mushroom tip and σ_{22}/σ_a the stress normalized by the applied stress.

2.4.3 Roughness and adhesion

Roughness strongly affects adhesion and, for example, limits the maximum pull-off stress.^{84,85,111–113} Several studies were performed which examine the influence of surface roughness on adhesion as a function of the real contact area and elastic material properties.^{83,84,114} An increase in roughness typically leads to a significant loss in contact area and larger distances over which the short-range intermolecular forces have to act. It is important to note that the real contact area is much smaller than the apparent contact area.¹¹⁵ In addition, surface asperities locally induce regions with high strain energy, which also counteracts adhesion. In order to improve adhesion, higher preloads and, in case of viscoelastic materials, longer times in contact with the substrate can help as they tend to enlarge the contact area.^{114,116}

In the presence of surface roughness, the stress distributions and detachment mechanisms are strongly influenced by the substrate asperities. It has for instance been shown by Chiche et al.¹¹⁷ that the amplitude of surface roughness plays a major role and asperities serve as initiation points for cavities, but at the same time seem to diminish the crack propagation speed and yield a more dissipative delamination process.

It has been shown by Briggs et al.¹¹⁸ that microscale roughness can increase adhesion. Similar to this observation, Purtov et al.¹¹⁹ measured adhesion of a specially cured, very soft silicone half-sphere to epoxy surfaces with increasing roughness. The authors did not observe the maximum pull-off force for

the smoothest substrate, but for a substrate with nanoscale roughness. They argue that some roughness can enhance adhesion due to increased contact area, while higher roughness leads to a reduction in adhesion strength due to partial contact. Similar observations were described by Davis et al., who studied the adhesion of wrinkled, rigid surfaces to a silicone elastomer with varying stiffness caused by different amounts of crosslinker.¹²⁰ They found that small scale wrinkles yield higher pull-off stress compared to a smooth substrate for the elastomer with higher crosslinker content while large scale wrinkles decrease the pull-off stress. Almost no difference between pull-off stress on the smooth control and the patterned substrates was observed for the softer elastomers with lower concentrations of crosslinker. This implies that the sensitivity of adhesion to roughness depends on the mechanical properties. However, based on the argument that increased contact area is responsible for larger pull-off stresses on surfaces with nanoroughness, an even stronger effect would be anticipated for softer materials, which was not observed by the authors.

The insensitivity to surface roughness, therefore, calls for another hypothesis of underlying mechanisms than an increase in surface area. Interestingly, Davis et al.¹²⁰ observed that the detachment mechanisms differed strongly on different substrates depending on the material properties. The authors base their interpretation on previous work by Persson et al.¹¹² and Hui et al.¹²¹, who established a material-defined length scale, δ_c , describing the range of adhesive interactions. δ_c primarily depends on the critical strain energy release rate, G_c , and the elastic modulus, E ,⁹³ for semi-infinite soft films:

$$\delta_c^\infty \approx \frac{G_c}{E}. \quad (2.9)$$

In case of a confined elastic layer, δ_c depends on the thickness of the elastomer, h_{film} :

$$\delta_c^{h_{film}} \approx \sqrt{\frac{G_c \cdot h_{film}}{E}}. \quad (2.10)$$

According to this argument, surface roughness influences the adhesive interaction and thereby pull-off stress and work of separation if the surface asperities are in the range or higher than δ_c . On the other hand, adhesion is not impeded by surface topography if the height differences are smaller than the characteristic length, δ_c , as in the case of the lightly crosslinked elastomers presented in the work by Davis et al.¹²⁰ If an interaction between surface profile and polymer takes place, surface roughness does not necessarily reduce adhesion, but can also guide crack propagation, slow down propagation and thereby increase adhesion.

2.4.4 Adhesion on skin

In the case of medical applications, adhesives must sometimes fulfil a multitude of functions at a time: They have to adhere to an extremely complex surface, be biocompatible, allow breathability through the adhesive, prevent skin irritation, cause minimal damage of the skin upon removal, and sometimes deliver drugs to facilitate the healing process.^{122,123} One of the biggest challenges, however, is the variance of the surface roughness of skin^{124–128}: The properties of the skin not only depend on the patient's age and life style (smoking, skin products), but additionally very much on the position on the

body (forearm, wrist, cheek,...) where they even vary locally. Additionally, skin can include grease, sweat, hair follicles and also skin care products on its surface. All of these factors make skin a very complex substrate, which is difficult to mimic for testing the adhesives.

Thus, quantifying the adhesive performance is very difficult. Measuring on real skin is not a practical option to test adhesives because of ethical and legal issues, therefore other substrates are used to test adhesion. Often, standardized tests are performed on stainless steel or smooth polymer blocks. While this is a very reproducible and convenient method, this gives at most an estimate of the adhesion behavior to be expected. Especially time and preload stress dependency cannot be captured by this simplified testing method. Therefore, several artificial skin substrates exist. Some models of interest for pharmacological studies are reconstructed from human epidermis, for instance SkinEthic (SkinEthic laboratories, Nice, France), EpiSkin (EpiSkin, Lyon, France) or Epiderm (MatTek Corporation, Ashland, MA, USA).¹²⁹ These are, however, developed for describing penetration into skin and not suitable for adhesion testing. VitroSkin from IMS Inc. is a synthetic polymer sheet of non-biological origin designed to mimic not only the topography but also physico-chemical properties like the pH value or surface tension. It is used in the cosmetics industry to test formulations of sun-screen, but also to perform adhesion measurements. Additionally, replication techniques have been used to replicate the skin roughness into a polymer with properties similar to those of skin.¹³⁰

Materials used for medical adhesives include a wide variety of polymers and polymer composites with components such as acrylates, synthetic rubber or silicones for instance. Tissue adhesives used to seal small wounds or vesicles can be structural adhesives, or adhesives in a liquid state that cure with a stimulus like UV-light or moisture present.¹³¹ Kheyfets et al.¹³² reported tack tests of such commercially available liquid wound-treatment polymers on explanted porcine skin. They measured pull-off strength from 10 to 14 kPa and a work of separation ranging from 25 to 40 J/m². In contrast to structural adhesives, most bandages contain pressure-sensitive adhesives (PSA), which do not need any external stimulus like heat or moisture to attach, but reach high adhesion strength upon applying light pressure. This makes them very versatile adhesives usable without any equipment and without waiting times for curing.

Adhesives for skin are not just used to attach to skin, but usually incorporate more complex functions. Adhesives can be designed in a way that the wound edges are approached and kept under tension.¹³³ This device is at present past medical trials and has been shown to reduce scar formation. Some adhesives are especially made for particularly delicate skin, for example the skin of premature infants.¹³⁴ Here, the adhesive together with its backing layer were designed to make the detachment easier, preventing damage of the skin while being able to secure devices in place.

For the growing need for sensors temporarily attached to the body, so-called electronic skin has attracted interest of scientists worldwide.^{135–137} These devices are designed to sense temperature, pressure, stretch, measure physiological body signals or enable interaction with humans. Several aspects are challenging to succeed in building such devices: They have to adapt very well to the skin topography, be at least partly conductive or able to feature conductive circuits and interface to a power supply. Some groups have integrated electronic circuits on temporary tattoo paper to attach to skin.^{138,139} The electronics were printed by customized inkjet printing or screen printing for instance. These techniques are also used to transfer circuits on thin elastomer sheets.¹⁴⁰ Another approach is based on integrating carbon nanotubes in elastomers and using percolation of the networks to achieve conductivity.¹⁴¹ Some groups have even succeeded in making the e-skin self-healing, like real human

skin.¹⁴² Another challenge is the biodegradability of the polymers if the e-skin is serving as a prosthetic to restore skin functions.^{143,144}

Fibrillar bioinspired adhesives are a promising technology for applications on skin as they can be designed to secure multiple attachments on rough surfaces while maintaining high adhesion, which would be useful for attachment of sensors. However, to design adhesives for rough surfaces, it is common to use existing designs of fibrillar adhesives with minor modifications when comparing to smooth surfaces.⁴⁹ A difficulty in manufacturing them can be the compromise between low elastic modulus materials for good adaptability and high elastic modulus to avoid collapsing or clustering of the features.¹⁴⁵ In the case of mushroom-shaped structures, some groups have tried to combine different materials.^{48,49} One of the first approaches was proposed by Bae et al.⁴⁹ and consisted of manufacturing mushroom structures where the tips were inked with a softer material for application as skin adhesive. They restricted their experiments to one pillar geometry with a diameter of 5 μm and a height of 15 μm as these were optimal parameters identified in their previous study to achieve highest adhesion against skin while preventing collapse of the structures.¹⁴⁶ To modulate the mechanical properties, Sylgard 184 with different amount of crosslinking agent was used, with best results for 15 wt% crosslinker in the stiffer pillars and 5 wt% crosslinker for the soft tip coating, yielding adhesion strength of up to 18 kPa.

Theoretical studies predict that large, thin mushroom flaps are best to increase adhesion.⁴¹ These studies usually assume smooth, rigid surfaces and perfect contact. Therefore, this conclusion cannot directly be translated to surfaces with significant surface roughness. In addition, Barreau et al.⁸⁹ showed that, for fibrillar adhesives, the size of the structure needs to be correlated to the roughness of the counter surface. They found that adhesion was maximized when the microstructures had a diameter slightly larger than the horizontal distance of roughness peaks at small scale. If pillars are smaller, they bend to conform to roughness valleys which caused high strain energies and a drop in adhesion. When structures are much bigger, they only come in contact with the tips of asperities and cannot conform to the surface.

Furthermore, the height of the pillars as well as the backing layer thickness play an important role. Kwak et al.¹⁴⁶ developed a simplified mechanical model to provide design criteria for the backing layer and the fibril height of a dry adhesive patch with mushroom caps for adhesion to skin. Their argumentation considers the skin to be a surface with dual roughness: The first level of roughness includes the contour of the body and wrinkles, while the second level of roughness includes height differences at the micron scale. They consider two contributions to the adaptation of a patch to the skin: the backing layer adapts to the first level of roughness, elongation of the fibrils enables adaptation to the second level of roughness. The backing layer was simplified to be a thin, elastic membrane of thickness t wrapped around a curved surface. The minimum curvature radius R_{min} is calculated based on the equilibrium of bending-induced strain energy per unit area A and adhesion energy γ .

They estimate the minimum radius of curvature R_{min} to be:

$$R_{min} = \sqrt{\frac{E t^3}{24 \gamma}}, \quad (2.11)$$

where E is the elastic modulus of the membrane. This means that the minimum radius of curvature increases with increasing thickness of the backing layer ($R_{min} \propto t^{\frac{3}{2}}$) and increasing elastic modulus ($R_{min} \propto \sqrt{E}$).

For the adaptation to the second level of roughness, the evaluation of Kwak et al.¹⁴⁶ is based on the equilibrium between the elastic restoring energy and the adhesion strength of single fibrils, yielding a minimum height of the pillars of:

$$h_{min} = \frac{E A_p}{2 \gamma_t A_t} \delta^2, \quad (2.12)$$

where E is the elastic modulus of the fibrils, A_p and A_t the cross sectional area of the pillar and the tip (i.e. mushroom cap), γ_t the adhesion energy per pillar and δ the displacement of the pillars necessary to form contact which is correlated to the amplitude of the roughness. Extending this relation to pillars with an overall cylindrical shape ($A_p = A_t$) results in:

$$h_{min} = \frac{E}{2 \gamma_t} \delta^2. \quad (2.13)$$

Many factors influence adhesion of bioinspired adhesives on rough surfaces like skin. It is for instance possible to tune material, microstructure dimensions and the backing layer. One possible application for the fibrillar adhesives on skin, where all these parameters need to be optimized, are new patches to heal tympanic membrane ruptures.

2.4.5 Tympanoplasty

Tympanoplasties are reconstructions of ear drum perforations. Eardrum perforations occur following exposure to trauma in the ear, for instance caused by explosions or mechanical impact, or infections. If the perforations are small, spontaneous closure can occur. In the case of large defects, a surgery is necessary to enable closure of the membrane and restore hearing capabilities.^{147,148} The standard procedure involves the explantation of a tissue graft from the patient and application on the ruptured ear drum. However, this procedure involves expensive surgery necessitating microsurgical skills, partial or full anesthesia of the patient, immobilization of the ear with cotton in the ear canal for over a week and is still associated with a chance of reoccurrence due to shrinkage of the tissue or shift of the graft.^{149,150} There is no suitable method to fixate the graft in place as the tympanic membrane is very fragile with only 50 to 70 μm in height, there is moisture present and liquid structural adhesives cannot be used as the risk to glue the hearing bones is too high. Other approaches already involve synthetic grafts like paper, bioinspired silk or hydrogels.¹⁵¹⁻¹⁵³ An important aspect during the closure of the tympanic membrane is that the three cell layers of the membrane are restored.¹⁵⁰ Otherwise, the membrane does not exhibit full vibrational properties and might be prone to failure.¹⁵⁴ However, with most methods, the middle layer does not regain its original morphology, which causes reduction in hearing. One hypothesis for this is attributed to the lack of tension compared to the intact tympanic membranes, as it was shown that some cell types grow better in the presence of tension and scar formation can be reduced by application of a stress.^{133,155}

An important aspect of this surgery is, however, that the placement of the graft is a very delicate procedure, and might require several attempts to replace the patch. In this case, removing the patch should not damage the ear drum. In the case of non-biodegradable polymers, the patch also needs to be removed upon complete healing of the membrane without causing damage. Developing a patch with good adhesion to the tympanic membrane could enable to pre-stretch the ruptured membrane during tympanoplasty, and in this way potentially enable healing under tension followed by a more successful restoration of hearing ability. Additionally, shifting of the graft during the recovery and the period in which the patient needs to be shielded from sound could potentially be reduced.

Preliminary experiments evaluated the application of microstructured patches on mice ear skin.^{156,157} De Souza et al.¹⁵⁷ performed adhesion measurements with micropatterned and flat reference samples made from Sylgard 184 and found that, even though the pull-off forces were similar, the adhesion energy increased in presence of microstructures and adhesion curves strongly depended on the humidity of the skin. Kaiser et al.¹⁵⁶ systematically studied the influence of the pillar diameter of Sylgard 184 and biodegradable poly(lactic-co-glycolic)acid (PLGA) microstructures on different substrates: mice ear skin, gelatin-glycerol mixtures as artificial skin substitute and polished glass. Similarly to de Souza et al.¹⁵⁷, Kaiser et al. observed similar adhesion strength for patterned and non-patterned Sylgard 184 samples on mice ear skin, with a high scattering of the results. They attributed this partly to degradation of the properties of explanted tissue, variability and misalignment, underlining that the material choice is not optimal for this application in the presence of roughness. Even if the stiffer PLGA micropatterns with diameters between 10 and 20 μm exceeded adhesion stresses of unpatterned PLGA substrates and all Sylgard 184 samples on the soft gelatin-glycerol substrate, no experiments of PLGA samples on mice ear skin were presented, thus neglecting the influence of roughness. For the real application as tympanic membrane graft, both the adhesion and adaptation to the natural curvatures of the inner ear have to be equally considered in the development process.

3 Scope of this work

Adhesion is a field that has been explored for many decades and a concept everybody encounters daily with stamps, medical adhesives or sticky notes for example. However, there are still many challenges based on the properties of the substrate, especially related to surface roughness. Nature has evolved versatile tools for attachment to any surface in the habitat of animals, addressing issues such as environmental factors, surface properties, and reduction of contamination of the attachment system. This is an immense source of inspiration for artificial adhesives as those are still usually very specific for a special application. Through biomimetics, concepts are developed to simplify those systems and reduce them to the essential features, retaining the adhesion characteristics while simplifying the overall structure and adapting it for manufacturing. To ultimately find better solutions for this problem, a profound understanding of the interaction of adhesive structures and materials with complex surfaces is needed. This thesis will address associated challenges and contribute to improved designs and understanding of dry adhesives in the future.

In this work, new approaches have been explored to increase the adhesive performance of artificial, dry adhesives to rough surfaces. In creating a successful artificial dry adhesive, many parameters must be taken into account to tune the structure (**Figure 3.1**). The **backing layer** is the backbone of the whole system, responsible for flexibility and adaptation to macroscopic roughness. **Microstructures** distribute the applied stress across the surface and enable contact splitting.²⁰ By having many points of contact rather than one, the stress necessary to separate the surfaces is predicted to increase.²⁰ The **contact region** is responsible for adaptation to microscopic roughness, and can consist of an adapted tip shape or material, for example. Lastly, the material **interface** in multi-material structures can be tuned to influence the mechanical behavior of the system and the stress distribution at the substrate interface.

The present thesis comprises three parts with different approaches to improve adhesion to rough substrates.

In the first part of this work, a novel dry adhesive with tunable interface is presented which achieves higher adhesion without changing tip shape (**Chapter 4**). The study comprises an experimental part on single macroscopic pillars with a composite structure and finite element model simulations. The tunable adhesion is based on a combination of interface geometry variation between two materials with considerable differences in elastic modulus, as well as tip thickness.

In the second part, unpatterned soft adhesive SSA MG 7-9800 by Dow Corning is characterized and tuned to explore its potential for biomedical applications (**Chapter 5**). In the case of medical adhesives, especially in the case of open wounds, additional challenges arise as the material must be biocompatible and enable cells to proliferate. This can for instance be realized by plasma treatment, which in turn influences the adhesion especially on rough surfaces. Therefore, it is important to find compromises between good adhesive performance and biocompatibility. In addition, a comprehensive study of adhesion on surfaces with roughness similar to skin was performed to understand the behavior of the polymer in terms of surface roughness, contact time and material relaxation behavior (**Chapter 6**).

In the third part, a different approach to enhance the performance of existing artificial adhesives is investigated. An alternative tip shape is presented to enhance adaptability of mushroom shaped structures to the surface (**Chapter 7**). Funnel-shaped microstructures have thin, inclined flaps and a cavity in the center. During the approach of the structures to the substrate, the flaps adapt to the surface due to their high compliance and form intimate contact. Adhesion experiments performed on single microstructures with a nanoindentation system and finite element simulations systematically reveal the influence of different geometrical parameters on the deformation and adhesion strength of the polymeric structures.

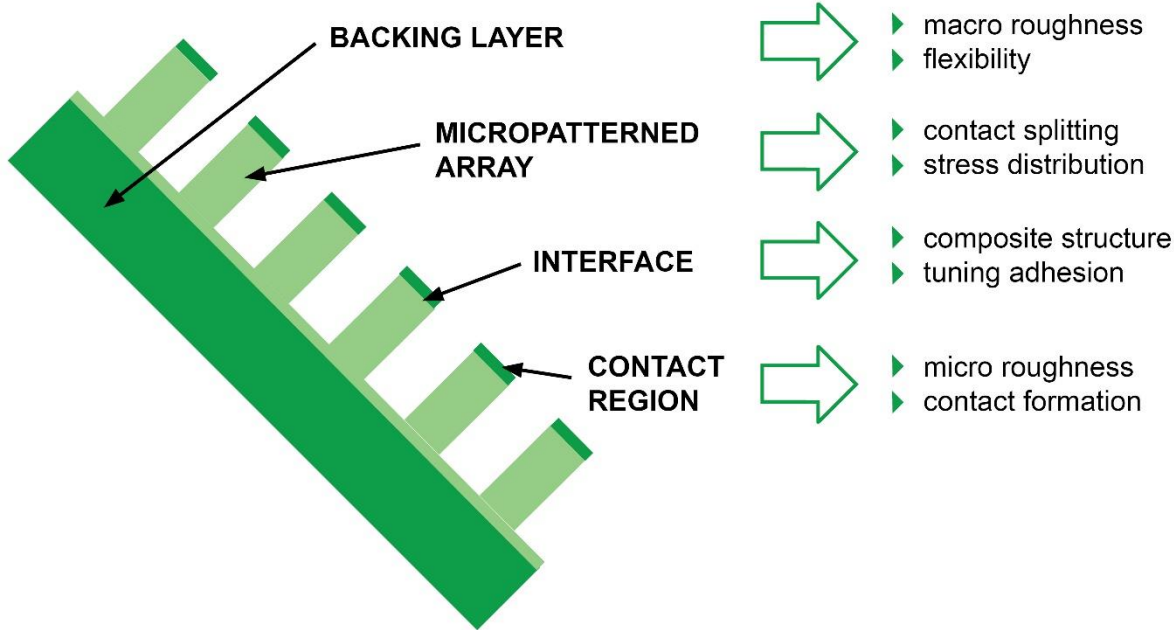


Figure 3.1. Microstructures with functional regions. Different aspects of microstructures can be used to tune the adhesion, including the backing layer, the micropatterned array, the contact region, and the interface between microstructure and contact region.

PART I:

Composite pillars

4 Composite Pillars with Tunable Interface for Adhesion to Rough Substrates *

4.1 Abstract

The benefits of synthetic fibrillar dry adhesives for temporary and reversible attachment to hard objects with smooth surfaces have been successfully demonstrated in previous studies. However, surface roughness induces a dramatic reduction in pull-off stresses and necessarily requires revised design concepts. Towards this aim, we introduce cylindrical two-phase single pillars, which are composed of a mechanically stiff stalk and a soft tip layer. Adhesion to smooth and rough substrates is shown to exceed that of conventional pillar structures. The adhesion characteristics can be tuned by varying the thickness of the soft tip layer, the ratio of the Young's moduli and the curvature of the interface between the two phases. For rough substrates, adhesion values similar to those obtained on smooth substrates were achieved. Our concept of composite pillars overcomes current practical limitations caused by surface roughness and opens up fields of application where roughness is omnipresent.

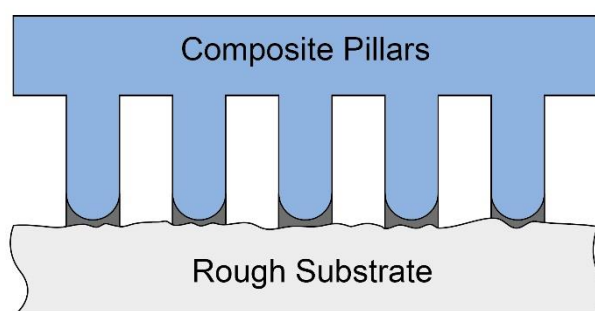


Figure 4.0. Graphical summary of chapter 4. Schematic of composite structures with tunable interface in contact with a rough surface.

* This chapter was published in *ACS Applied Materials and Interfaces*:

Fischer, S. C., Arzt, E., & Hensel, R. (2016). Composite pillars with a tunable interface for adhesion to rough substrates. *ACS applied materials & interfaces*, 9(1), 1036-1044.

The article is available under: <http://pubs.acs.org/doi/abs/10.1021%2Facsami.6b11642> .

4.2 Introduction

Fibrillar dry adhesives attract much attention as they are instrumental for emerging technologies such as wall climbing robots³⁷ and novel gripping systems.^{35,36} In such applications, most real walls and objects exhibit surface roughness on different length scales. It is known that roughness strongly affects adhesion and, for example, limits the maximum lifting force.¹⁵⁸ Several studies were performed which examine the influence of surface roughness on adhesion as a function of the real contact area and elastic material properties.^{83,84,114} An increase in roughness typically leads to a significant loss in contact area and larger distances over which the short-range intermolecular forces have to act. In addition, higher elastic strains typically occur in the contact zone, which also counteract adhesion. In order to improve adhesion, higher preloads and, in case of viscoelastic materials, longer times in contact with the substrate can help as they tend to enlarge the contact area.^{114,116}

An alternative approach to enhance adhesion to rough substrates are fibrillar adhesives.^{89,159–162} Such structures are now well known from sticky footpads found in nature^{6,163}: The fibrillar structures of adhesive organs, developed during evolution for instance in geckoes, make up soft and compliant surfaces which allow easy adaption to roughness at the expense of little strain energy.^{18,20,43,164} The toe pads exhibit several hierarchical levels, with a stalk splicing into successively finer fibrils and, finally, spatula terminal elements.¹² Several groups have mimicked such hierarchically assembled structures in artificial designs^{51–54} but many unsolved questions remain: introduction of hierarchy, for example, generally reduces the available contact area in synthetic adhesives and increases the propensity to elastic buckling.^{56,57}

The ladybug provides another blueprint for the design of fibrillar adhesives.¹⁶ In contrast to the gecko, its adhesive pad consists of cuticular fibrils without hierarchy, but each fibril possesses an axial gradient of Young's modulus. Experiments using nanoindentation have demonstrated that the Young's modulus decreases by three orders of magnitude from the stalk to the tip.¹⁶ A numerical study revealed that such a material gradient can also prevent clustering of an array of fibrils, especially for fibrils with high aspect ratio coming into contact with rough substrates.¹⁷ Similar effects were observed in smooth adhesive pads of other insects.⁶⁷ Recently, first experimental and numerical studies have been performed for fibrils with axial variations of the Young's modulus adhering to smooth surfaces.⁴⁷ It was found that very thin soft tip layers promise the best adhesion enhancements for smooth substrates. Interestingly, Bae *et al.* demonstrated that a soft tip coating added to a micropatterned fibrillar array improved adhesion to skin, i.e. a compliant and rough surface.⁴⁹ However, the underlying adhesion mechanism of composite fibrils on rough substrates is only poorly understood.

The objective of this work is to evaluate the potential of composite fibrils as a new design concept for adhesion to rough and smooth substrates. As model structures, single macroscopic composite pillars were fabricated in a two-step molding process with a systematic variation of soft layer thickness, Young's modulus ratio, and interface curvature. The influence of these design parameters on adhesion performance and observed detachment events was assessed experimentally. As a result, composite pillars with hemispherical interface, thin soft tips and high Young's modulus ratio were identified as promising candidates to enhance adhesion to rough substrates.

4.3 Material and methods

4.3.1 Fabrication of composite pillars

Composite pillars with macroscopic dimensions in the mm range were fabricated using a two-step molding process as illustrated in **Figure 4.1**. The pillars consisted of a relatively stiff stalk of poly(ethyleneglycol) dimethacrylate (PEGdma, Polysciences, Warrington, PA, USA; Young's modulus of about 350 MPa) or polydimethylsiloxane (PDMS, Sylgard 184, Dow Corning, Midland, MI, USA; Young's modulus of about 2 MPa). The softer tip layer consisted of polyurethane Polyguss 74-41 (PU, PolyConForm GmbH, Duesseldorf, Germany) with a Young's modulus of about 900 kPa. Thus, composite pillar structures with a Young's modulus ratio of stiff to soft of about 350 and 2, and two interface geometries, flat and hemispherical (with a curvature radius half the diameter), were generated. As control samples, pillars consisting entirely of PU were manufactured.

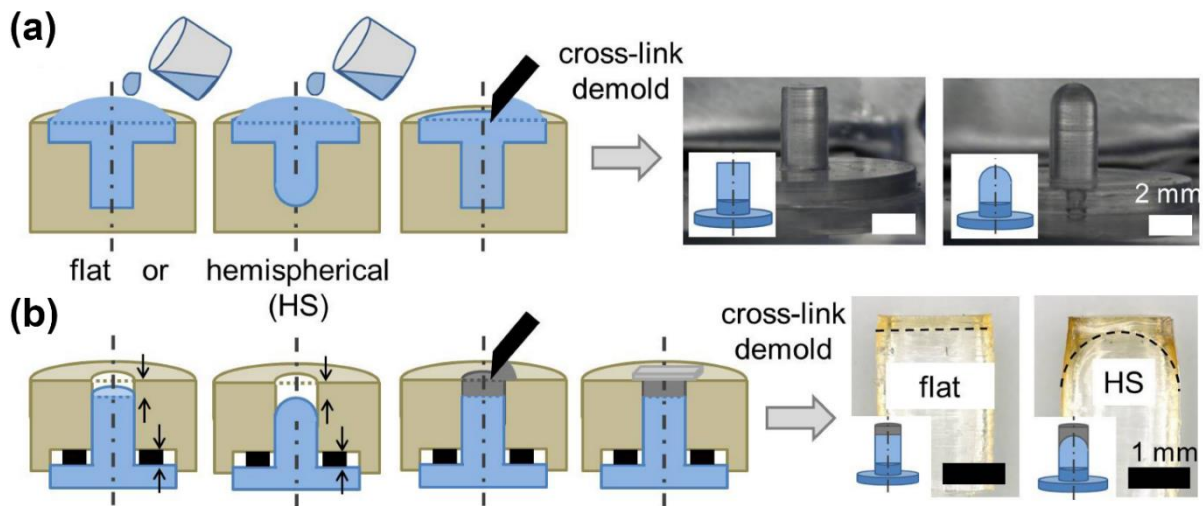


Figure 4.1. Two-step molding process for composite pillar fabrication. (a) Stalks are manufactured in two separate molds depending on the interface geometry of the final composite. The optical micrographs show exemplary PDMS stalks with a flat (left) and a hemispherical (right) pillar face. (b) Adding of soft polyurethane tip layers using a second mold. The thickness of the soft layer is determined by spacers (black) between the mold and the backing layer. Optical micrographs show cross-sections of the final composite structures for both interface geometries.

In the first step of composite fabrication, stalks were replicated using a custom-made aluminum mold as shown in the optical micrograph in **Figure 4.1a**. The resulting stalks had a diameter of 2 mm, a height of 4 mm and either a flat or a hemispherically-shaped face with radius 1 mm. The manufacturing process varied for the two materials. The PDMS prepolymer (10 weight parts of the base to 1 weight part of the curing agent) was degassed under vacuum for 5 min at 2000 rpm in a SpeedMixer (DAC600.2 VAC-P, Hauschild Engineering, Hamm, Germany). It was then filled into the mold, degassed for 10 min and cured at 125°C for 20 min on a heating plate. In case of PEGdma, 0.5 wt% of the photoinitiator 2-Hydroxy-2-methylpropiophenone (Sigma-Aldrich, St. Louis, MO, USA) was added to the prepolymer. Subsequently, 1 wt% of 2-Aminoethyl methacrylate hydrochloride (Sigma-Aldrich, St. Louis, MO, USA) was added to enhance the adhesion of PU on PEGdma. The liquid mixture was poured into the mold,

exposed to nitrogen for 20 min and then UV-cured for 300 s using a UV lamp (Omnicure S1500, Excelitas Technologies, Waltham, MA, USA).

The soft layer was added to the pillar in the second molding step (**Figure 4.1b**): The PU prepolymer solution was mixed under vacuum for 2 min at 2000 rpm in a SpeedMixer. The PDMS stalks required activation with oxygen plasma for 2 min at 60 % power (PICO plasma system, Diener electronic, Ebhausen, Germany) prior to this second step to enable covalent bonding of PU to the PDMS. The PU prepolymer was applied at the free end of the pillars and degassed for 2 min. Afterwards the excess polymer was removed with a razor blade and the mold was subsequently covered with a smooth Teflon film glued onto a glass slide. To realize different thicknesses of the soft tip, spacers with different thickness were inserted at the back end. The PU was cured at room temperature for at least 16 hours and finally gently demolded.

4.3.2 Adhesion experiments

Adhesion experiments were performed using a custom-built, slightly modified setup (**Figure 4.2a**) following Kroner *et al.*¹⁶⁵ A nominally flat glass substrate cut from a soda lime glass microscope slide (Marienfeld, Lauda-Königshofen, Germany) was used as a probe. The glass substrate exhibited two differently rough areas both of which were used for the adhesion tests (**Figure 4.2b**): region 1 (designated as “smooth”) exhibited a mean absolute roughness $R_a = 0.006 \mu\text{m}$, and a mean peak-to-valley profile roughness $R_z = 0.041 \mu\text{m}$, while for region 2 (designated as “rough”), $R_a = 0.271 \mu\text{m}$ and $R_z = 2.174 \mu\text{m}$ obtained from surface profilometer measurements (DekTak, Bruker, Billerica, MA, USA). Roughness power spectra (**Figure 4.2c**) of both substrate regions were calculated by Surface Topography Analyzer developed by Lars Pastewka (<http://contact.engineering/>)¹⁶⁶ based on AFM topography scans (JPK instruments AG, Berlin, Germany). Both regions were on the same substrate and were used for testing without changing the initial alignment performed on the smooth region of the substrate.

Normal forces were recorded with a load cell (3 N, Tedeo-Huntleigh 1004, Vishay Precision Group, Basingstoke, UK). Before each measurement, the substrate was cleaned with ethanol. A camera and a prism, mounted below the sample, were used to optically align the specimen and the substrate and to observe the contact area between the pillars and the substrate *in situ*. Upon adhesion measurements, samples were sectioned in axial direction and the thickness of the soft tip layer was measured in an optical microscope (Eclipse LV100ND, Nikon, Alzenau, Germany) with an accuracy of $\pm 10 \mu\text{m}$.

In the adhesion experiments, specimen and substrate were brought together until a maximum force, corresponding to compressive preloads between 30 and 180 mN, was reached. After a hold time ranging from 0 to 120 s, the specimen was withdrawn until it detached from the substrate. The measurements were repeated at two different positions on each of the two substrate regions (smooth and rough). For the PEGdma/PU and PDMS/PU composites, the effective elastic moduli of the pillars varied over two orders of magnitude. As a result, the applied force rate in adhesion tests varied dramatically. To keep the force rate similar for all samples, the following test velocities were chosen: For PDMS/PU composites and the PU control pillars, experiments were conducted at $10 \mu\text{m/s}$. For PEGdma/PU composites, experiments were performed at $2 \mu\text{m/s}$. Thus, the force rate was about 10 mN/s and comparable for all tested structures.

For the analysis, the recorded force and displacement values were transformed into nominal stress, σ , and displacement, Δ . We accounted for the deformation of the setup by a correction of the displacement with the previously measured machine compliance ($C = 0.12 \mu\text{m}/\text{mN}$). Pull-off stress values were determined from the maximum tensile force, divided by the nominal contact area.

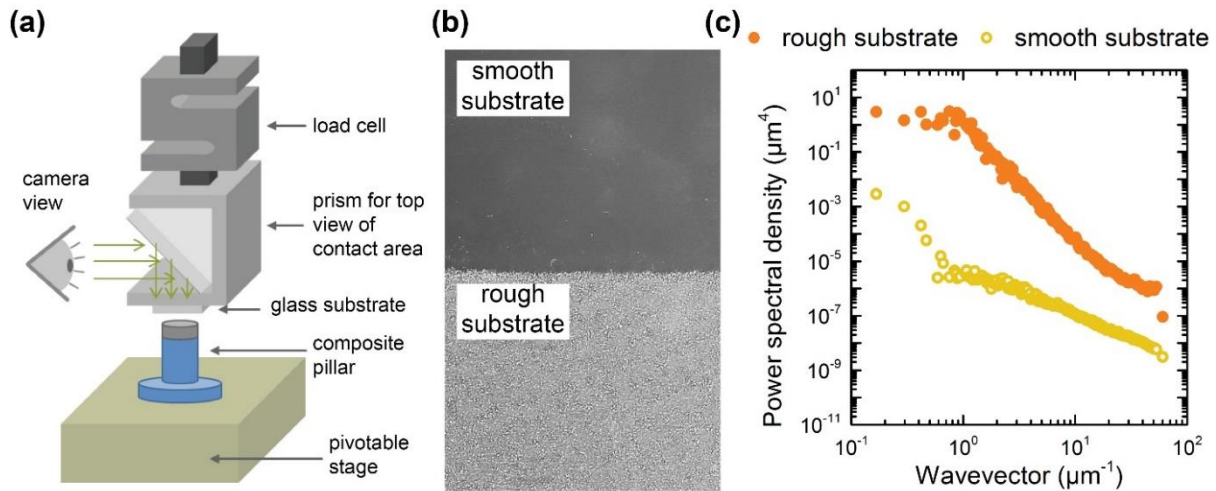


Figure 4.2. Experimental setup for adhesion measurements on smooth and rough substrates. **(a)** Adhesion measurement setup that consists of a load cell to record normal forces, a pivotable stage for alignment and sample manipulation, and an optical camera for *in situ* observations of the contact area. **(b)** The glass slide substrate exhibits two regions: “smooth” and “rough”, and **(c)** the corresponding power spectra calculated from AFM data using Surface Topography Analyzer (<http://contact.engineering/>)¹⁶⁶.

4.4 Results

The macroscopic composite pillars fabricated by the technique described above are shown in **Figure 4.1**. Flat and hemispherical (curvature radius about 1 mm) interfaces, with soft PU layers in the range between 20 and 500 μm , were successfully generated. The actual soft layer thickness, t , were determined upon adhesion measurements and showed some variation due to slight material shrinkage during the cross-linking reaction. For PEGdma/PU composites, manufacturing difficulties occurred for tip thicknesses below 120 μm and, therefore, no measurements were performed for those parameters. As a control structure, conventional pillars with the same dimensions made entirely from PU were used.

In a first step, the adhesion characteristics of conventional pillar structures are reported. **Figure 4.3** shows that their adhesion to the smooth substrate was always higher than to the rough substrate: for small preloads (about 50 mN), the pull-off stress was about 25 kPa for the smooth substrate and about 10 kPa for the rough substrate, corresponding to a ratio of about 2.5. This behavior is in line with a recent study by Barreau *et al.*⁸⁹ Unlike smooth substrates, rough substrates gave significantly higher

adhesion after applying higher preloads or after longer hold times (**Figure 4.3**). Thus for high preloads (about 150 mN), the ratio decreased to 1.5 for 0 s hold time and to about 1.2 for 120 s hold time. These findings very likely reflect the viscoelastic nature of PU that produces an increase in contact area by material relaxation over time.

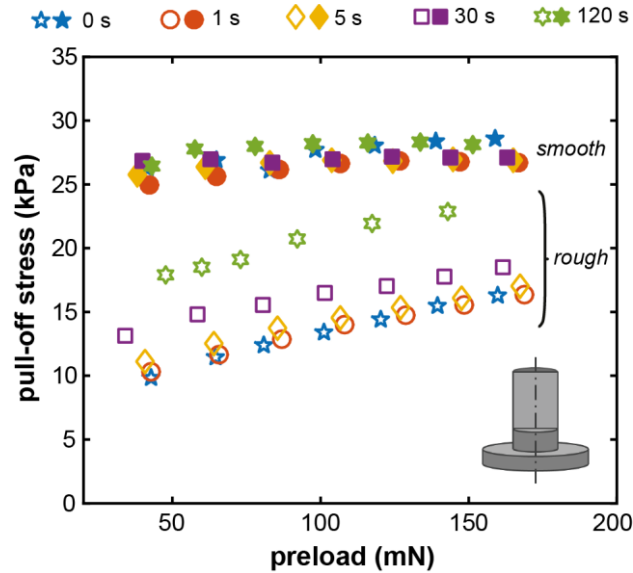


Figure 4.3. Pull-off stress of conventional pillars (controls) made entirely from polyurethane on smooth (filled symbols) and rough substrates (open symbols) as a function of preload and for different hold times : 0 s (blue star), 1 s (red circle), 5 s (yellow diamond), 30 s (purple square) and 120 s (green hexagram).

The pull-off stress of the composite pillars as a function of the soft layer thickness is shown in **Figure 4.4** for two distinct force ranges: low preloads with 50 mN and high preloads with 150 mN. **Figures 4.4a** and **4.4b** illustrate the results for composites with flat interface: On the smooth substrate, the pull-off stress increased with decreasing soft layer thickness up to a maximum pull-off stress of about 55 kPa (for PDMS/PU composites) and 60 kPa (PEGdma/PU composites); these values are about twice those for the PU control specimen (**Figure 4.4a**). The Young's modulus ratio had an influence on the critical thickness, at which the maximum adhesion value was achieved. The critical thickness was about 250 μm for $E_1/E_2 = 350$ and about 120 μm for $E_1/E_2 = 2$. With higher preloads, the adhesion of the composites increased slightly (dashed lines). In contrast, the adhesion of the composites with a flat interface on the rough substrate (**Figure 4.4b**) was similar to that of the PU control and insensitive to the Young's modulus ratio as well as the soft layer thickness. Only for high preloads (150 mN) was a strong increase in pull-off stress, by a factor of two, observed. **Figures 4.4c** and **4.4d** illustrate the pull-off stress of the composites with hemispherical interface under small and high preload. On the smooth substrate, adhesion was similar for both preloads whereas it increased with preload for the rough substrate. For both substrates, it was found that the pull-off stress continuously increased with decreasing layer thickness. Particularly for very thin soft layers ($t = 30 \mu\text{m}$), the value of about 75 kPa was similar on the smooth and rough substrate and, therefore, much higher than for the PU control sample. Thus, we obtained an increase in pull-off stress, over conventional pillars, of about three times on the smooth substrate (**Figure 4.4c**) and about five times on the rough substrate (**Figure 4.4d**).

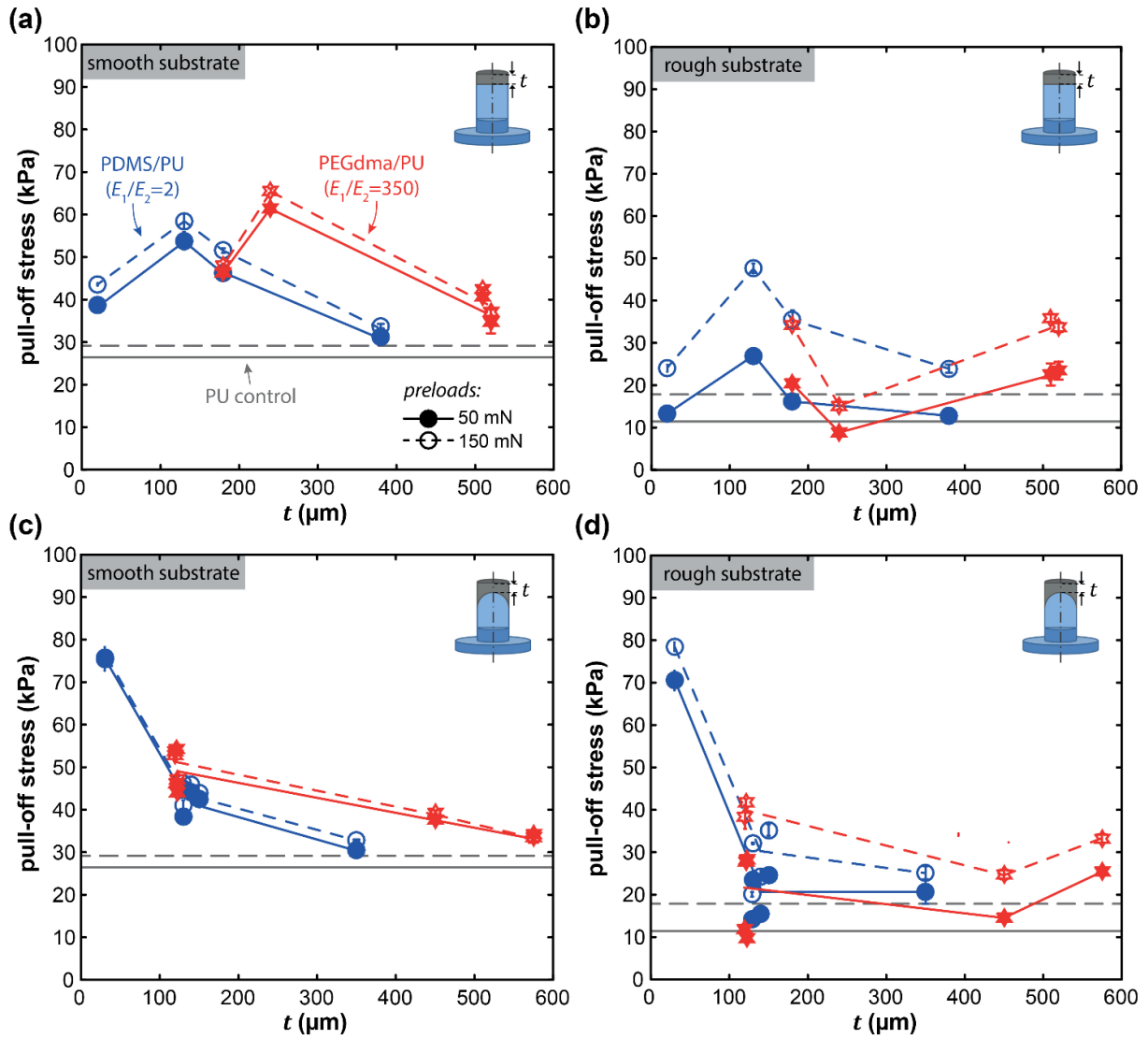


Figure 4.4. Pull-off stress of composite pillars as a function of the soft layer thickness, t . Composite pillars made from PDMS/PU (blue circles) and PEGdma/PU (red stars) were tested at different preloads (solid lines and filled symbols for 50 mN, dashed lines and open symbols for 150 mN). The grey horizontal lines represent the pull-off stress of the PU control sample in the low and high preload regime. The time in contact with the substrate was zero seconds. (a,b) Composite structure with flat interface tested on (a) smooth and (b) rough substrate. (c,d) Composite structure with hemispherical interface tested on (a) smooth and (b) rough substrate.

In the adhesion tests, three distinct detachment mechanisms as a function of the soft layer thickness, elastic modulus ratio and interface curvature could be identified (Figure 4.5):

- (i) Edge crack detachment: The crack was initiated at the edge of the pillar and propagated spontaneously through the contact area (Figure 4.5a). All composite pillars with thick soft layers ($t \geq 250 \mu\text{m}$ for PEGdma/PU and $t \geq 120 \mu\text{m}$ for PDMS/PU), composites with flat interface, $E_1/E_2 = 2$ and thinner soft layers as well as all conventional pillars exhibited this mechanism.

- (ii) Finger-like crack propagation: Several cracks initiated at the edge and slowly propagated towards the center (**Figure 4.5b**). Composites with flat interfaces, $E_1/E_2 = 350$ and thinner soft layers displayed this mechanism.
- (iii) Center crack delamination: A circular crack initiated at the center of the pillar and slowly propagated towards the edge until fast detachment started upon reaching a critical loss in contact area. The crack covered more than 40 % of the original contact area (**Figure 4.5c**). Composites with hemispherical interfaces and thinner soft layers displayed this behavior.

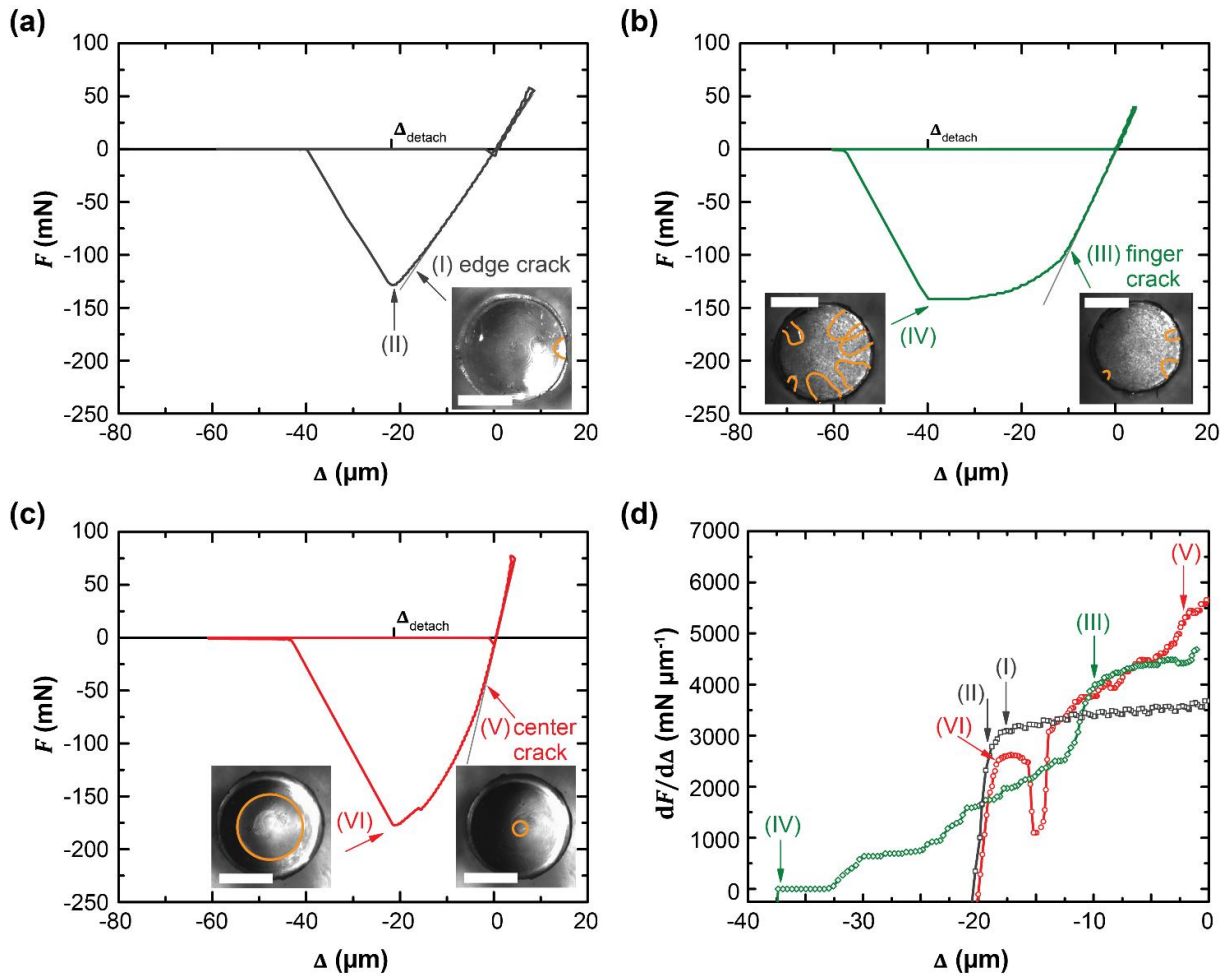


Figure 4.5. Detachment mechanisms of composite pillars. **(a-c)** Force (F)-displacement (Δ) curves of PEGdma/PU composite pillars ($E_1/E_2 = 350$) adhered to the smooth substrate. **(a)** Pillar with hemispherical interface and a 450 μm thick soft tip: crack initiation (I) spontaneously lead to complete detachment (II) via edge crack. **(b)** Pillar with flat interface and a 180 μm thick soft tip: finger cracks (III) appear and grow towards the center (IV) before complete detachment occurs. **(c)** Pillar with hemispherical interface and a 120 μm thick soft tip: a center crack (V) is formed and propagate towards the edge (VI) before complete detachment occurs. **(d)** Derivative of the force-displacement curves in the retracting part of the force-displacement curves. It represents the decrease in stiffness during crack initiation and propagation. Optical micrographs (insets) visualize the cracks upon initiation and propagation (scale bars: 1 mm). The crack fronts were highlighted with orange lines for better visualization.

Interestingly, edge crack detachment was always spontaneous and resulted in detachment directly upon crack initiation within a few seconds. In contrast, finger-like and center cracks propagated more slowly; the time for the complete detachment could be controlled by the pulling velocity of the displacement controlled setup and ranged from about 10 to 15 s (at 2 $\mu\text{m/s}$) to 2 to 3 s (at 10 $\mu\text{m/s}$). The different crack types can be distinguished by inspecting the derivatives of their respective force-displacement curves where crack initiation and propagation corresponds to characteristic drops in stiffness (**Figure 4.5d**). The initial stiffness of the pillars correlates with the soft tip layer thickness and is highest for the thinnest tip. Overall, crack initiation resulted in a significant drop in stiffness (see points I, III, and V in **Figure 4.5d**) and directly to detachment in case of edge cracks (point II). A less pronounced decrease in stiffness upon crack initiation relates to stable crack propagation driven by further withdrawal of the pillar structure. Unlike edge cracks, the center and finger cracks were not immediately unstable. The transition from edge to finger or center crack with decreasing soft tip thickness was similarly observed on the smooth and the rough substrates.

Similar to conventional pillars (**Figure 4.3**), extended hold times yield higher pull-off stress for all composite pillars (**Figure 4.6**). The magnitude and rate of increase of the hold time effect were significantly higher for rough substrates and varied with tip layer thickness, the Young's modulus ratio and the interface curvature. Upon contact to the rough substrate, local stresses at the pillar faces induced by surface asperities decreased with time due to viscoelastic material relaxation. In addition, the contact area most likely increased. Hence, reduced local strains and larger contact areas led to higher pull-off stresses as shown in **Figure 4.6**. The data obtained from the hold time experiments were fitted using an equation that phenomenologically describes viscoelastic material relaxation. Thus, the pull-off stress, σ , as a function of hold time, τ can be expressed as follows:

$$\sigma(\tau) = \sigma_{\infty} - (\sigma_{\infty} - \sigma_0) \cdot \exp\left(-\frac{\tau}{\tau_0}\right) = \sigma_{\infty} - \Delta\sigma \cdot \exp\left(-\frac{\tau}{\tau_0}\right), \quad (4.1)$$

where σ_0 is the initial pull-off stress at $\tau = 0$ s, σ_{∞} is the maximum pull-off stress for infinite hold times, $\Delta\sigma = \sigma_{\infty} - \sigma_0$ and τ_0 is the characteristic relaxation time. The fitting parameters were calculated using a nonlinear regression model in Matlab (MathWorks, Ismaning, Germany) based on the Marquardt-Levenberg algorithm.^{167,168} All fit parameters can be found in the **Supporting Information Table S 4.1** and **Table S 4.2**.

For the smooth substrate, the increase in $\Delta\sigma$ was small (2 to 5 kPa) for all samples, signifying that adhesion did not significantly depend on hold time (**Figure 4.6**). For the rough substrate, in contrast, longer hold times resulted in higher values of $\Delta\sigma$. Composites with thick soft tip layers, irrespective of interface curvature, exhibited a value of $\Delta\sigma \approx 7$ kPa similar to the value found for the PU control. For thinner tip layers, a strong increase in $\Delta\sigma$ was observed, rising up to 24 kPa for PDMS/PU composites (with hemispherical interface and 30 μm thick tip) or 32 kPa for PEGdma/PU composites (hemispherical, 120 μm). **Figure 4.7a** displays that σ_{∞}/σ_0 , i.e. the relative increase in adhesion, was higher for thinner soft layer thickness and higher Young's modulus ratio. For PEGdma/PU composites with hemispherical interface the maximum time-related adhesion ratio was about 6, which is four times higher than for the PU control ($\sigma_{\infty}/\sigma_0 = 1.6 \pm 0.2$) and the PDMS/PU composites with hemispherical interface ($\sigma_{\infty}/\sigma_0 = 1.7 \pm 0.3$). For composites with flat interface, the ratio increased from 2 to 4 with smaller tip thickness, but decreased again after a threshold thickness. To assess how fast viscoelastic relaxation occurred, we compared the gradients of $\sigma(\tau)$, i.e. the first derivative of the

fit equation (Eq. 4.1) at $\tau = 0$ s, which equals $\Delta\sigma/\tau_0$. **Figure 4.7b** shows that the rate is similar or higher, for all composites, when compared to the PU control, suggesting that composite pillars adapt faster to rough substrates. Furthermore, the rate increased with thinner soft tip thickness, but did not vary systematically for the different pillar compositions. The considerable scatter of the values is most likely caused by the strong variation of τ_0 obtained from the fits (see **Supporting Information Table S 4.1** and **Table S 4.2**).

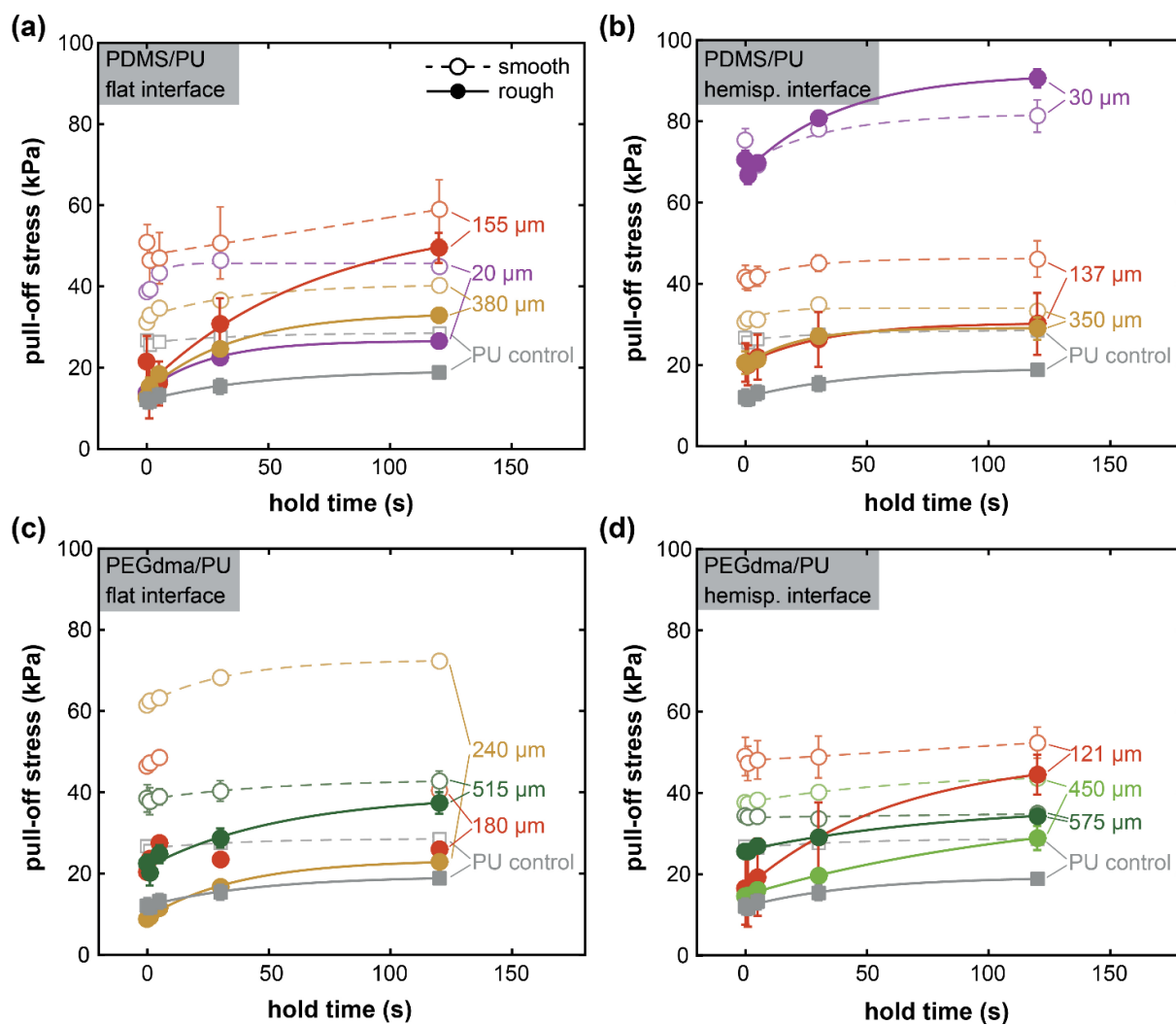


Figure 4.6. Hold time effects on pull-off stress of composite pillars with varying soft layer thickness. **(a)** PDMS/PU pillar with flat interface. **(b)** PDMS/PU pillar with hemispherical interface. **(c)** PEGdma/PU pillar with flat interface. **(d)** PEGdma/PU pillar with hemispherical interface. The data marked PU control (gray squares) correspond to conventional pillars (cf. **Figure 4.3**). The adhesion experiments (preload of 50 mN) were performed against smooth (open circle, dashed lines) and rough (filled circle, solid lines) substrates. The solid and dashed lines were fitted using **Eq. 4.1**.

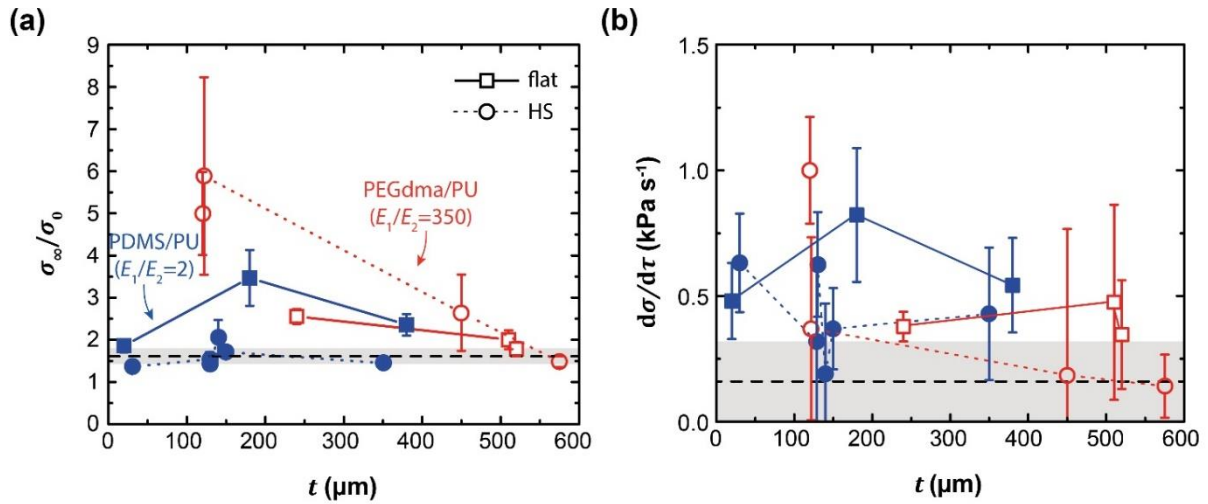


Figure 4.7. Hold time-related relative increase in adhesion σ_{∞}/σ_0 and rate of adhesion enhancement $\Delta\sigma/\tau_0$ of composite pillars adhered to rough substrates. **(a)** The ratio σ_{∞}/σ_0 is displayed as a function of the soft tip thickness, t . The ratio is calculated from the pull-off stress at infinite hold times, σ_{∞} , divided by the initial pull-off stress, σ_0 at zero hold time. **(b)** The rate of adhesion enhancement provides a measure of the time dependent adaptation to the surface topography obtained from the derivative of the fit equation (Eq. 1) at $\tau = 0$ s and is displayed as function of the soft tip thickness, t . All values for PDMS/PU composite pillars are shown as filled blue and, for PEGdma/PU composite pillars, as open red symbols. Flat interfaces are marked with squares and hemispherical interfaces with circles. The values of the PU control are shown as dashed black lines and their error bars are represented by grey areas.

4.5 Discussion

The results presented in this paper showed that pull-off forces of composite pillars can significantly exceed the values of conventional pillar structures. The adhesion was found to be affected by interface geometry, material combinations and variations in preload as well as hold time. A particularly significant result was that composite pillars exhibited similar adhesion values to both smooth and rough substrates, while the adhesion dropped by more than 50% for conventional pillars.

In the pull-off experiments, the adhesion of composites to the smooth substrate was increased by reducing the soft tip thickness (Figure 4.4) in accordance with a similar concept recently presented by Minsky and Turner.⁴⁷ In addition, numerical simulations revealed that the stress distribution along the pillar-substrate interface dramatically varied with the soft layer thickness, Young's modulus ratio and materials interface curvature as shown in Supporting Information Figure S 4.1. Particularly, the stresses at the center of the fibril increased with decreasing soft layer thickness, i.e., increasing confinement. Hence, the propensity for edge crack detachment (as always observed for the PU control) decreased and a transition to other crack forms was observed. The distinct crack types depend on the interface geometry and elastic modulus ratio (Figure 4.5).

For flat interfaces, finger crack detachment with an undulating crack front was initiated close to the perimeter and subsequently propagated towards the center of the contact for high elastic modulus ratio (Figure 4.5b) and edge crack for the lower elastic modulus ratio. Finger cracks were frequently

reported in pull-off tests on confined viscoelastic layers such as pressure sensitive adhesives or other thin soft films.^{94,169} It was also demonstrated that fingering instabilities in thin, soft layers are caused by the viscoelastic properties of the material.^{170–172} Indeed, the shape of the crack front forms such that the compliance of the layer is maximized for the current contact area and displacement.⁶⁸ Theoretical arguments are in agreement with the observed transition from edge to finger cracks for thinner soft layers: Webber *et al.* calculated the energy release rate as a function of the confinement, which is analogous to the ratio of the pillar radius to the tip layer thickness in our study.⁶⁸ Based on their results, one can distinguish between spontaneously propagating edge cracks (energy release rate always higher than the critical energy release rate) and controlled crack propagation of finger cracks (energy release rate always lower than the critical energy release rate). The critical value of the confinement for a rigid punch⁶⁸ is about 0.45 and, thus, much smaller than our values obtained for the transition, which are about 4 and 7 for the PEGdma/PU and PDMS/PU composites, respectively. We assume that the increase in the critical confinement value is due to the reduced Young's modulus of the stalk materials compared to the rigid glass punch used in the work of Webber *et al.*

For hemispherical interfaces (and thin soft layers), detachment occurred at the center of the contact under the high stress concentrations there (**Supporting Information Figure S 4.1**), leading to a circular crack front propagating towards the edge (**Figure 4.5c**). Similar detachment mechanisms have been reported for mushroom structures by Micciché *et al.*¹⁰⁷ and Heepe *et al.*⁶². Also in these studies, the tip geometry modification reduced the propensity for edge cracks induced by corner stress singularities, while a transition to center cracks was induced.^{41,59,104} A more detailed numerical study on the interfacial stress distribution and, in particular, on the intensity of the corner stress singularities as a function of the composite design parameters is currently underway.¹⁷³ In addition to the variation of the interfacial stress distribution, reduced pressure inside the cavities upon center crack formation might contribute to the adhesion. However, a pressure difference would require perfect sealing at the contact area to avoid gas flow. On the rough substrate, such a sealing would be difficult to obtain. It is, therefore, very interesting that the adhesion of composite pillars with hemispherical interface and particularly thin tips exceeded the adhesion of composites with flat interfaces and conventional pillars. The higher adhesion probably results from larger contact areas that were most likely induced by the high center stresses under compressive preloads, which translate into high center stresses in tension during detachment. Such stresses are more beneficial than high stresses at the perimeter in case of conventional pillars (or thick tips) due to edge stress intensities.

In addition to interface geometry, the preload and hold time had a significant impact on the adhesion to rough surfaces, which is in accordance with previous reports.^{116,113} Higher preloads enforce the conformation of the pillar faces to the asperities of the substrate topography. Longer hold times most likely reduce local stress concentrations at the pillar faces based on material relaxation. The different material combinations revealed that composite pillars with high Young's modulus ratio and thin tips adapted more quickly to rough substrates as expressed by the highest pull-off stress ratio σ_{∞}/σ_0 . Again, the stress concentration at the center of the contact area most likely enforces the best adaption to the rough substrate in short hold times. These findings have implications for many areas where dry adhesives can be applied, particularly when objects exhibit microscale roughness in conjunction with short cycle times, as is the case e.g. in pick-and-place technologies.

4.6 Conclusion

We presented a detailed study on composite pillars that overcome previous limitations in adhesion to rough glass substrates. For the first time, a systematic variation of structure parameters such as soft tip layer thickness, Young's modulus ratio and interface geometry was experimentally performed and analyzed in relation to parameters such as surface roughness, preload and hold time. The following conclusions can be drawn:

- Composite pillars improved adhesion to the smooth and rough substrates by a factor of three and five compared to conventional pillar structures made from a single material.
- To take advantage of this effect, composite structures should exhibit thin soft tips atop a stiffer stalk. Curved material interfaces were found to be beneficial compared to flat interfaces as high center stresses enforce the adaption to surface asperities and, therefore, result in higher adhesion.
- The edge crack detachment due to sharp corners of the pillars undergoes a transition to center crack (hemispherical interface) or finger crack (flat interface) below a critical tip layer thickness that depends on the Young's modulus ratio.
- Preload and hold time have a strong impact on adhesion of the composite pillars to the rough substrate, but affect only slightly the adhesion to the smooth substrate. For the rough substrate, the pull-off stress ratio between infinite and zero seconds hold times as well as the rate to adapt to the surface topography are highest for the composite pillar with hemispherical interface and Young's modulus ratio of 350.

We believe that these results are particularly relevant for the design of fibrillar adhesives suitable for applications in the presence of surface roughness.

4.7 Supporting information

List of parameters obtained from fit equation (Eq. 4.1). FE analyses on interfacial stress distributions for different composite pillars.

4.7.1 Parameters obtained from fit equation

Supplemental Table S 4.1. Complete overview of fit parameters from Eq. 4.1 (see main manuscript) for the hold time dependent pull-off stress of composite pillars on the smooth substrate.

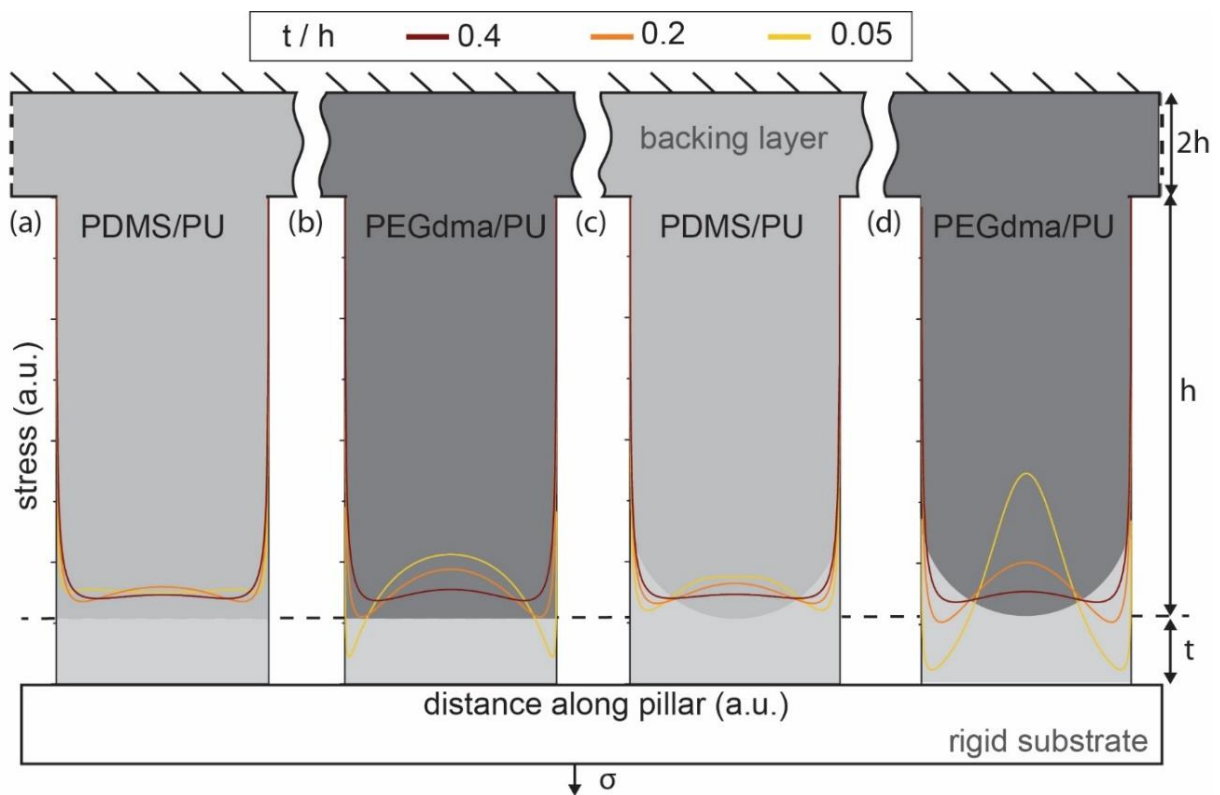
pillar material	interface geometry	thickness (μm)	SMOOTH		
			σ_{∞} (kPa)	σ_0 (kPa)	τ_0 (s)
PU	control	-	28.59 \pm 0.62	26.14 \pm 0.29	37.99 \pm 28.94
PDMS with PU	HS	30	81.79 \pm 2.90	69.29 \pm 1.60	32.48 \pm 26.77
PDMS with PU	HS	129	50.38 \pm 3.12	43.85 \pm 0.43	75.96 \pm 81.55
PDMS with PU	HS	130	41.23 \pm 0.62	37.91 \pm 0.47	9.90 \pm 8.35
PDMS with PU	HS	140	51.81 \pm 0.87	43.38 \pm 0.27	47.25 \pm 11.30
PDMS with PU	HS	150	47.72 \pm 0.82	41.97 \pm 0.19	54.82 \pm 18.62
PDMS with PU	HS	350	34.00 \pm 0.38	30.62 \pm 0.33	9.91 \pm 5.49
PDMS with PU	flat	20	45.70 \pm 0.46	38.38 \pm 0.46	4.83 \pm 1.28
PDMS with PU	flat	130	41.73 \pm 2.45	53.82 \pm 3.33	1.05 \pm 0.84
PDMS with PU	flat	180	62.31 \pm 0.71	46.97 \pm 0.53	29.01 \pm 4.46
PDMS with PU	flat	380	40.51 \pm 0.81	32.48 \pm 0.39	37.86 \pm 11.46
PEGdma with PU	HS	120	54.45 \pm 0.50	52.84 \pm 0.37	16.66 \pm 19.14
PEGdma with PU	HS	121	- \pm -	- \pm -	- \pm -
PEGdma with PU	HS	122	64.12 \pm 233.1	44.42 \pm 0.62	577.95 \pm 7625.60
PEGdma with PU	HS	450	44.74 \pm 1.76	37.47 \pm 0.32	66.35 \pm 36.80
PEGdma with PU	HS	575	- \pm -	33.86 \pm 0.36	- \pm -
PEGdma with PU	flat	180	- \pm -	47.47 \pm 0.41	- \pm -
PEGdma with PU	flat	240	72.61 \pm 0.58	61.80 \pm 0.33	32.64 \pm 5.51
PEGdma with PU	flat	510	45.26 \pm 2.29	40.38 \pm 0.38	76.03 \pm 75.84
PEGdma with PU	flat	520	38.96 \pm 0.78	34.61 \pm 0.87	7.13 \pm 5.95

Supplemental Table S 4.2. Complete overview of fit parameters from Eq. 4.1 (see main manuscript) for the hold time dependent pull-off stress of composite pillars on the rough substrate.

pillar material	interface geometry	thickness (μm)	ROUGH		
			σ_{∞} (kPa)	σ_0 (kPa)	τ_0 (s)
PU	control	-	19.36 \pm 1.48	12.01 \pm 0.44	45.85 \pm 23.01
PDMS with PU	HS	30	91.73 \pm 2.02	67.49 \pm 0.95	38.96 \pm 9.69
PDMS with PU	HS	129	20.58 \pm 1.06	13.78 \pm 0.65	22.68 \pm 11.26
PDMS with PU	HS	130	33.81 \pm 0.70	23.37 \pm 0.42	16.81 \pm 4.26
PDMS with PU	HS	140	31.22 \pm 4.85	15.78 \pm 0.49	84.73 \pm 50.30
PDMS with PU	HS	150	41.20 \pm 2.23	24.47 \pm 0.56	46.39 \pm 14.13
PDMS with PU	HS	350	29.11 \pm 0.98	20.11 \pm 0.65	21.60 \pm 8.21
PDMS with PU	flat	20	26.61 \pm 1.00	14.28 \pm 0.57	25.94 \pm 6.86
PDMS with PU	flat	130	- \pm -	- \pm -	- \pm -
PDMS with PU	flat	180	52.13 \pm 3.34	14.95 \pm 1.60	45.37 \pm 11.85
PDMS with PU	flat	380	33.51 \pm 1.58	14.33 \pm 0.77	35.96 \pm 8.98
PEGdma with PU	HS	120	50.58 \pm 2.54	10.69 \pm 1.22	40.85 \pm 7.73
PEGdma with PU	HS	121	45.91 \pm 3.32	29.32 \pm 0.85	56.09 \pm 24.93
PEGdma with PU	HS	122	53.52 \pm 13.67	9.14 \pm 0.90	119.42 \pm 58.93
PEGdma with PU	HS	450	37.56 \pm 10.54	14.83 \pm 0.61	124.77 \pm 94.19
PEGdma with PU	HS	575	37.11 \pm 2.75	25.84 \pm 0.34	85.70 \pm 40.02
PEGdma with PU	flat	180	25.64 \pm 0.62	20.39 \pm 1.15	0.95 \pm 0.64
PEGdma with PU	flat	240	23.33 \pm 0.69	9.14 \pm 0.33	37.30 \pm 5.44
PEGdma with PU	flat	510	38.28 \pm 2.38	19.68 \pm 0.84	50.75 \pm 18.36
PEGdma with PU	flat	520	41.19 \pm 2.66	23.41 \pm 0.62	51.95 \pm 20.08

4.7.2 Numerical simulations.

Finite element simulations (plain strain) were performed using Comsol (Version 5.1, COMSOL Inc., Burlington, MA, USA) and Matlab (MathWorks, Ismaning, Germany) for post-processing. A single composite fibril with flat or curved interface atop a backing layer (with fully constrained backside) was adhered to a stiff substrate assuming perfect contact and sticking friction, which totally suppressed sliding of the fibril against the rigid substrate. The stiff stalk had a height, h , of 40 μm and an aspect ratio of two while the soft tip layer was varied in height. Both regions were assigned linear elastic material properties with a Poisson's ratio of 0.49 and a density of 980 kg/m^3 . The soft tip was given an elastic modulus of 1 MPa and the stiff stalk an elastic modulus of 2 MPa or 350 MPa. A remote tensile stress was applied on the substrate, resulting in a stress distribution with stress singularities at the edge of the contact of fibril to substrate.



Supplemental Figure S 4.1. Stress distributions along the substrate-pillar interface obtained from FEM simulations (plain strain). FEM simulations were performed for different material combinations and interface geometries: (a) PDMS/PU with flat interface, (b) PEGdma/PU with flat interface, (c) PDMS/PU with curved interface, (d) PEGdma/PU with curved interface. The ratio of the soft layer thickness, t , to the height of the stiff stalk, h , was 0.4, 0.2 and 0.05 to demonstrate the influence of the tip thickness on the stress distribution.

PART II:

Smooth adhesive structures

5 Adhesion and Cellular Compatibility of Silicone-Based Skin Adhesives *

5.1 Abstract

Pressure-sensitive adhesives (PSAs) based on silicone materials have emerging potential as adhesives in healthcare products, in particular for gentle skin adhesives. To this end, adhesion to rough skin and biocompatibility are crucial factors for a successful implementation. In this study, the mechanical, adhesive and biological properties of the two-component poly(dimethylsiloxane) Soft Skin Adhesive MG 7-9800 (SSA, Dow Corning) have been investigated and compared to Sylgard 184. Different mixing ratios of SSA's components allowed for tuning of the shear modulus, thereby modifying the adhesive properties of the polymer. To give a comprehensive insight, we have analysed the interplay between pull-off stress, adhesion energy and stretch of the adhesive films on smooth and rough surfaces. The focus was placed on the effects of substrate roughness and on low pressure oxygen plasma treatment of the adhesive films. SSA showed superior biocompatibility in *in vitro* cell culture experiments. High pull-off stresses in the range of 3 N/cm² on a rough surface were achieved, promising broad application spectra for SSA based healthcare products.

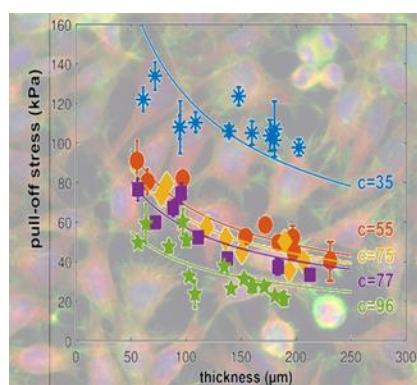


Figure 5.0. Graphical summary of chapter 5. Both mechanical and biological experiments were performed to assess the properties of the silicone elastomers in a biomedical context. Normal tack measurements were performed to quantify the pull-off stress as a function of material and film thickness (foreground). Cells were seeded on the materials to characterize biocompatibility and cell spreading analyzed (background).

* This chapter was published in *Macromolecular Materials and Engineering*:

Fischer, S. C., Kruttwig, K., Bandmann, V., Hensel, R., & Arzt, E. (2017). Adhesion and Cellular Compatibility of Silicone-Based Skin Adhesives. *Macromolecular Materials and Engineering*, 302(5).

The article is available under: <http://onlinelibrary.wiley.com/doi/10.1002/mame.201600526/full> .

5.2 Introduction

Skin adhesives are essential in medical therapies and diagnostics as they provide secure placement of wound dressing, catheters, extensions or electrodes.^{156,174} Pressure-sensitive adhesives (PSAs) are widely used due to their ability to adhere to skin with small applied pressure and a short contact time.^{116,175} Several studies focused on the investigation of mechanical and adhesive behaviour of PSAs from natural or synthetic origin, including research on delamination phenomena.^{96,169,176–179} The adhesive properties of PSAs can be varied by e.g. the incorporation of different monomers during the polymerization process.¹⁸⁰ The modification of the viscoelastic properties of different materials directly influences their pull-off (tack) and peel strength to yield optimum properties for a wide field of applications including surface protection or medicine.^{181–184} The three major classes of PSAs are acrylics, polyisobutylenes and silicones.¹⁸⁵

Acrylate-based PSA polymer systems dominate the market for medical adhesives due to their typical high adhesion strength.¹⁸⁶ However, the strong adhesion induced by acrylate formulations may induce irritations or even damage to the outermost skin layers during removal of the adhesive.^{122,134,187} Thus, alternatives for gentle skin attachment are needed, particularly for sensitive skin of neonates or hardly regenerating skin of elderly people.^{134,188,189} Another class of PSAs are silicones, exhibiting unique adhesion characteristics to surfaces of both high and low surface energy and showing low initial tack and adhesion. Silicones are a versatile class of polymeric material, showing a low surface energy of 20 mJ/m^2 and a high flexibility of the silicone network.¹⁹⁰ One of the most used silicone elastomers is poly(dimethyl siloxane) (PDMS), which exhibits a broad application spectrum in adhesive and biomedical technology. It has been widely used for medical devices, contact lenses manufacture and cell culture purposes including lab-on-a-chip applications.¹⁹¹ Its low surface reactivity, surface free energy and the relatively high amount of low-molecular weight components causes PDMS to generate poor adhesion joints leading to the risk of adhesion failure.¹⁹² One possible modification to increase the free surface energy of PDMS and hence its pull-off strength on smooth substrates¹⁹² is the treatment with low-pressure plasma. This versatile technique, which is also one of the most frequently applied¹⁹³ techniques to increase the hydrophilic properties, results in a decreased adsorption of molecules to the surface, while promoting cellular attachment and cellular spreading behaviour.¹⁹² The Young's modulus of PDMS can be varied to below 1 MPa as it is a function of the cross linker concentration and/or the curing time.^{194,195} For Sylgard 184 the manufacturer's recommendation is a ratio of 10:1 for the elastomer base to crosslinker ratio. The crosslinker concentration has been subsequently decreased to 50:1 in order to produce softer gels with Young's moduli around 50 kPa.^{194,196} Because of these physiologically relevant Young's modulus values, such elastomers have great potential in cell culture research application.¹⁹⁶ Both parameters may influence the interaction between cells and polymer. Little research has been conducted so far with a view to a comprehensive and systematic investigation and optimization of the adhesive properties of silicone elastomers in response to surface roughness parameters.⁸⁹ Additionally, a direct comparison of different polymers with respect to their biocompatibility, adhesive properties and physiologically relevant Young's modulus has scarcely been reported in literature.¹⁹⁷

Here, we focused on the characterization of the adhesive behaviour of Sylgard 184 and SSA MG 7-9800 depending on the roughness of the substrate and as a function of low pressure oxygen plasma

treatment. Additionally, *in vitro* adhesion and cytotoxicity effects of L929 murine fibroblasts on the two PSAs were analysed in detail.

5.3 Materials and Methods

5.3.1 Preparation of polymer samples

Thin polymer films of two different PDMS formulations were manufactured: Soft Skin Adhesive SSA MG 7-9800 (Dow Corning, Midland, MI, USA) and Sylgard 184 (Dow Corning, Midland, MI, USA). Different mixing ratios of the two components of SSA 9800 were produced to yield polymers with different mechanical properties. The SSA prepolymer (50:50 / 47:53 / 45:55 / 40:60 weight parts of component A: component B) as well as the Sylgard 184 prepolymer (10 weight parts of the basement to 1 weight part of the curing agent) were degassed under vacuum for 3 min at 2000 rpm in a SpeedMixer (DAC600.2 VAC-P, Hauschild Engineering, Hamm, Germany). The prepolymer mixtures were placed onto a glass slide (Marienfeld, Lauda-Königshofen, Germany) that was previously activated with oxygen plasma for 2 min at 60 % power (PICO plasma system, Diener electronic, Ebhausen, Germany). Films with various thicknesses ranging from 50 to 230 μm were prepared by the doctor blade technique using a film applicator (Erichsen, Hemer, Germany). All polymer films were cured at 95 °C for 60 min. The thickness of the polymer films was measured using an optical microscope (VHX-2000, Keyence, Osaka, Japan) with an accuracy of $\pm 20 \mu\text{m}$. In selected experiments, cured polymer films were post-treated by plasma activation in an argon/ -oxygen atmosphere for 2 min (Parameters: Forward RF target 50W; forward RF range 5W; maximum reflected RF 5W; O₂ gas flow 11.5 sccm; Ar gas flow 35.0 sccm; Solanus model 950, Gatan, Munich, Germany).

5.3.2 Adhesion measurements.

In adhesion experiments, normal forces were recorded with a load cell (3 N, TedeA-Huntleigh 1004, Vishay Precision Group, Basingstoke, UK) mounted on a custom-built setup (**Figure 5.1A**). As nominally flat probes, two different glass substrates were used (**Figure 5.1B**). Substrate #1 (designated as “smooth”) exhibited a mean absolute roughness $R_a = 0.006 \mu\text{m}$, and a mean peak-to-valley profile roughness $R_z = 0.041 \mu\text{m}$, while for substrate #2 (designated as “rough”), $R_a = 0.271 \mu\text{m}$ and $R_z = 2.174 \mu\text{m}$. The substrates exhibited a circular contact area of 3.2 mm² for the smooth and 6.7 mm² for the rough substrate. The roughness values of the substrates were measured using a stylus profilometer (Surfcom 1500SD3, Carl Zeiss, Ostfildern, Germany) and an atomic force microscope (JPK instruments AG, Berlin, Germany). Before measurement, the substrate was cleaned with ethanol or isopropanol. A camera and prism, mounted below the sample, were used to optically align the specimen and the substrate while observing initial contact. To maximize contact between both surfaces the setup was mounted on a pivotable table allowing misalignment angle adjustment.

For adhesion experiments, specimen and substrate were converged at a velocity of 30 $\mu\text{m/s}$ until a maximum force was reached, corresponding to a compressive preload of $10 \pm 2 \text{ kPa}$. After a hold time of 1 s, the specimen was withdrawn at a velocity of 10 $\mu\text{m/s}$ until detachment. The measurements were repeated with different parameters at one position and three different positions on each

individual specimen were tested. In selected measurements, the withdrawal velocity was changed from 2 to 50 $\mu\text{m/s}$ or the hold time from 0 to 300 s.

Force, F , and displacement, s , were recorded. The displacement was corrected using the machine compliance ($C = 0.12 \mu\text{m/mN}$) to account for deformation of the setup. Values were then transformed into stress, $\sigma = F/A$, with the contact area, A , and relative displacement, $\varepsilon = (s - s_0)/h_{\text{film}}$, where h_{film} is the initial film thickness and s_0 is the displacement at which the force became zero and tensile deformation started. The maximum stress was defined as the pull-off stress, σ_{max} . The maximum relative displacement of the adhesive film, ε_{max} , was defined as the displacement at which detachment occurred.

The work of separation, W_{sep} , was calculated as follows:

$$W_{\text{sep}} = \int_{s_0}^{s_{\text{end}}} \sigma ds, \quad (5.1)$$

where s_{end} is the displacement at which the tensile stress returned to zero.

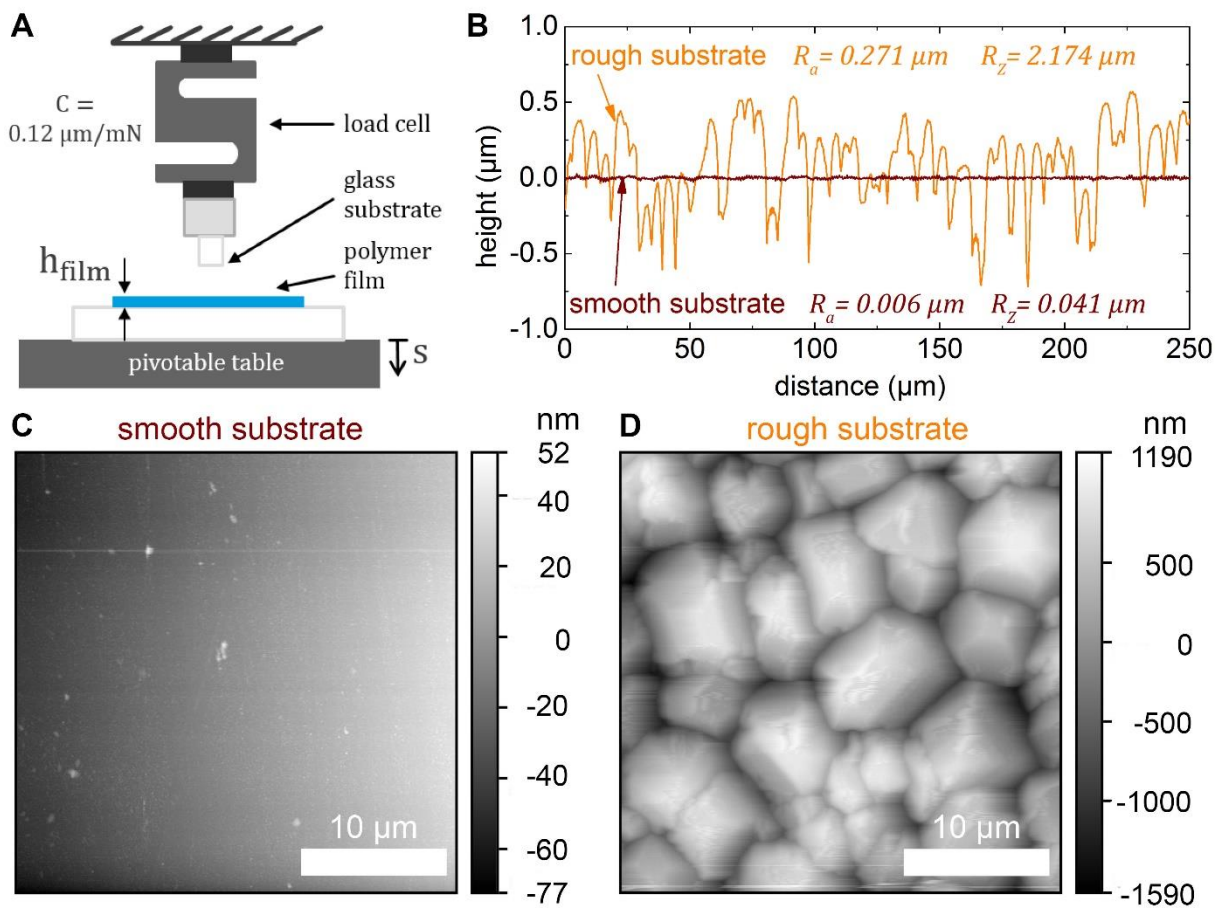


Figure 5.1. Experimental setup for adhesion testing. **(A)** Schematic illustration of the adhesion measuring setup; h_{film} is the thickness of the silicone film and C the machine compliance. **(B)** Surface profiles of the smooth and rough substrate used as probes for the normal (tack) adhesion tests; R_a is the mean absolute roughness and R_z the mean peak-to-valley roughness. In addition, AFM scans of the surface topography ($30 \mu\text{m} \times 30 \mu\text{m}$) are shown for **(C)** the smooth and **(D)** the rough substrate.

5.3.3 Materials characterization.

Frequency dependent storage, loss and complex shear moduli (G' , G'' , G^*) as well as the damping factor ($\tan \delta$) were determined using a rheometer Physica MCR-300 (Anton Paar, Graz, Austria) equipped with a cone/plate setup (diameter 25 mm, gap height 0.054 mm). The prepolymer mixtures were placed on the device, the plates approached and the polymer was cured at 90 °C for 30 min. Upon cooling to 25 °C, a frequency sweep from 0.01 to 100 Hz at constant amplitude of 0.1 % was carried out.

5.3.4 Contact angle goniometry.

The static water contact angle θ was measured using a goniometer (dataphysics, Filderstadt, Germany) by depositing a drop of 3 μ l or 5 μ l water with the needle inside the drop onto the surfaces, recording a side-view and subsequent image analysis.

5.3.5 Cell culture experiments.

Murine mouse fibroblasts L929 were obtained from the American Type Culture Collection (ATCC, Rockville, MS, USA) and cultured in RPMI 1640 (Thermo Fisher Scientific, Dreieich, Germany) supplemented with 10 % fetal bovine serum and 1000 U/ml Penicillin and Streptomycin at 37 °C, 5 % CO₂. Cells were routinely passaged with Accutase (Capricorn Scientific, Ebsdorfergrund, Germany) and cultured in sterilized tissue culture polystyrene flasks. For cell adhesion experiments, cells were seeded on glass slides coated with Sylgard 184 and SSA 50:50 on a mean surface area of 4.68 cm². Thickness of the polymer films was approx. 150 μ m. Polymer coated slides were placed for 24 h in phosphate buffered saline (PBS) before cell culture experiments. After 24 h culture period single cells were obtained by treatment with 0.25 % trypsin-EDTA solution. The cell number was determined using an automatic cell counter (CASY, OLS OMNI Life Science, Bremen, Germany) or a Neubauer chamber.

In order to characterize the cell cytotoxicity, release of lactate dehydrogenase (LDH) was measured with the CytoTox-ONE™ homogeneous membrane integrity assay (Promega, Madison, WI, USA). Supernatant was removed from cells cultured for 24 h on polymeric materials and analyzed with a Tecan plate reader (Tecan, Crailsheim) according to manufacturer instructions. Cells were removed from the polymeric surface by brief incubation with trypsin. Fluorescence intensity was recorded at an excitation wavelength of 560 nm and an emission wavelength of 590 nm. As LDH positive control 9 % TritonX-100 solution was added to cells cultured for 24 h on cell culture treated polystyrene. The initially seeded cell amount was 3 x10⁵ cells per well. Six independently performed experiments were used for statistical analysis. Additionally, trypan blue exclusion test was performed on n=3 independently performed experiments. Two tailed students t-test was performed at a significance level of $\alpha=0.05$, where indicated.

5.3.6 Immunofluorescence analysis.

Cells were fixated for 25 min with 4 % paraformaldehyde and permeabilized with 0.25 % TritonX-100 for 10 min. Blocking of unspecific antibody binding was reduced with a 60 min treatment of 5 % bovine serum albumin (BSA) in PBS. Incubation with a 1:80 dilution of Phalloidin conjugated Alexa488 (Thermo Fisher Scientific) in PBS was performed over night at 4 °C. After an additional blocking step with 5 % BSA cells were incubated with anti- α -tubulin (1:500, Sigma Aldrich) for 2 h at room temperature. As a secondary antibody, Alexa 546 (1:1000, Invitrogen) was used. For nuclear staining, cells were

incubated with Hoechst Dye 33342 (1 $\mu\text{g}/\text{ml}$, Sigma) for 10 min and embedded with Aquamount (Polyscience, Eppelheim) in CELLVIEW™ cell culture dishes (Greiner bio-one). Microscopic analysis was performed with an inverted microscope (Leica, Wetzlar, Germany). Image brightness and contrast was adjusted with Leica LAS AF Lite software and ImageJ. Phase contrast images were acquired with a Zeiss inverted microscope.

5.3.7 Protein adsorption test.

Sylgard 184, SSA 40:60 and SSA 50:50 exhibiting a thickness of 150 μm and mounted on glass slide were incubated with a solution of 1 mg/ml FITC conjugated albumin (A9771, Sigma) for 3 h at 37 °C, 5 % CO_2 . After the incubation period, samples were subsequently washed with PBS and transferred to a new plate to minimize the influence of unspecific binding of albumin to the polystyrene surface during incubation. Fluorescence intensity was recorded with a Tecan plate reader. To correlate fluorescence intensity units to adsorbed protein amount, dilution series were performed and included in every measurement. The surface area of the samples was photographically documented, analysed using ImageJ and included in the calculation. Values are presented as microgram protein adsorbed to 1 cm^2 area.

5.4 Results and Discussion

5.4.1 Mechanical and adhesion properties

The dynamic-mechanical properties of Sylgard 184 and SSA 9800 in different mixing ratios, obtained from rheometer measurements, are shown in **Figure 5.2**. As a general observation for all materials, the storage (G'), loss (G''), complex (G^*) shear moduli as well as the damping factor ($\tan \delta$) increased with increasing frequency, hence, they became stiffer and more viscoelastic. The viscoelastic properties of SSA could be tuned by varying the mixing ratio from 50:50 to 40:60, which led to higher values of G' , G'' and G^* and a lower damping factor. For example, G^* increased from 20 to 120 kPa (for 20 Hz) while $\tan \delta$ decreased from 0.75 to 0.2 when the mixing ratio was changed from 50:50 to 40:60. These results indicate that the cross-linking density of the polymer network increases and the mobility of polymer chains simultaneously decrease by changing the mixing ratio. Sylgard 184 exhibited a complex shear modulus of about 500 kPa (for 20 Hz), i.e. more than one order of magnitude higher than SSA 50:50. Furthermore, Sylgard 184 showed the lowest damping factor of only 0.1 at 20 Hz. Thus, Sylgard 184 is a rather elastic material at low frequencies, which is in line with literature.¹⁹⁸ The softest material analysed in the current investigation, SSA 50:50, exhibits a much more pronounced viscoelastic characteristic that is reflected by a steep increase of the damping factor from 0.2 to 0.8 for a frequency sweep from 0.01 to 20 Hz.

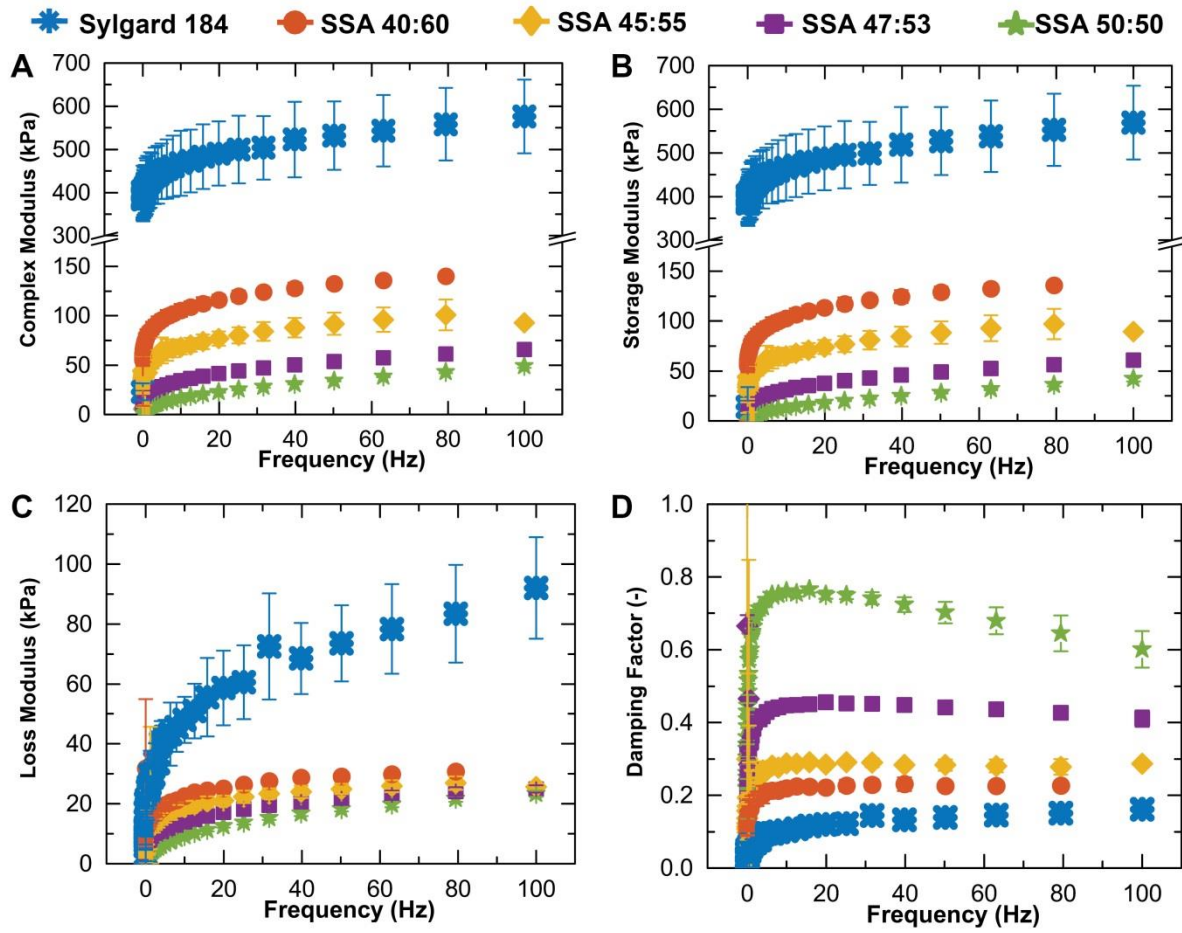


Figure 5.2. Determined material properties of the polymer materials from rheometer measurements. (A) Complex, (B) storage and (C) loss shear moduli as well as (D) damping factor as a function of frequency. SSA 50:50 (stars, green), SSA 47:53 (squares, purple), SSA 45:55 (diamonds, yellow), SSA 40:60 (red, circles) and Sylgard 184 (asterisk, blue).

The adhesive characteristics of polymer films, with uniform thicknesses ranging from 50 to 230 μm , of SSA 9800 in different mixing ratios and Sylgard 184 to the smooth substrate are displayed in **Figure 5.3**. The following trends can be observed:

- Film thickness effect: For all materials, the pull-off stress increased with decreasing film thickness, t (**Figure 5.3A**). Particularly for the different SSAs, we obtained a twofold increase of the pull-off stress for 50 μm thin films compared to the 230 μm thick films. This increase most likely corresponds to the scaling between interfacial and volume effects as in Chung and Chaudhry.⁹⁵ The authors propose that for very thin films, the pull-off stress is proportional to the function $\sigma_{max} = c \cdot \sqrt{E/t}$, where E is the Young's modulus; this is in good agreement with our data as shown by the fitting curves (**Figure 5.3A**). Based on the Young's modulus at 10 Hz, i.e. three times the shear modulus from rheometer measurements assuming a Poisson's ratio of $\nu = 0.5$, the coefficients c were evaluated and are displayed in **Figure 5.3A**.
- Modulus effect: A higher shear modulus resulted in higher pull-off stresses. For example, the pull-off stress σ increased from 55 kPa (SSA 50:50) to 90 kPa (SSA 40:60) and 120 kPa (Sylgard 184) for a constant film thickness of about 50 μm . The increase of the pull-off stress,

σ_c , with increasing shear modulus is in accordance to Kendall's and Gent's models, according to which σ_c scales with \sqrt{E} .^{199,200}

- Work of separation: The work of separation that similarly increased with thinner films as shown in **Figure 5.3B**. The highest values of about 3500 mJ/m², obtained for Sylgard 184, were twice as high as for the SSA mixtures 40:60, 45:55 and 47:53; the latter exhibit very similar values of up to 1750 mJ/m² for 50 μ m thick films. Only for the mixing ratio 50:50, were values of up to 2500 mJ/m² obtained, most probably due to the high maximum relative displacement (**Figure 5.3C**).
- Maximum relative displacement: In contrast to all other materials, SSA 50:50 remained in contact with the smooth substrate up to 50 % relative displacement for thicker films (200 μ m) and 200 % maximum relative displacement for thin films (50 μ m). For SSA 47:53 and SSA 45:55, a transition from almost zero to about 30 % maximum relative displacement was observed for films with a thickness of 120 μ m and 200 μ m, respectively. Thus, the transition is shifted towards higher film thickness with increasing shear modulus. For SSA 40:60 and Sylgard 184, the maximum relative displacement was almost zero for all films. Detachment mechanism: The maximum relative displacement appears to be connected with the detachment mechanisms observed. Instead of detaching abruptly from the edge, SSA 50:50 shows a rather ductile detachment. Cavitation and finger cracks are initiated throughout the contact area and the material deforms over a large displacement range, forming long threads between substrate and indenter.^{201,202} This effect is, however, less pronounced, as the film thickness or elastic modulus increases.^{68,203}

The adhesion measurements presented above were all carried out at a constant pull-off velocity of 10 μ m/s. Additional measurements with different velocities ranging from 2 to 50 μ m/s were performed for thicker film with $170 \pm 35 \mu$ m (**Figure 5.3D**). Higher velocities resulted in higher pull-off stresses for all materials. For SSA 50:50, the pull-off stress increased by almost 100 % from 20 to 40 kPa; the relative increase was less prominent as the storage shear modulus increased and the damping factor decreased, i.e. for SSA 40:60 and Sylgard 184. These results reflect the various viscoelastic properties of the materials as obtained from the rheometer measurements (**Figure 5.2**). SSA 50:50 exhibits the highest damping factor and therefore the highest sensitivity to the testing velocity. In contrast, Sylgard 184 has the lowest damping factor, but the pull-off strength still varied with velocity in accordance with a previous report.¹⁹⁸

In summary, the mechanical properties of SSA could be tuned by varying the mixing ratio from 50:50 to 40:60, which strongly affected the adhesive properties. Sylgard 184, SSA 40:60 and SSA 50:50 showed a clearly distinguishable behaviour in the adhesion experiments on the smooth substrate. Therefore, we restricted the further investigations to these three materials.

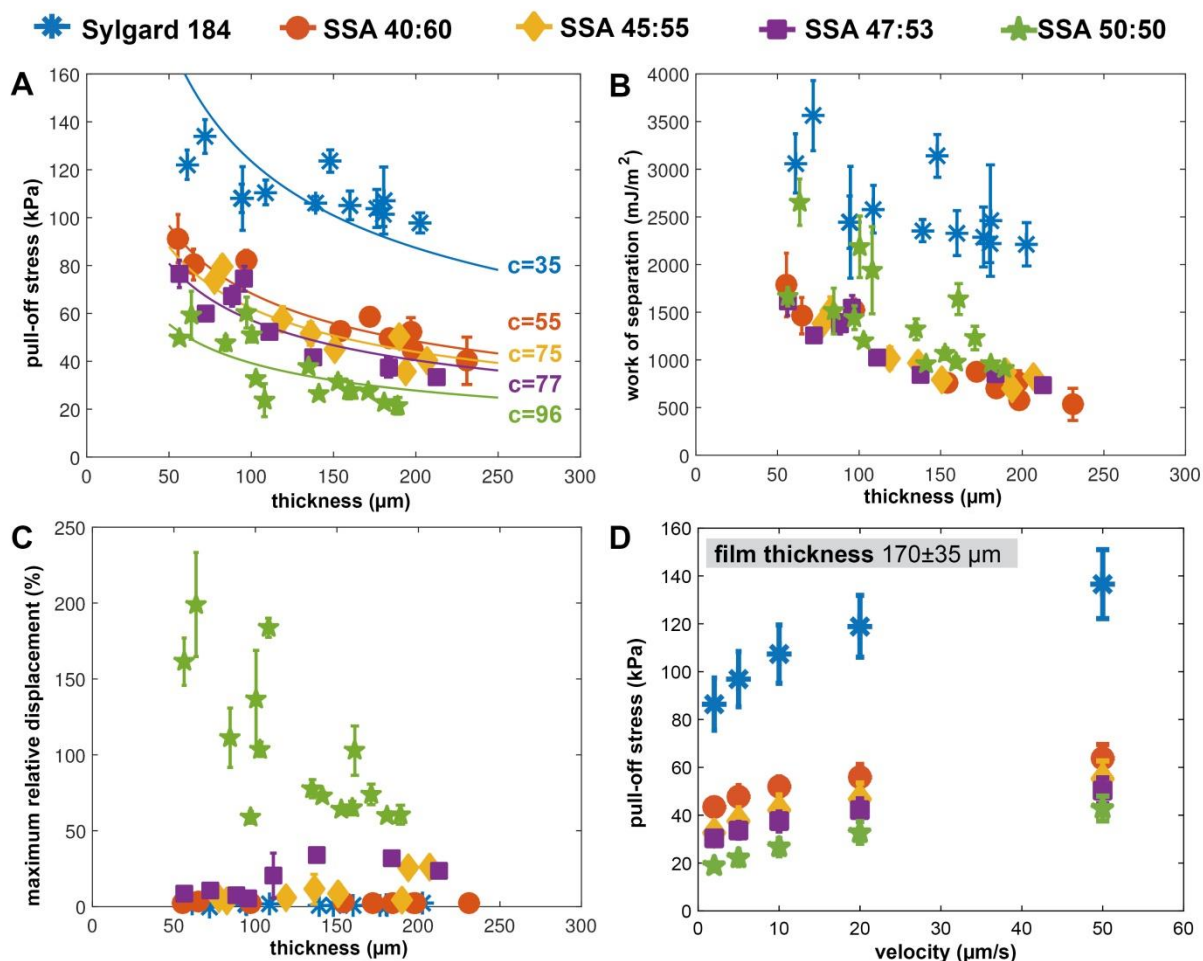


Figure 5.3. Adhesion measurements on the smooth substrate as a function of film thickness and pull-off velocity. **(A)** Pull-off stress, **(B)** adhesion energy and **(C)** maximum relative displacement as function of the film thickness of SSA 50:50 (stars, green), SSA 47:53 (squares, purple), SSA 45:55 (diamonds, yellow), SSA 40:60 (red, circles) and Sylgard 184 (asterisk, blue). The solid curves in **(A)** indicate the fit function $\sigma_{max} = c \cdot \sqrt{E} \cdot t^{-1}$ where c is the fit coefficient (see main text). The pull-off velocity for these measurements was 10 μm/s. **(D)** Pull-off stress as a function of pull-off velocity for polymer films with a thickness in the range 170 ± 35 μm.

5.4.2 Biological properties

Next, we present experiments relevant for the biological characterization of the materials. To enhance biocompatibility of the hydrophobic polymers two principle methods, protein adsorbance and oxygen plasma treatment were explored. Sylgard 184, SSA 40:60 and SSA 50:50 were incubated with FITC-conjugated albumin to visualize protein adsorption. No statistical significant difference in the adsorption of FITC conjugated BSA could be discriminated between the tested polymeric materials (**Supplemental Figure S 5.1**). We detected $2.46 \pm 0.37 \mu\text{g} \cdot \text{cm}^2$ on Sylgard 184, $2.28 \pm 0.32 \mu\text{g} \cdot \text{cm}^2$ on SSA 50:50 and $2.39 \pm 0.33 \mu\text{g} \cdot \text{cm}^2$ on SSA 40:60 polymeric surfaces. The amount of protein coverage of surfaces depends amongst others, on the bulk protein concentration to which the polymers have been exposed.²⁰⁴ Protein surface densities ranging from $0.2 \mu\text{g} \cdot \text{cm}^2$ to $5 \mu\text{g} \cdot \text{cm}^2$ have been reported.^{204–207} The values we observed in the adsorption assay (**Supplemental Figure S 5.1**)

are comparable to previously reported data. The static water contact angles, tested before and after oxygen plasma treatment, for Sylgard 184 are shown in **Table 5.1**. They reveal the significant increase in surface energy after plasma treatment, in line with published results.¹⁹³ The initial static water contact angle of SSA 40:60 of 116° is comparable to the value obtained for Sylgard 184. Shifting the SSA ratio to 50:50 resulted in a significantly higher contact angle of 136°. This phenomenon has been reported for soft materials because of an elastic deformation due to capillary forces.²⁰⁸

Table 5.1. Water contact angle measurements. Contact angle of Sylgard 184, SSA 40:60 and SSA 50:50 was determined before (-) and after (+) oxygen plasma treatment.

plasma treatment	Sylgard 184	SSA 40:60	SSA 50:50
-	117°	116°	136°
+	25°	21°	29°

To test the cellular adherence, L929 cells were cultured for 24 h on Sylgard 184, SSA 50:50 and Sylgard 184, SSA 50:50 treated with plasma. Independent of the polymer, significantly more cells adhered to the plasma treated surfaces, while no statistically relevant difference was found between both polymers (**Figure 5.4A**).

To determine cellular cytotoxic effects of the materials, release of lactate dehydrogenase (LDH) was analyzed after 24 h culture period (**Figure 5.4B**). The cytotoxicity on Sylgard 184 or SSA was comparable and not higher than on the Triton X-100 control (0.4 % ± 1.8 % cytotoxicity for cells cultured on Sylgard 184, 1.7 % ± 1.9 % cytotoxicity for cells cultured on plasma treated Sylgard 184, 1.7 % ± 3.8 % cytotoxicity for cells cultured on SSA 50:50 and 0.9 % ± 3.1 % cytotoxicity for cells cultured on plasma treated SSA 50:50) (**Figure 5.4B**). To further validate the results of the LDH determination, a trypan blue exclusion test as additional cytotoxicity assay was performed. We observed 1.2 % ± 1.1 % cytotoxicity for cells cultured on Sylgard 184, 1.2% ± 2.0 % cytotoxicity for cells cultured on plasma treated Sylgard 184, 1.0 % ± 0.9 % cytotoxicity for cells cultured on SSA 50:50 and no cytotoxicity for cells cultured on plasma treated SSA 50:50. Therefore, we conclude that no statistically significant cytotoxicity was detectable while comparing both polymers to each other. In general, silicones are known for their low toxicity and high biostability, also in long-term applications.²⁰⁹ However, polymeric materials may contain additional components, e.g. residual monomers or catalysts²¹⁰, which might eventually influence physiological processes. Therefore a cytotoxic evaluation with a specific cell line can be beneficial for further applications. Interestingly, In order to analyze the cellular adherence and cell spreading on the polymer surfaces, L929 cell were seeded for 24 h on both native, non-plasma treated polymers and polymers treated with oxygen plasma (**Figure 5.4**). Visualization of actin filaments and microtubules revealed the emanation of lamellipodia protrusions on native Sylgard 184 and SSA 50:50 elastomers (**Figure 5.4C1** and **Figure 5.4C2**). We could not detect qualitative differences related to the cellular morphology while comparing both polymers. As expected, plasma treatment significantly improved cellular spreading on both surfaces resulting in remarkable extension of cellular body and lamellipodia protrusions (**Figure 5.4C3** and **Figure 5.4C4**).

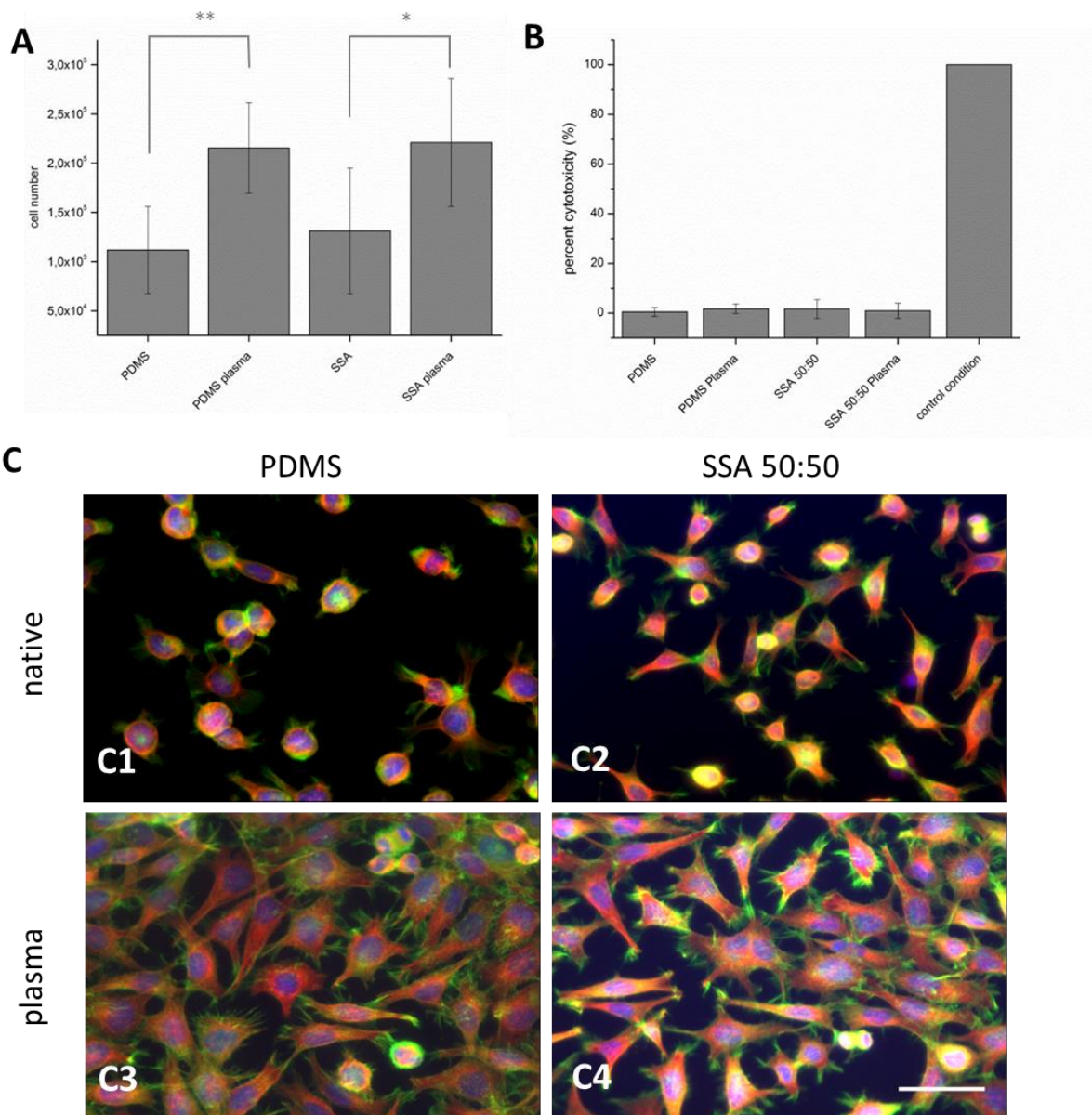


Figure 5.4. Cellular morphology after 24 h culture on polymeric surface. To determine cellular adhesion and assessment of cytotoxicity L929 cells were cultured for 24 h on PDMS, PDMS activated with plasma, SSA 50:50 and SSA 50:50 activated with plasma. **(A)** Cell number attached to the different surfaces was determined. **(B)** Release of lactate dehydrogenase was analyzed after release into the medium supernatant. As positive control for LDH release, cells were treated with 9 % Triton X-100 solution. **(C)** L929 cells were seeded for 24h on **(C1)** Sylgard 184 and **(C2)** SSA 50:50. **(C3)** Sylgard 184 plasma treated and **(C4)** SSA 50:50 plasma treated. To visualize the actin cytoskeleton, fixated cells were incubated with FITC conjugated phalloidin (green). Additionally alpha tubulin was visualized (red). Nucleii were stained with Hoechst dye 33342 (blue). On native surfaces cells adhere poorly **(A, B)**. Scale bars 25 μm . * denotes significance level $p < 0.05$, ** denotes significance level $p < 0.0005$.

5.4.3 Comparison between smooth and rough substrates

The results of the adhesion tests to smooth glass substrates (as shown in **Figure 5.3**) are not directly transferable to rough substrates, e.g. skin, which is our preferentially targeted application area. Several previous publications have already highlighted that roughness plays an important role in adhesion processes.^{117,211} In addition, for biological testing purposes, all samples were plasma treated as it is a common method to increase cellular adhesion to plastic materials,^{212,213} to sterilize materials and to make them more hydrophilic.²¹⁴ Additionally, it has been reported that plasma treatment leads to an increase in the root-mean-square roughness of polymers.²¹⁵ Thus, oxygen plasma treatment likely exerts fundamental effects onto adhesion properties and could influence the function of skin adhesives.

In **Figure 5.5**, the adhesion properties of Sylgard 184, SSA50:50 and SSA 40:60 films with a thickness between $170 \mu\text{m} \pm 30 \mu\text{m}$ on the smooth and rough glass substrate are compared before and after plasma treatment. Pull-off stresses, adhesion energy as well as maximum relative displacement of Sylgard 184 and SSA 40:60 decrease significantly on the rough substrate compared to the smooth substrate without plasma treatment. For Sylgard 184 we observed a nearly 95 % decrease in pull-off stress, while it is roughly 50 % for SSA 40:60; SSA 50:50 shows lower, but comparable pull-off stress values on the smooth and the rough substrate (**Figure 5.5A**). Similar effects are seen in the adhesion energy values (**Figure 5.5B**), with one notable exception: SSA 50:50 exhibits a twofold *increase* in adhesion energy on the rough substrate, reaching values similar to Sylgard 184 on the smooth substrate. A similar maximum is seen in the maximum strain (**Figure 5.5C**). The impact of roughness on adhesion behaviour is further illustrated in **Supplemental Figure S 5.2**. The detachment mechanisms remained similar on the rough substrate: Sylgard 184 and SSA 40:60 showed abrupt detachments, while SSA 50:50 remained in contact with the substrate for an extended time, detaching by fibrillation and withstanding high relative displacement (**Supplemental Figure S 5.2**). Compared to the detachment of the investigated PSAs from smooth surfaces, where fewer, but larger cavitation areas were observed, higher nucleation frequency was generally more prevalent on a rough surface.

In these measurements, plasma treatment had no influence on the pull-off stress, the adhesion energy and the maximum relative displacement on the smooth substrate for all tested materials. Interestingly, we observed a decrease of these values on the rough substrate, especially for Sylgard 184 and SSA 40:60. Oxygen plasma treatment is commonly used to increase adhesion between PDMS and glass.²¹⁶ Furthermore, plasma treatment modifies the mechanical properties of the surface layer of polymers^{217,218} as it results in the formation of an inorganic, wettable, brittle silica-like phase.^{212,219} Presumably, this influences adhesion to the rough substrate as it reduces the adaptability to the surface.

The effect of the hold time on pull-off stress on the rough substrate is shown in **Figure 5.5D**. Pull-off stress increased with increasing hold time for not plasma-treated polymers, but saturated at long hold times. In the case of plasma treated polymers, we observed a gradual increase of the pull-off stress with increasing hold time. A saturation of the pull-off stress was not reached in the evaluated time scale. When using a smooth substrate, the hold time did not greatly affect the results (not shown).

Depending on the particular application, different parameters may be controlling the adhesion performance. We conclude that combining all three parameters adequately describes the adhesion performance on complex surfaces and should therefore be included in the evaluation of dry adhesives.

In our study, we focussed on the investigation of thin films composed of SSA 50:50, where pull-off stresses up to 3 N/cm² could be reached on a rough substrate. The comparison of pull-off stresses between SSA 40:60 and SSA 50:50 implies almost no differences in adhesion as shown in **Figure 5.5A**. However, adhesion energy and maximum relative displacement on rough surfaces are significantly higher for SSA 50:50 as visualized in **Figure 5.5B and 5.5C**. SSA 50:50's excellent adhesion performance on rough surfaces allows the development of novel adhesives for skin applications like wearable sensors.

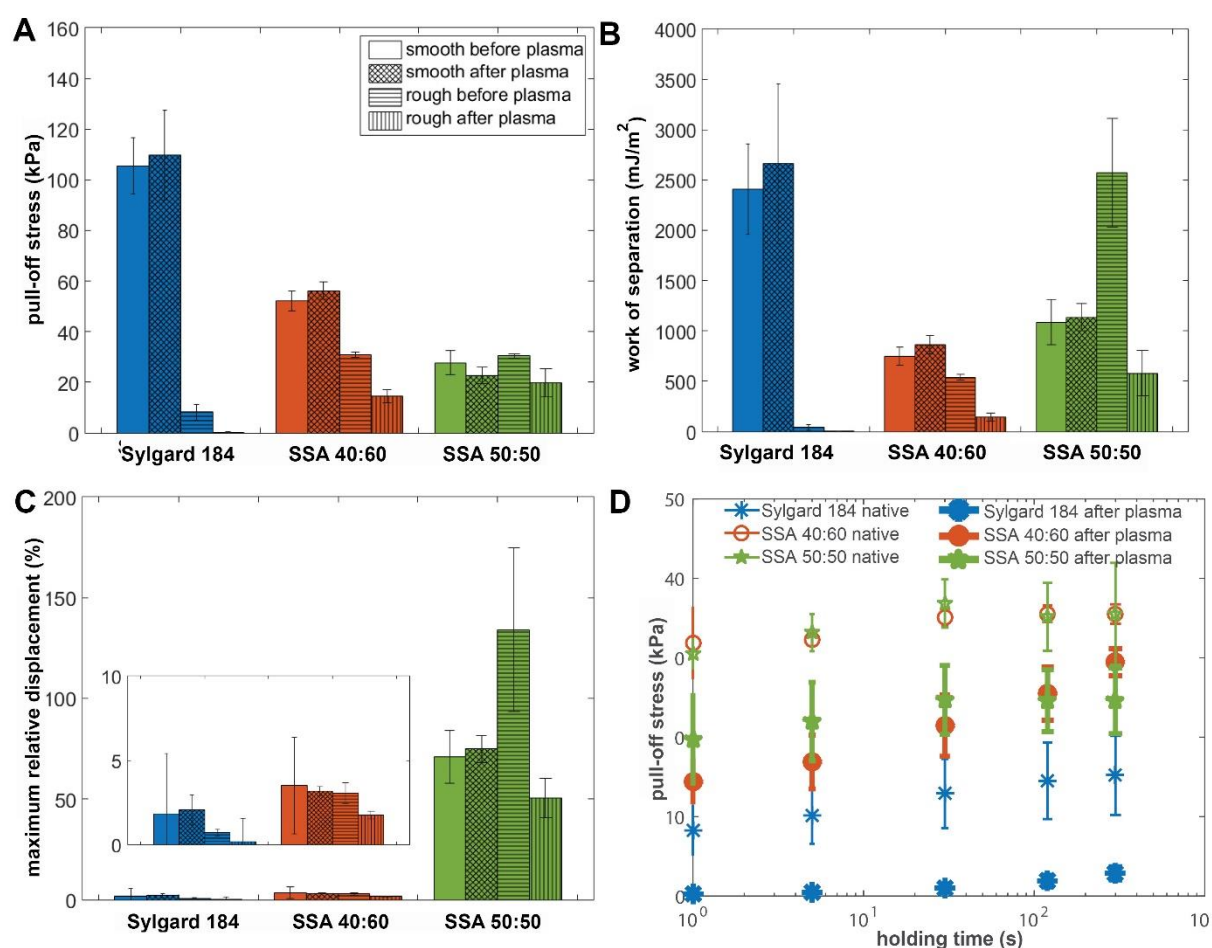


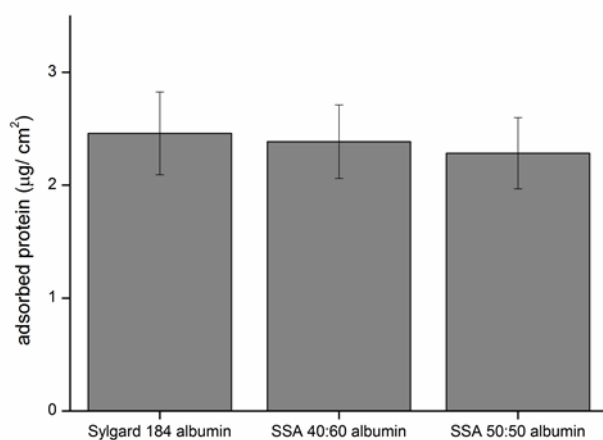
Figure 5.5. Comparison of the characteristic adhesion parameters obtained from smooth and rough substrates for Sylgard 184, SSA 40:60 and SSA 50:50 with and without plasma treatment. **(A)** Pull-off stress, **(B)** adhesion energy and **(C)** maximum relative displacement for experiments with a pull-off velocity of 10 $\mu\text{m/s}$ and a hold time of 1 s. The insert is a close-up version of the data for Sylgard 184 and SSA 40:60 in **(C)**. **(D)** Influence of the hold time on the adhesion to the rough substrate. Only films with a thickness of $170 \pm 35 \mu\text{m}$ were considered for this analysis.

5.5 Conclusions

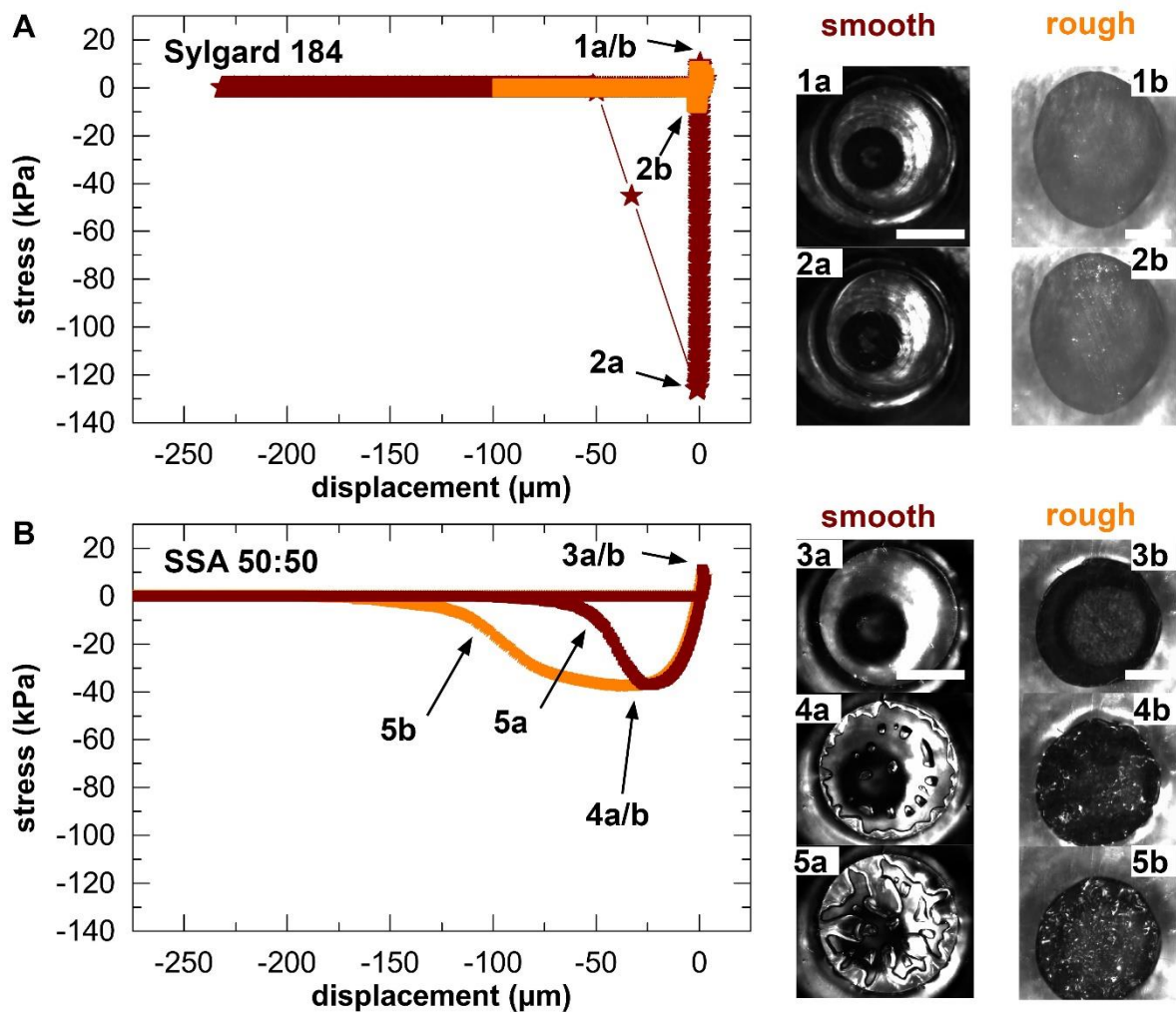
The mechanical, adhesive and biological properties of SSA have been investigated and compared to Sylgard 184 with a special focus on roughness and low pressure oxygen plasma treatment.

- No cytotoxic effects could be detected when culturing murine fibroblast on SSA surfaces and cellular adhesion was enhanced after plasma treatment.
- We have clearly shown that pull-off stress of the investigated Sylgard 184 and SSA 40:60 is highly dependent on the substrate type used, while almost no differences were observed, when focusing on SSA 50:50.
- Pull-off stress values can be expected to increase furthermore when the roughness increases, which makes this material very promising for applications as skin adhesive.
- Pull-off stress of SSA 50:50 was also not negatively affected by the treatment with oxygen plasma, therefore balancing biocompatibility and mechanical strength.

5.6 Supplemental information



Supplemental Figure S 5.1. Determination of protein adsorption. Polymers were incubated with FITC conjugated bovine albumin for 3h and fluorescence intensity determined at a wavelength of 488nm. No difference in protein adsorption was detected after the incubation period.



Supplemental Figure S 5.2. Comparison of the characteristic stress displacement curve of Sylgard 184 and SSA 50:50 on both substrates and detachment mechanisms. Two exemplary measurement curves of (A) Sylgard 184 and (B) SSA 50:50 and the smooth (red) and rough (orange) substrate are shown. Optical micrographs on the right depict the detachment process (top to bottom) from both substrates. The arrows indicate approximate positions in the force-displacement curve where the pictures were taken. Scale bars 1 mm.

6 Adhesion and relaxation of a soft elastomer on surfaces with skin like roughness

6.1 Abstract

For designing new skin adhesives, the complex mechanical interaction of soft elastomers with surfaces of various roughnesses needs to be better understood. We systematically studied the effects of a wide set of roughness characteristics, film thickness, hold time and material relaxation on the adhesive behaviour of the silicone elastomer SSA MG 7-9800 (Dow Corning). As model surfaces, we used epoxy replicas obtained from substrates with roughness ranging from very smooth to skin-like. Our results demonstrate that films of thin and intermediate thickness (60 and 160 μm) adhered best to a sub-micron rough surface, with a pull-off stress of about 50 kPa. Significant variations in pull-off stress and detachment mechanism with roughness and hold time were found. In contrast, 320 μm thick films adhered with lower pull-off stress of about 17 kPa, but were less sensitive to roughness and hold time. It is demonstrated that the adhesion performance of the silicone films to rough surfaces can be tuned by tailoring the film thickness and contact time.

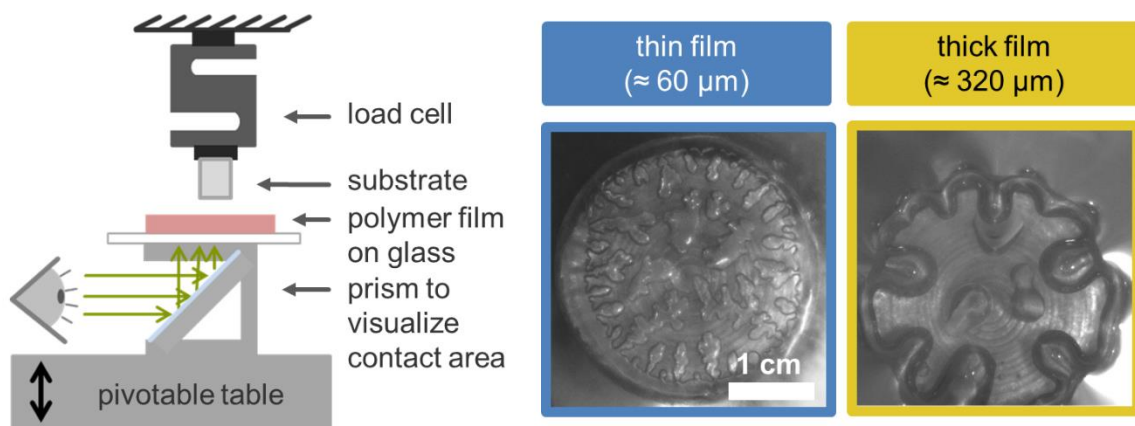


Figure 6.0. Graphical summary of chapter 6. Adhesion experiments were performed using the probe tack test setup (left). Adhesion measurements were analysed quantitatively through force-displacement curves and qualitatively through optical micrographs of the delamination processes (right).

6.2 Introduction

The surface and contact topography strongly affects the adhesive interaction between two materials.^{84,89,118} It is well recognized that the adhesion to rough surfaces is reduced due to the absence of full surface contact.^{85,115,112,220} Several parameters, such as compressive preload and hold time as well as film thickness and mechanical properties, influence the adhesive behaviour.^{84,103,119,120} Only a few systematic adhesion studies exist on surfaces exhibiting roughness in the micron range. Especially contact time and relaxation of the adhesive materials are factors whose influence needs to be better understood. Roughness, material properties and the thickness of the adhesive material notably affect the detachment mechanism from the surface.^{1,120,169} While edge cracks often yield unstable, spontaneous detachment, other mechanisms including cavitation and center cracks can result in stable crack growth and thus can increase the work of separation and the pull-off strength.^{1,96,103,169}

Skin is an example of a particularly complex, rough surface with properties depending on several factors including humidity, secretion, environmental conditions and the presence of skin care products.^{221,222} Adhesion to skin is needed for wound dressings or for emerging consumer applications, e.g. wearable electronic devices and activity trackers.^{134,186,223} The adhesive performance of skin dressings is often characterized by peel or tack tests on substitute materials such as stainless steel or polycarbonate substrates, both exhibiting nanoscopic or sub-micron roughness.^{224,225} For the development and improvement of innovative skin adhesives, a fundamental understanding of the material interaction with surfaces exhibiting skin-like roughness is necessary. Standardized measurements are complicated by the fact that human skin exhibits mean peak-to-valley distances in the range of 50 to 70 μm depending on age and location on the body surface.²²⁶ Because these variations influence measurements significantly, skin substitutes composed of synthetic and natural materials have been evaluated.^{129,183,227}

In previous work, we analysed the mechanical properties, adhesion properties and biocompatibility of the soft skin adhesive SSA MG 7-9800 (SSA, Dow Corning, Auburn, MI, USA) and Sylgard 184 (Dow Corning, Auburn, MI, USA). Their applicability to biomedical applications was studied as a function of the mixing ratio of the base to crosslinker of the two-component systems.² In these investigations we limited our study to glass substrates with low roughness ($R_z = 0.04$ to $2.2 \mu\text{m}$) and a restricted range of film thicknesses (50 to $230 \mu\text{m}$). The pull-off strength was found to increase with decreasing film thickness and increasing elastic modulus on the smooth substrate, and significantly decreased on the rough glass substrate except for SSA in the mixing ratio 50:50.

The present paper provides comprehensive insight into the effects of film thickness and surface roughness on the adhesion of the silicone adhesive SSA MG 7-9800. Parameters included film thickness (from 60 to $320 \mu\text{m}$), substrate roughness (R_z from 0.1 to $84.2 \mu\text{m}$) and hold time (from 1 to 300 s). Surface roughness comparable to skin was produced by replicating epoxy resins from glass surfaces or from the artificial skin model VitroSkin.²²⁸ VitroSkin has been shown to exhibit mechanical properties and surface roughness comparable to animal skin.^{130,228} From the results, we conclude that two different regimes are present, fundamentally affecting the adhesive behaviour: a roughness insensitive regime when the film thickness is higher than the material-specific critical roughness parameter and a roughness sensitive regime in the other case.

6.3 Materials and Methods

6.3.1 Manufacturing of adhesive film samples

Polymer films were manufactured from SSA MG 7-9800 (Dow Corning, Auburn, MI, USA) in a mixing ratio of 1:1 weight parts by a doctor blade technique with an automatic thin film applicator (AFA-IV, MTI Corporation, Richmond, CA, USA). After deposition on glass, the films were cured at 95°C for one hour. The film thickness was measured by optical microscopy (Eclipse LV100ND, Nikon, Duesseldorf, Germany). Thickness values were $60 \pm 10 \mu\text{m}$ (denoted as “thin”), $160 \pm 25 \mu\text{m}$ (“medium”) and $320 \pm 30 \mu\text{m}$ (“thick”). The samples were prepared on glass plates with an area of about $7 \times 20 \text{ cm}^2$, and subsequently cut into samples of about 4 cm^2 for adhesion testing.

6.3.2 Adhesion measurements and analysis

Adhesion measurements were performed using a custom-built setup as described previously.² The approach and retraction velocity were set to $30 \mu\text{m/s}$ and $10 \mu\text{m/s}$, respectively. The hold time, t_{hold} , was varied from 1 to 300 s. The compressive preload stress, σ_0 , was kept constant at $10 \pm 3 \text{ kPa}$. Measurements were performed with at least four independent adhesive films and at three different locations on each surface

From the measured values of the force, F , and the displacement, s , we calculated the stress, $\sigma = F/A$, where A is the nominal contact area (about 7 mm^2 for the epoxy substrates). The relative displacement was defined as $\varepsilon = (s - s_0)/h_{film}$, where h_{film} is the film thickness and s_0 the displacement at force zero. To analyse and compare the adhesive behaviour, three parameters were chosen: the maximum pull-off stress, σ_{max} ; the maximum relative displacement, ε_{max} ; and the work of separation, $W_{sep} = \int_{s_0}^{s_{end}} \sigma ds$ where s_{end} is the displacement at which complete detachment occurred.

6.3.3 Substrate manufacturing

Substrates of different materials and surface roughness were used (cf. **Figure 6.1** and **Figure 6.2**). The reference substrates consisted of a polished glass slide (denominated as GS 1, area $A = 3.2 \text{ mm}^2$) (Hellma Optik GmbH, Jena, Germany), frosted glass (GS 2, $A = 6.7 \text{ mm}^2$) (Marienfeld, Lauda Königshofen, Germany), VitroSkin (IMS inc., Portland, ME, USA) backside (VS 1, $A = 7.6 \text{ mm}^2$) and VitroSkin frontside (VS 2, $A = 7.6 \text{ mm}^2$). While for GS 1 the glass was purchased as a cylinder with 2 mm diameter, a circular substrate with about 3 mm diameter was machined out of a frosted glass slide for GS 2. For the VitroSkin, circular substrates with about 3 mm diameter were extracted using a biopsy punch (Integra Miltex Inc., York, PA, USA).

Epoxy substrates were replicated from different master substrates: a regular glass slide (ES 1, $A = 6.1 \text{ mm}^2$) (Marienfeld, Lauda Königshofen, Germany), a frosted glass slide (ES 2, $A = 7.0 \text{ mm}^2$) (Marienfeld, Lauda Königshofen, Germany), VitroSkin (IMS inc., Portland, ME, USA) backside (ES 3, $A = 7.1 \text{ mm}^2$) and VitroSkin frontside (ES 4, $A = 7.2 \text{ mm}^2$). The epoxy resin (Résine epoxy R123, Soloplast-Vosschemie, Fontanil-Cornillon, France) was mixed in 100:45 weight ratio of base to curing agent as specified by the supplier, cured on the respective substrate at room temperature for over 12 hours and then extracted with a biopsy punch of 3 mm diameter.

All substrates were attached to an aluminium mount compatible with our adhesion setup using UV adhesive (Bohle Ltd., Cheshire, UK), for GS 1-2 and ES 1-4, or epoxy resin, for VS 1-2. The displacements

measured during the tests were corrected for the system compliance $C = 0.12 \mu\text{m} \cdot \text{mN}^{-1}$ for glass and $C = 0.13 \mu\text{m} \cdot \text{mN}^{-1}$ for epoxy and VitroSkin.

6.3.4 Substrate characterisation

The exact nominal area of each substrate was measured using optical microscopy (Keyence, Osaka, Japan) and used in the stress calculations. Their roughness parameters were measured by stylus profilometry (Surfcom 1500SD3, Carl Zeiss, Oberkochen, Germany). Roughness power spectra were determined using the Surface Topography Analyzer developed by Lars Pastewka (<http://contact.engineering/>).¹⁶⁶

6.4 Results

In this section, we first present the results of the substrate surface characterization. Subsequently, the results of the adhesion test with the different adhesive samples are reported as a function of film thickness, surface roughness and hold time.

6.4.1 Substrate surfaces

Figure 6.1 and **Figure 6.2** show the results of the substrate surface characterization. As can be seen, the replication process led to slight differences in the topographies between master and replica. From the table in **Figure 6.2** we can see that, except for ES 3, the roughness parameters R_a and R_z seem to slightly decrease after replication. **Figure 6.2** reveals also slight differences between the respective power spectra. The power spectra of the glass and the VitroSkin substrates have considerably different slopes and thus height distributions.

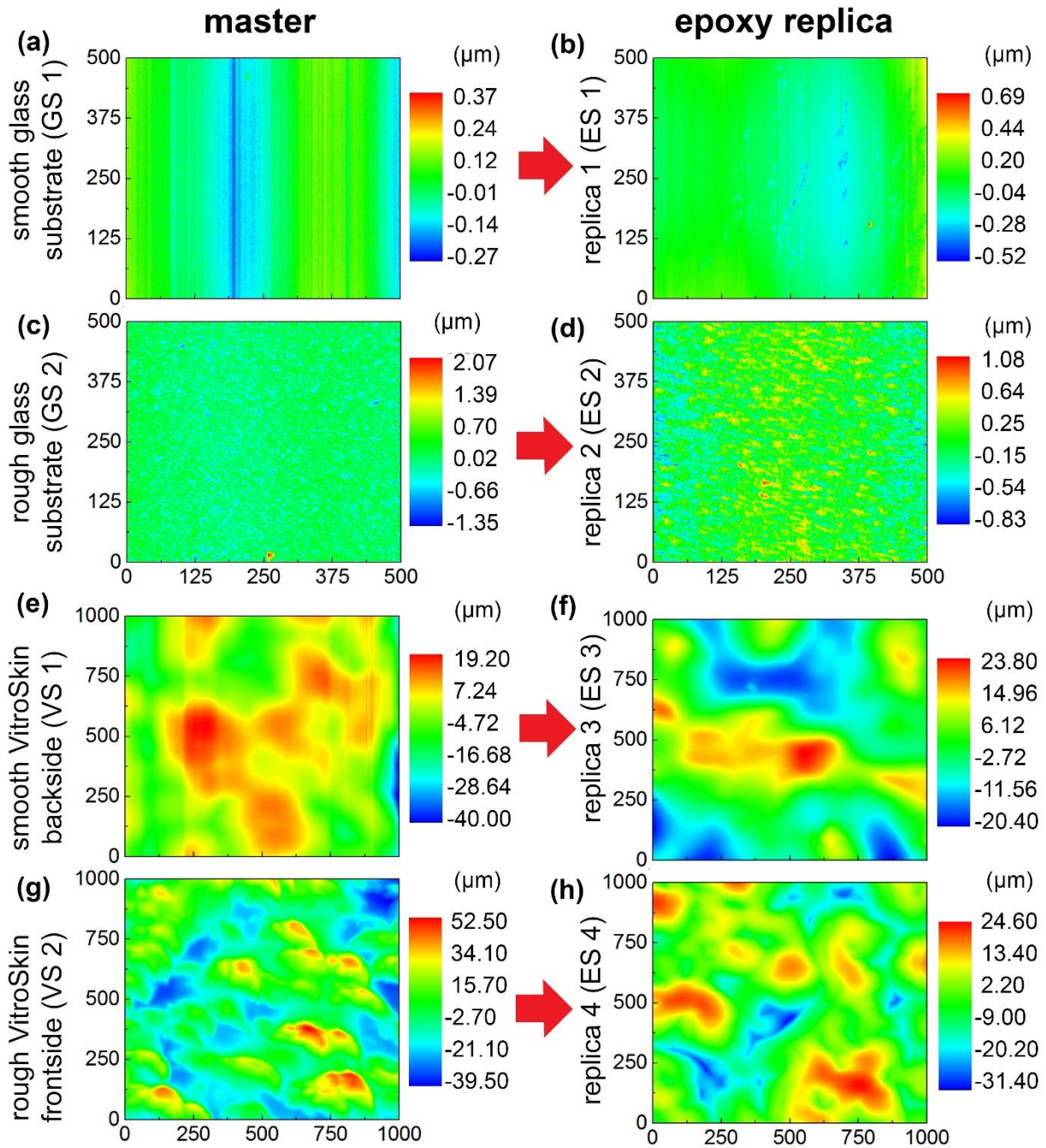


Figure 6.1. Topography of substrates used for adhesion testing, as characterized by stylus profilometry. (a)-(d) glass substrates (GS 1 and GS 2) and their epoxy replicas (ES 1 and ES 2), scans of $500 \times 500 \mu\text{m}$. (e)-(h) VitroSkin substrates (VS 1 and VS 2) and their epoxy replicas (ES 3 and ES 4), scans of $1000 \times 1000 \mu\text{m}$. Due to the large roughness range, the roughness scales differ.

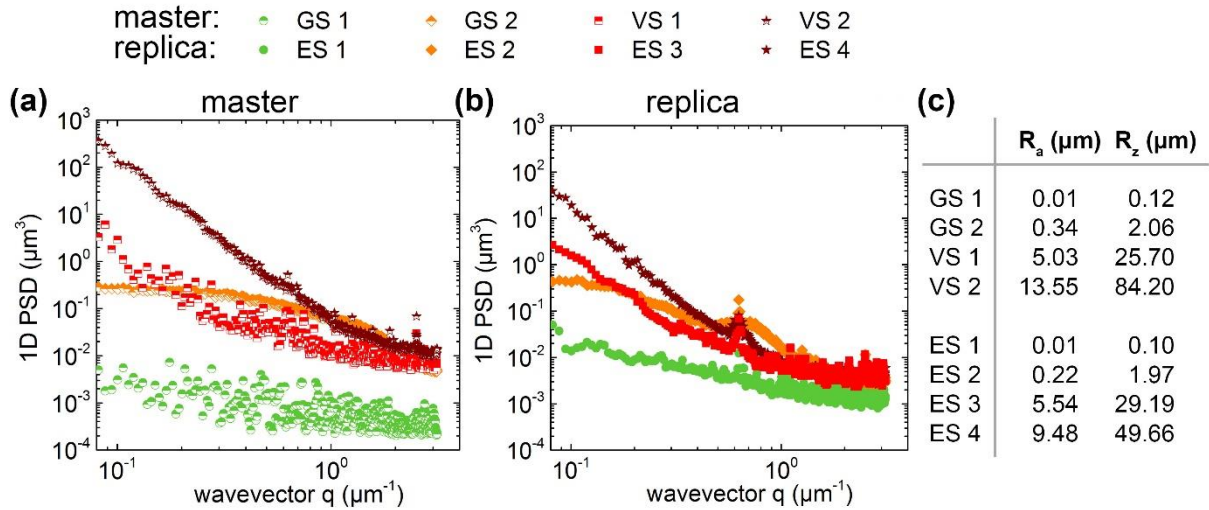


Figure 6.2. Roughness power spectra of the substrates used for adhesion testing. 1D power spectra of (a) the glass and VitroSkin master surfaces (GS 1-2; VS 1-2) and (b) the epoxy replica (ES 1-4) based on profilometer scans and generated with the Surface Topography Analyzer (<http://contact.engineering/>).¹⁶⁶ (c) Resulting roughness parameters of all surfaces: average roughness R_a and average peak-to-valley distance R_z .

6.4.2 Influence of film thickness and roughness

Figure 6.3 depicts the adhesion parameters measured, with a hold time of 1 s, for the different film thicknesses and substrate topographies. Each data point corresponds to the average of about twelve measurements, corresponding to at least four independent adhesive films with three positions on each film. The “thick” films exhibited similarly low pull-off stresses on all four substrates of about 17 kPa (Figure 6.3a and 6.3b). The “medium” and “thin” films, in contrast, showed a dependence of the pull-off stress on the substrate. Within the error bars, the behaviour of the two films on glass was virtually indistinguishable (Figure 6.3a); the adhesion to the smoothest substrate ES 1 was about 40 kPa and, interestingly, seemed to increase for the rougher ES 2 substrate to between 40 and 50 kPa. It is debatable whether this increase is statistically significant in view of the error margins, a point that will be discussed below. On the roughest substrates (ES 3 and ES 4), the pull-off stress decreased substantially, with the “thin” film showing a stronger decrease.

The work of separation was found to be lowest for the “thin” films, with values of about 2 J m^{-2} and a slight maximum of 2.5 J m^{-2} for ES 2 (Figure 6.3c). The “medium” and “thick” films displayed almost twice this value and are again virtually indistinguishable within the error margins. A small, probably insignificant variation for the different substrates could be observed, with maximum values of 6.5 J m^{-2} and 7.5 J m^{-2} for substrates ES 2 and ES 3, respectively. The maximum relative displacement observed for all three films on all four substrates was, within the error margin, of similar magnitude between 180 and 300% (Figure 6.3d).

In addition to quantitative differences, the detachment mechanisms of the films varied depending on film thickness and substrate roughness (Figure 6.4). Finger-like cracks originating from the contact edge were observed in all cases, with dimensions increasing with increasing film thickness. Thus, in thinner films, the fingers were finer than in thicker films. On the smoothest substrate, cavitation in the interior of the contact area was exclusively seen in thinner films. Increasing the surface roughness lead

to augmented occurrence of cavitation in the medium and thick films. These differences influenced the adhesion strength on the different substrates as quantitatively described before.

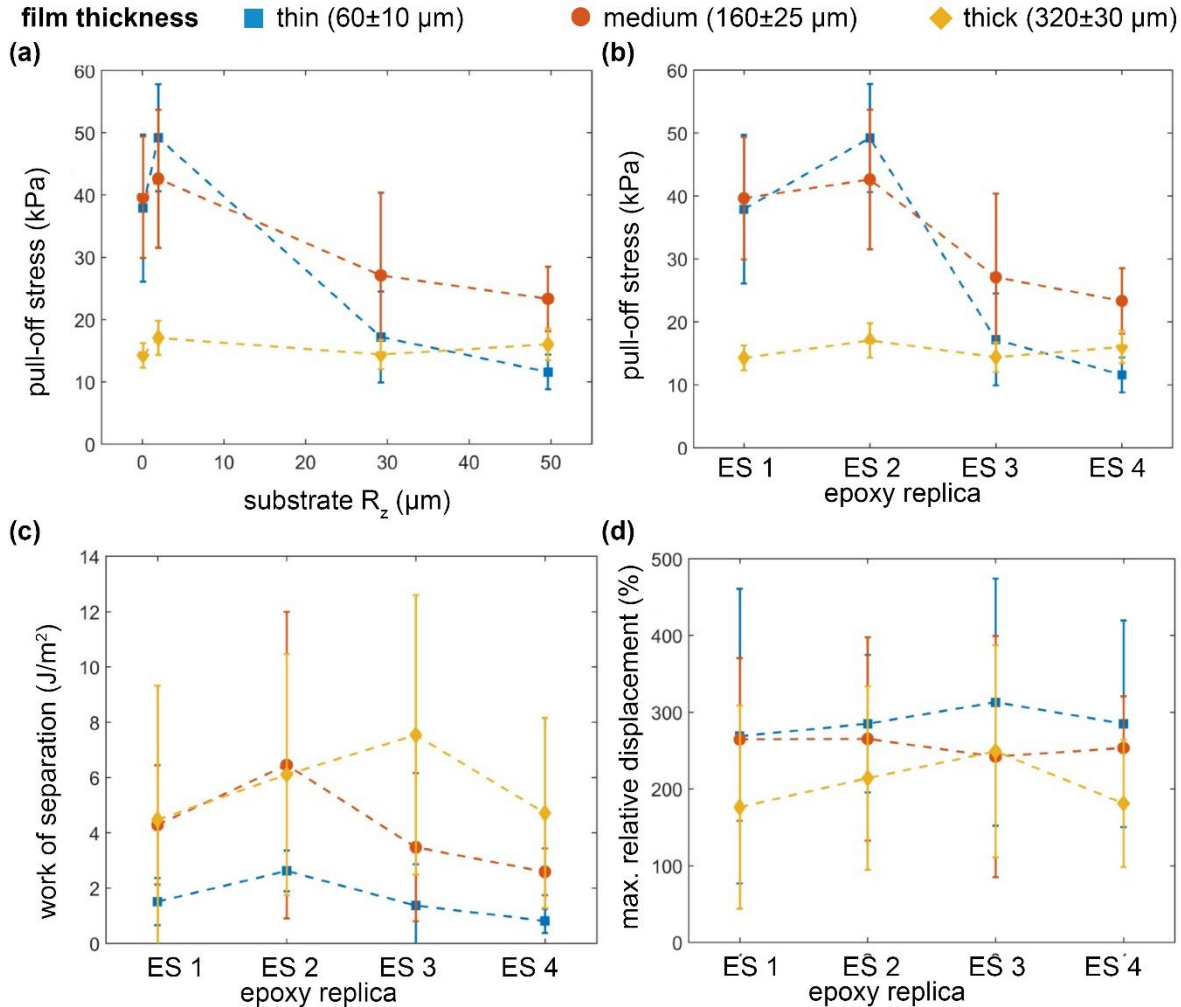


Figure 6.3. Adhesion measurement results as function of film thickness and substrate roughness. (a) Pull-off stress as a function of the roughness parameter R_z and (b) pull-off stress, (c) work of separation and (d) maximum relative displacement for the films with three different thickness on four epoxy substrates. The hold time was 1 s.

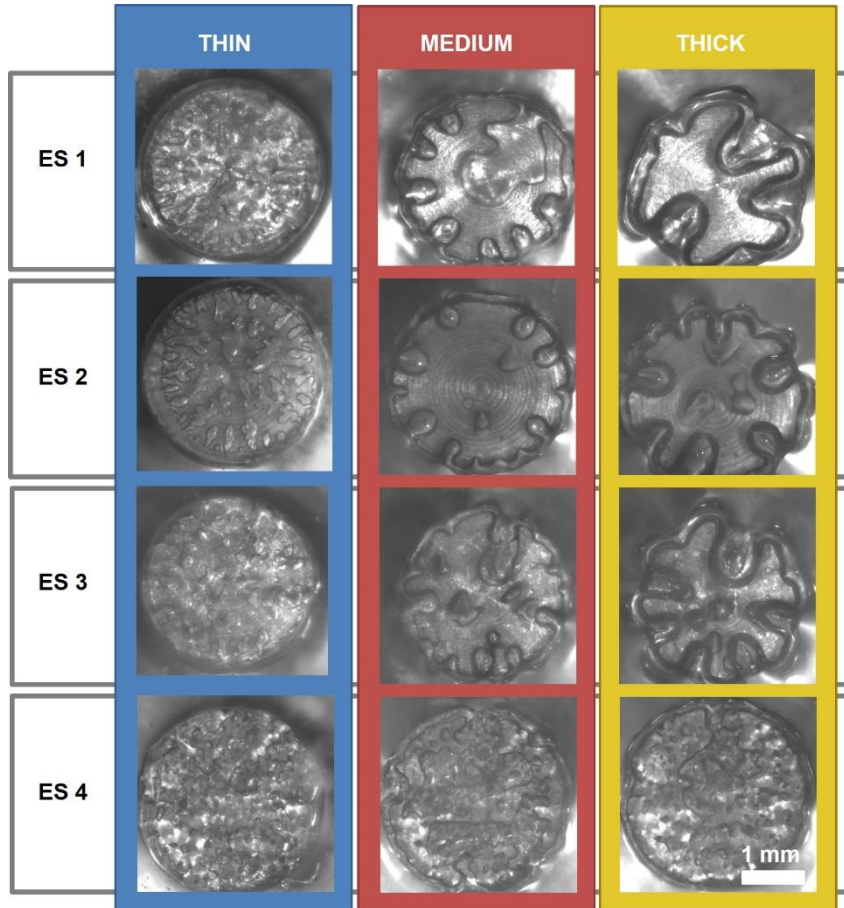


Figure 6.4. Exemplary pictures of the detachment mechanisms. Debonding of a “thin” (blue), “medium” (red) and “thick” (yellow) film from the epoxy substrates with increasing surface roughness. Finger-like cracks originating from the contact edge are observed in all cases. In thicker films, the fingers are coarser than in thinner films. Additional crack formation in the interior of the contact (cavitation) is seen in thinner films, especially in contact with substrates of higher roughness.

6.4.3 Influence of hold time and material relaxation

Viscoelastic materials exhibit time-dependent stress relaxation during a hold time at constant displacement.¹ The compressive stress σ as a function of time t can be approximated by the following equation based on the Kelvin model.^{102,229,230}

$$\sigma = \sigma_{\infty} + \sigma_1 \cdot \exp\left(-\frac{t}{\tau_1}\right) + \sigma_2 \cdot \exp\left(-\frac{t}{\tau_2}\right), \quad (6.1)$$

where σ_1 and σ_2 are stress constants and τ_1 and τ_2 are time constants, and σ_{∞} is the stress value for infinite hold time ($t \rightarrow \infty$). The initial stress, denoted as σ_0 , is given by $\sigma_{\infty} + \sigma_1 + \sigma_2$. For $\tau_1 < \tau_2$, the short time relaxation behaviour is described by τ_1 and σ_1 , whereas τ_2 and σ_2 describes the long-term behaviour. By fitting the parameters σ_{∞} , σ_1 , σ_2 , τ_1 , and τ_2 , the stress relaxation during 120 s hold time at an initial pre-stress of 10 ± 2 kPa was reproduced in **Figure 6.5** and **Supplemental Figure S 6.2** (all fit parameters can be found in the **Supplemental Table S 6.1**).

Figure 6.5a shows that the normalized stress relaxation was higher for “thick” films, with a stress drop of 42% after 120 s compared to only 23% for the “thin” films. For all films, the stress at 120 s hold time

was already very close to the estimated stress, σ_∞ , at infinite contact times (see **Supplemental Table S 6.1**), which means that the material relaxation is close to saturation after 120 s. The relaxation time τ_1 was similar for all film thicknesses and substrates with a value of about 2.4 ± 0.3 s (**Figure 6.5b**). The relaxation time τ_2 varied with film thickness and substrate roughness: for the “medium” and the “thick” films, τ_2 slightly increased with roughness (from 28 ± 4 s to 47 ± 6 s and from 27 ± 21 s to 31 ± 2 s, respectively). The highest τ_2 of 60 ± 22 s was obtained for the “thin” film in contact with ES 2, but dropped dramatically in contact with the rougher substrates ES 3 and ES 4.

The pull-off stresses as a function of hold time, varied between 1 and 300 s, are displayed in **Figure 6.6**. Unlike the “thick” films, the “thin” and the “medium” films showed a pronounced increase in pull-off stress with longer hold times. For “medium” films, the pull-off stress increased by a factor ranging from 1.7 to 3 per time decade (**Figure 6.6b**); the “thin” films exhibited the highest sensitivity to the hold time, with a factor of 2.4 to 5 per time decade (**Figure 6.6a**). In line with the results of **Figure 6.3**, the sensitivity of the pull-off stress to the surface roughness decreased with increasing film thickness.

The results indicate that “thick” films are very insensitive to the hold time, while the adhesion of “thin” and “medium” films can be adjusted by varying the hold time. The rate of pull-off stress increase with time decreases at longer hold times, but a saturation could not be measured in our experiments. However, from the relaxation experiments (**Figure 6.5**), we observe that the characteristic material relaxation time was between 27 and 60 s, the stress decrease being highest for the thickest films and yielding a plateau after less than 120 s. This indicates that the stress relaxation is not primarily influencing the pull-off stress increase at elongated hold times, as the influence of hold time is more pronounced for thinner films, and does not plateau, even after 300 s hold time.

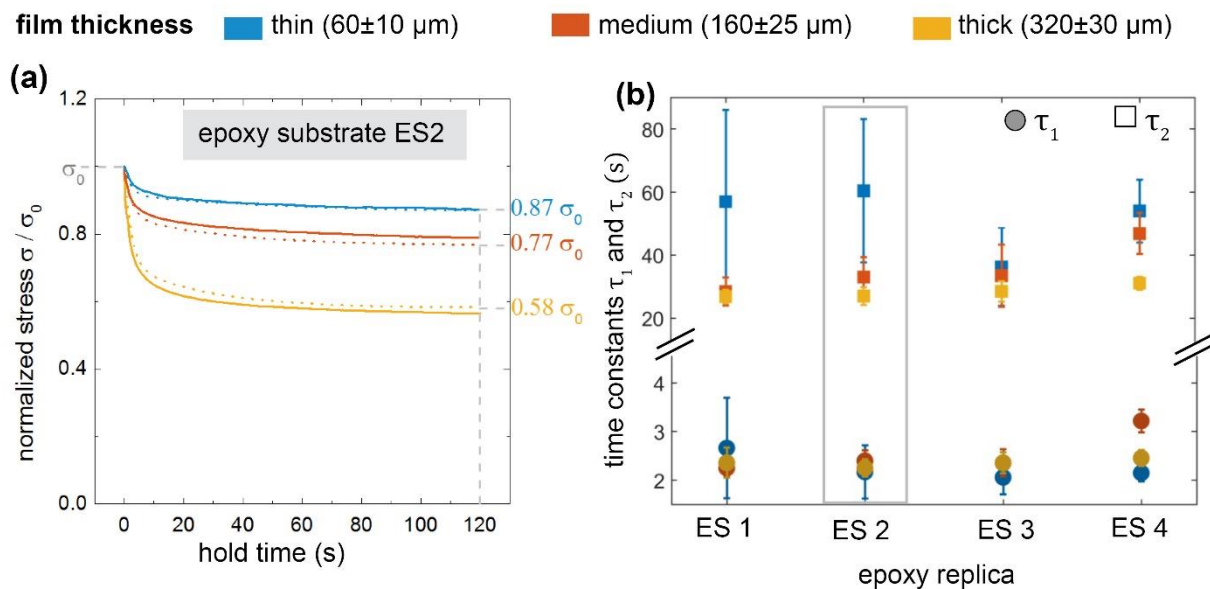


Figure 6.5. Stress relaxation behaviour of the films on the different substrates. (a) Stress, normalized by the compressive pre-stress σ_0 of about 10 kPa, vs. hold time. Data shown are for the epoxy replica ES 2. Dots are experimental data, lines represents fits to eq. 1. The values right to the curves represent the stress decreases at 120 s contact time relative to the initial pre-stress. (b) Time constants τ_1 (circles) and τ_2 (squares) obtained as a function of substrate and film thickness (see color code).

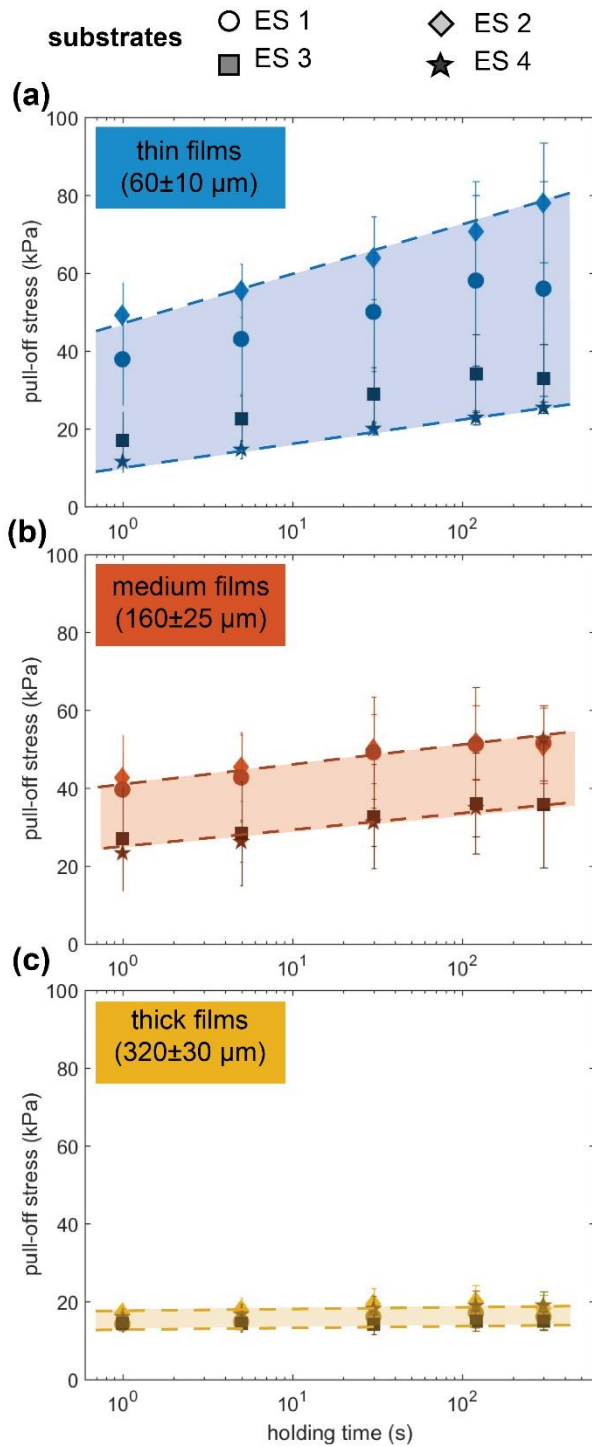


Figure 6.6. Hold time effect on adhesion. Pull-off stress as a function of hold time for (a) thin ($60 \pm 10 \mu\text{m}$), (b) medium ($160 \pm 25 \mu\text{m}$) and (c) thick films ($320 \pm 30 \mu\text{m}$) on the different epoxy substrates. The dashed lines are intended to guide the eye of the reader.

6.5 Discussion

In this work, we presented adhesion measurements on epoxy substrates replicated from different surfaces, from polished glass to VitroSkin, an artificial model skin. The replicas exhibited slightly different roughness profiles compared to the original surfaces. This is most likely due to shrinkage of the epoxy resin during the curing process or to limited epoxy molding of fine asperities. However, we believe that this will not drastically influence the outcome of our study. Adhesion measurements showed that, with increasing confinement, i.e. an increasing ratio between the punch diameter and the film thickness, the pull-off stress typically increases most likely because lateral retraction of the material is suppressed.^{95,231,232} That explains the generally observed trend that the pull-off stress increased with decreasing film thickness. However, this is limited if the film thickness is in the same size scale as the mean peak to valley distance (R_z) of the substrates, as observed for epoxy substrates ES 3 and ES 4 for the thinnest film (**Figure 6.3a**). Davis et al. discussed a material-defined length scale, δ_c , that describes the distance over which adhesive forces act and that qualitatively provides a measure of the critical size scale of surface roughness to impact adhesion.¹²⁰ For confined elastic layers $\delta_c = \sqrt{G_c \cdot h_{film}/E}$, G_c and E being the critical energy release rate and the Young's modulus, respectively.⁶⁸ This means that for a given adhesive material of a given thickness, there is a critical surface roughness parameter $R_{z,crit} = \delta_c$ above which the adhesion is strongly influenced by surface roughness. Conversely, for a given surface with roughness R_z there is a critical film thickness of the elastic material, $h_{film,crit} = R_z^2 \cdot E/G_c$, above which the adhesion will likely be insensitive to the surface roughness.

The lower bound of the critical energy release rate, in equilibrium conditions, equals the thermodynamic work of adhesion, typically about 50 mJ/m² for silicone materials. The Young's modulus of SSA 7-9800 is about 6 kPa as measured in our previous study assuming $E \approx 3 \cdot G$, G being the shear storage modulus measured at 0.01 Hz with a rheometer.² Hence, $R_{z,crit}$ ranges between 22 μm and 52 μm , for the thin ($h_{film} = 60 \mu\text{m}$) and thick ($h_{film} = 320 \mu\text{m}$) films, respectively. These values are larger than R_z obtained from ES 1 and ES 2; this most probably explains why the surface topography does not affect the adhesion performance of all films. In contrast, $R_{z,crit}$ is in the same order than R_z of the substrate ES 3 and ES 4. Here, the surface asperities most likely have an impact on the adhesion performance related to strain energy distortions, particularly for the thinner films (**Figure 6.3a**). For the "thick" film, $R_{z,crit}$ is larger than R_z for all substrates, which likely indicates the small influence of the roughness on the adhesion measurements.

The apparent trend that the pull-off stresses seemed to be highest for the slightly rough substrate (ES 2), rather than for the smoothest substrate (ES 1) (**Figure 6.3c**), requires further discussion. Unfortunately, the error bars are too large to make this an unambiguously significant observation. We note however that such a behaviour would be in line with earlier reports where similar effects of sub-micron roughness were found.¹¹⁸⁻¹²⁰ For the "thin" films, the pull-off stress increased by about 25% compared to the smoothest substrate, which cannot be explained by the slight increase of real contact area. In fact, a soft elastic body adhering to a sub-micron rough substrate creates elastic strain distortions at the surface asperities, surrounded by regions with smaller strain distortions.²³³ Guduru demonstrated that surface roughness resulted in a combination of stable and unstable crack growth: from the surface valleys, the crack moves continuously towards the top of asperities, where it is then hindered and requires higher stresses to continue to propagate, yielding dissipative zones for the small scale roughness.²³³ This results in crack trapping, which leads to increased work of separation and higher pull-off stresses.²³⁴

Contact time can have different superimposing effects on adhesion measurements, including stress relaxation in the material, defect annealing at the interface and development of chemical affinity at the interface. Stress relaxation experiments revealed that the characteristic relaxation times were much smaller than the hold times influencing the pull-off stresses in adhesion measurements. The stress relaxation reflects a combination of macroscopic and microscopic effects, i.e. a global deformation of the film due to the penetration of the punch and local deformation due to the surface asperities. Note that the indentation depth to achieve the pre-stress increased with increasing film thickness. Hence, bulk deformation most probably dominates the stress relaxation behaviour over microscopic defect annealing, particularly for film thicknesses much larger than R_z . For the thin films adhering to ES 3 and ES 4, where $h_{film} \approx R_z$, however, τ_2 varies as a function of the substrate, which likely indicates that the surface roughness affects the relaxation behaviour.

For “thick” films, we suggest that the low confinement yields stress concentrations at the edge of the contact zone, initiating detachment at the edge (**Figure 6.4**). This detachment process is relatively independent of defects and defect annealing with increasing hold time. Both chemical affinity and stress relaxation seem to only marginally influence adhesion. For thin and medium-thick films, detachment is driven by stress concentrations within the contact area, influenced drastically by defects, yielding cavitation driven detachment. Thus, defect annealing at the interface contributes towards the increased adhesion strength observed.

6.6 Conclusions

We presented a study of the adhesion and material relaxation of a medical grade silicone SSA MG 7-9800. Substrate roughness, hold time and film thickness were varied and epoxy replicas from glass and VitroSkin substrates were used as counter surfaces. In this way, a description of the time-dependent interaction of soft elastomers on skin-like surfaces was provided. The following conclusions can be drawn:

- The adhesion behaviour of the thin films in our study was found to be very sensitive to surface roughness and hold time. Thicker films exhibited smaller pull-off stresses which were almost unaffected by roughness and hold time.
- Hold times improved adhesion only for the thinner films, which is very likely due to a combination of stress relaxation and defect annealing at the contact.
- Small surface roughness resulted in increased pull-off stresses; this is believed to indicate the occurrence of crack trapping.
- Thin films can achieve very high adhesion, also on rough surfaces, with the limitation that the film thickness must fulfil $h_{film} > R_z^2 \cdot E/G_c$, where E is the Young’s modulus and G_c the critical energy release rate.

The results suggest that, for any application related to skin adhesion, the thickness of the adhesive layer should be judiciously chosen: While thick films provide smaller, but constant pull-off stresses, the adhesive behaviour of thinner films can be tuned with longer hold times. For the most versatile adhesives, thick layers should be chosen while thinner films achieve higher pull-off stresses on certain substrates.

6.7 Supplemental information

6.7.1 Adhesion measurements on master substrates compared to epoxy replicas

Normal adhesion measurements of polymer films with thin and medium thicknesses were performed against two glass substrates (GS 1 and GS 2) and their epoxy replica (ES 1 and ES 2) to study the influence of the substrate material used for adhesion testing. In this case, the hold time was kept constant at 1 s.

No significant differences between pull-off stresses have been detected while comparing adhesion measurements on the two glass substrates and their epoxy replica with identical film and substrate properties (**Figure S 6.1a**). In addition, no significant difference was observed while comparing the work of separation (**Figure S 6.1b**). Interestingly, differences in the average maximum relative displacement are detectable while focussing on the glass indenter (**Figure S 6.1c**). Independent of the surface roughness, a decrease in the displacement was observed for the medium film thickness compared to thin films (**Figure S 6.1c**). This effect is not observed with the epoxy indenter.

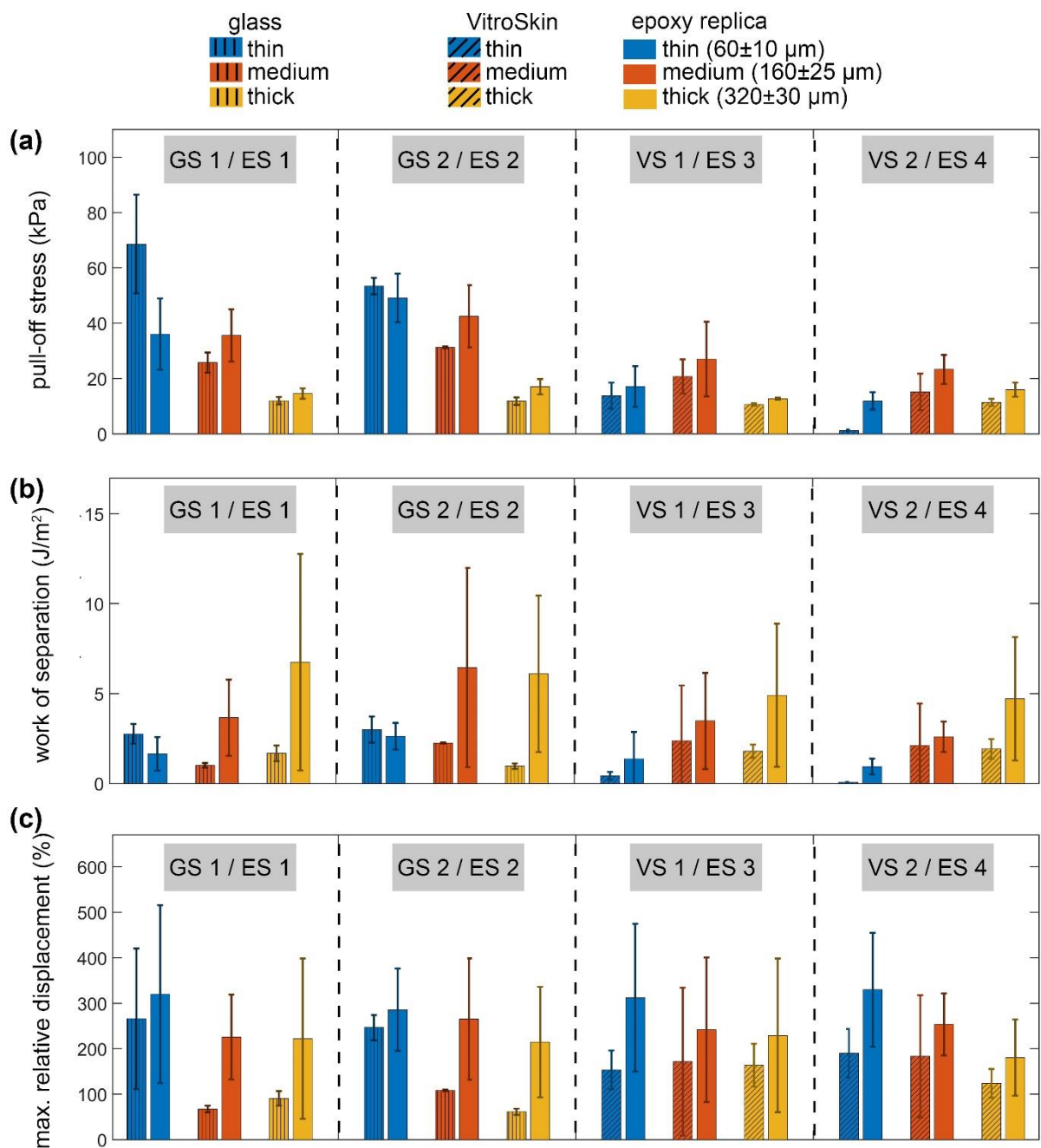
Detachment occurred with cavitation and fibrillation as described in many previous studies on debonding of soft, elastic films.^{96,169} We already observed this behaviour for SSA in our previous work.² The large measurement errors in the work of separation and maximum relative displacement arise from the fact that the fibrils elongate very differently for each measurement and can detach at very different time points.

Generally, a slight increase in pull-off stress was observed for both materials with increasing roughness (**Figure S 6.1a**). This is in contrast with classical literature stating that roughness leads to a decrease in roughness. However, these results are comparable with previously reported data.^{2,119}

To compare adhesion to the original VitroSkin and its epoxy replica, we performed adhesion measurements on VitroSkin backside (VS 1) and frontside (VS 2) and their respective epoxy replica, ES 3 and ES 4 (**Figure S 6.1**). VitroSkin (IMS inc., Portland, ME, USA) is a gelatin based synthetic film and has been used to test the influence of humidity, UV exposure and sunscreen function on the properties of the tissue.²³⁵ Chen et.al.²²⁸ demonstrated that the mechanical and tribological properties of VitroSkin are comparable to animal skin. Unfortunately, the surface roughness parameters in the commercially available VitroSkin product cannot be modified.

The pull-off stress was generally found to be smaller on the VitroSkin substrate (**Figure S 6.1a**). The difference was however generally only about 20% with the exception of the thinnest film on VS 2 and ES 4, where the pull-off stress was almost ten times higher on epoxy. Work of separation and maximum relative displacement were also generally smaller on VitroSkin, the discrepancies being more significant than for the pull-off forces (**Figure S 6.1b** and **S 6.1c**).

Taken together, replication in epoxy gave small deviations from values obtained on VitroSkin and glass master substrates in our case. The epoxy replica are, thus, considered suitable to characterize the influence of roughness on adhesion in a reproducible way.



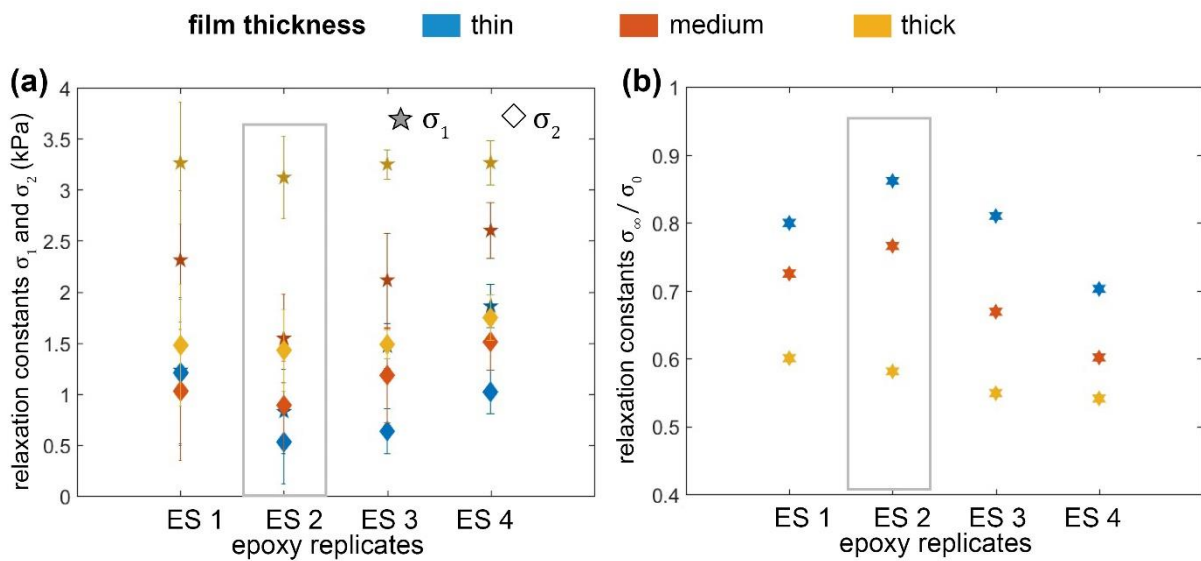
Supplemental Figure S 6.1. Adhesion measurements on glass substrates (GS 1 and GS 2), original VitroSkin (VS 1 and VS 2) and their respective epoxy replica (ES 1 to ES 4). (a) Pull-off stress, (b) work of separation and (c) maximum relative displacement on glass substrates (vertical dashes), VitroSkin (tilted dashes) and epoxy replicas (without dashes) for the different film thicknesses: thin (blue), medium (red) and thick (yellow). Measurements were performed on four independent samples and repeated at three positions of each sample. The error bars show the standard deviation.

6.7.2 Fitting parameters for compressive stress relaxation

Figure S 6.2 shows the fitting parameters σ_1 , σ_2 and σ_0 from the stress relaxation analysis. The parameters σ_1 and σ_2 indicate the magnitude of stress decrease, and generally seem to increase with increasing film thickness. While σ_1 strongly depends on the film thickness with up to three times higher values for the thick films compared to thin films. σ_2 is similar for all films with about 1.2 ± 0.75 kPa. (**Figure S 6.2a**)

Relative to the preload stress, σ_0 , the stress decrease at extended hold times is more significant for thicker films (reaching down to about $0.55 \sigma_0$ for ES 4) than for thin and medium films (**Figure S 6.2b**) with only about 12% and 23% respectively.

All parameters are furthermore listed in **Supplemental Table S 6.1**.



*Supplemental Figure S 6.2. Analysis of the stress relaxation behaviour of the films on different substrates. (a) σ_1 (circles) and σ_2 (squares) and (b) predicted stress decrease $\sigma_\infty \cdot \sigma_0^{-1}$ as a function of substrate and film thickness: thin (blue), medium (red) and thick films (yellow). The values highlighted in grey are the fitting parameters used to reconstruct stress relaxation curves of the three different films on ES 2 in **Figure 6.4** in the main text.*

Supplemental Table S 6.1. Fitting parameters from the relaxation analysis.

	epoxy substrate	σ_{∞} (kPa)	τ_1 (s)	τ_2 (s)	σ_1 (kPa)	σ_2 (kPa)
thin film	ES 1	9.7±1.4	2.7±1.0	56.9±29.0	1.2±0.7	1.2±1.3
	ES 2	8.4±1.1	2.2±0.5	60.4±22.7	0.8±0.4	0.529±0.2
	ES 3	8.9±1.1	2.1±0.3	36.3±12.4	1.5±0.2	0.6±0.2
	ES 4	6.8±0.6	2.1±0.5	53.9±10.0	0.8±0.4	1.0±0.1
medium film	ES 1	8.8±1.4	2.3±0.2	28.4±4.5	2.3±0.7	1.0±0.3
	ES 2	7.9±0.8	2.4±0.2	34.7±5.8	1.5±0.4	0.9±0.2
	ES 3	6.6±1.3	2.4±0.3	33.4±9.9	2.1±0.5	1.2±0.3
	ES 4	6.2±0.9	3.2±0.2	46.8±6.5	2.6±0.3	1.5±0.1
thick film	ES 1	7.1±0.8	2.4±0.3	26.8±2.2	3.3±0.6	1.4±0.2
	ES 2	6.3±0.5	2.3±0.2	26.9±2.8	3.1±0.4	1.4±0.1
	ES 3	5.8±0.3	2.4±0.2	28.4±3.3	3.3±0.1	1.7±0.1
	ES 4	5.9±1.0	2.5±0.2	31.0±2.1	3.3±0.2	1.5±0.1

PART III

Funnel-shaped microstructures

7 Funnel-shaped Microstructures for Strong Reversible Adhesion *

7.1 Abstract

We investigate the potential of a new design of adhesive microstructures in the micron range for enhanced dry adhesion. Using a two-photon lithography system, we fabricated complex 3D master structures of funnel-shaped microstructures for replication into poly(ethylene glycol) dimethacrylate polymer. The diameter, the flap thickness, and the opening angle of the structures were varied systematically. The adhesion of single structures was characterized using a triboindenter system equipped with a flat diamond punch. The pull-off stresses obtained reached values up to 5.6 MPa, which is higher than any values reported in literature for artificial dry adhesives. Experimental and numerical results suggest a characteristic attachment mechanism that led to intimate contact formation from the edges towards the center of the structures. Van-der-Waals interactions most likely dominate the adhesion, while contributions by suction or capillarity play only a minor role. Funnel-shaped microstructures are a promising concept for strong and reversible adhesives, applicable in novel pick and place handling systems or wall-walking robots.

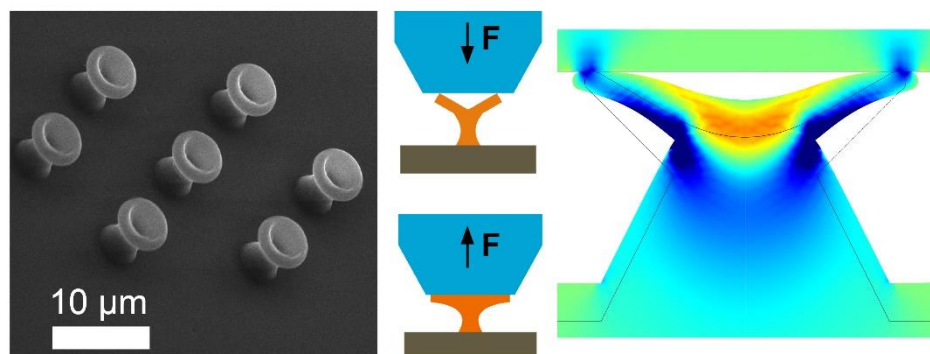


Figure 7.0: Graphical summary of the chapter. Funnel-shaped microstructures were successfully manufactured by two-photon-lithography and subsequent replication. Adhesion measurements were on single structures revealed high pull-off stresses. Numerical simulations of the approach to the substrate were performed to investigate the stress distributions in the structures and at the interface to the substrate.

* This chapter was published in *Advanced Materials Interfaces*:

Fischer, S. C., Groß, K., Torrents Abad, O., Becker, M. M., Park, E., Hensel, R., & Arzt, E. (2017). Funnel-Shaped Microstructures for Strong Reversible Adhesion. *Advanced Materials Interfaces*.

The article is available under: <http://onlinelibrary.wiley.com/doi/10.1002/admi.201700292/full> .

7.2 Introduction

Fibrillar foot pad organs of many animals such as insects, spiders and geckoes exhibit impressive adhesive performance to various substrates and have been studied by many research groups for almost two decades.^{18,236–238} The improved understanding has triggered the desire to mimic the natural principles by creating synthetic, reusable polymer adhesives that show high potential for emerging applications.^{40,49,89,239–243} The key is an optimized surface pattern tailored to the application that can be manufactured by techniques such as lithography, nanoimprint or self-organization.^{241,244–247} Patterned surfaces can exhibit better adhesion compared to non-patterned counterparts, e.g. due to a higher compliance and, therefore, reduced elastic strain energy penalties and a higher conformability to various substrate topographies; these benefits have been termed the “contact splitting” effect.^{18,20,43} The adhesion relies mainly on van der Waals interactions across the pattern-substrate interface. In addition, capillary forces may support the adhesive interaction.²⁴⁸ Van der Waals forces are significant only at short ranges, thus requiring intimate contact between the fibrils and the substrate. Based on the thermodynamic work of adhesion, theoretical pull-off stresses in the range of hundreds of MPa have been estimated.^{249,250} In practice, however, these stresses are typically in the range of several hundred of kPa or below.^{52,251–253} The discrepancy is most likely caused by non-ideal contact and detachment conditions: possible causes are, besides surface roughness, unequal load sharing²⁵⁴, or flaws and local stress concentrations.^{46,59,255,256} Therefore, tailoring the stress distribution along the fibril-substrate interface by reducing such stress concentrations is a major objective in fabricating synthetic fibrillar dry adhesives with high pull-off stresses.

Several experimental and numerical studies have already revealed that the tip shape of the fibrils strongly impacts the stress distribution. A conventional pillar structure with a constant axial cross-section exhibits a stress concentration at the edge of the contact area when the pillar is pulled normal to the surface, which always leads to detachment by edge cracks.^{59,62,256,257} A prominent strategy to reduce the stresses at the edge is a gradual widening of the tip area, i.e., the formation of a so-called mushroom tip. Numerical studies have revealed that the magnitude of the stress singularity at the edge can be decreased by simultaneously increasing the stresses at the center of the contact.^{41,44,256,257} Practically, such a tip can be manufactured using anisotropic etching or by modifying tips of previously manufactured pillar structures, which results in significantly higher pull-off values compared to conventional pillars.^{52,60–62} However, controlled generation of such tips remains difficult.

Another approach to modify the stress distribution is to vary the curvature of the pillar face coming into contact with the substrate. Convex (or conical) tips exhibit a parabolic stress distribution along the interface, but typically show low pull-off stresses due to the rather small contact area.^{42,52,61} In contrast, concave or flat tips lead to higher contact areas in complete contact, thus these microstructures can exhibit larger pull-off stresses.^{45,258} Gao and Yao theoretically demonstrated that such a concave tip geometry can lead to a homogeneous stress distribution.⁴⁶ Their calculations show that the edge stresses are reduced due to the fact that the edges are in compression while the inner contact area remains under tension. However, their approach requires very small curvatures, which are difficult to fabricate. In addition to the above mentioned concepts, triangular⁶³, spatula-shaped^{14,51} and slanted tips^{64,65} have been studied, introducing an asymmetry with potential improvements for directional or even switchable adhesion. Recently, we demonstrated that a combination of soft and stiff materials along the pillar axis improves the adhesion because the stress concentrations are reduced.¹⁷³

Furthermore, the soft component of the pillar, which is in contact with the substrate, may even increase adhesion to rough surfaces.¹

In the present work, we introduce funnel-shaped microstructures that resemble a structural combination of mushroom and concave shaped tips. The microscale structures were fabricated using two-photon lithography and a subsequent replication technique to transfer the pattern into a soft methacrylate-based material. Adhesion of single structures was tested using a triboindentation system and was rationalized in terms of the geometric parameters of the funnel such as opening angle, flap thickness and diameter of the structures. The attachment of the microstructures to the substrate was further observed *in situ* via scanning electron microscopy and theoretically elucidated by numerical simulations.

7.3 Materials and methods

7.3.1 Microstructure fabrication.

CAD models (**Figure 7.1a**) of different funnel-shaped microstructures were designed and generated on a glass substrate using a two-photon lithography system (Photonic professional GT, Nanoscribe, Eggenstein-Leopoldshafen, Germany) and the photoresist IP-L 780 (Nanoscribe, Eggenstein-Leopoldshafen, Germany). Three geometric parameters of the funnel-shaped tips were varied as follows (see **Figure 7.1d**): diameter (5, 10, and 15 μm), flap thickness (1 and 3 μm) and opening angle (90°, 120°, and 180° as a mushroom-shaped control structure).

Upon writing, the structures were developed in propylene glycol monomethyl ether acetate (PGMEA, STBD8433X, Sigma Aldrich, St. Louis, Missouri, USA) for 20 min and subsequently rinsed in isopropanol for 2 min. The IP-L master structures were coated with (1H,1H,2H,2H-perfluorooctyl) trichlorosilane (AB111444, ABCR, Karlsruhe, Germany) in a vapor deposition process to ensure a low energy and non-reactive surface for replication into polydimethylsiloxane (PDMS). IP-L master structures and 50 μl of the silane were placed in a vacuum chamber for about 60 min at reduced pressure and then used without any post treatment. PDMS (Sylgard 184, Dow Corning, Midland, MI, USA) with a mixing ratio of 10 weight parts of the base to 1 weight part of the curing agent was used to manufacture the molds (**Figure 7.1c**). The pre-polymer mixture was degassed under reduced pressure for 5 min at 2000 pm in a SpeedMixer (DAC600.2 VAC-P, Hauschild Engineering, Hamm, Germany), poured onto the master structures and subsequently cured at 75 °C for at least three hours. After demolding, PDMS molds were used to replicate the final structures made from poly(ethyleneglycol) dimethacrylate (PEGdma600; Polysciences, Warrington, PA, USA) with an average molecular weight of 600 g/mol. 0.5 wt% 2-Hydroxy-2-methylpropiophenone (Sigma-Aldrich, St. Louis, MO, USA) was mixed to the oligomer solution as a photoinitiator. A drop of the PEGdma600 oligomer solution was applied to the PDMS mold and covered with a glass slide, flushed with nitrogen for about 20 min and then crosslinked for 300 s by UV exposure (365 nm, Omnicure S1500, Excelitas Technologies, Waltham, MA, USA).

To ensure adhesion of the PEGdma600 microstructures to the glass substrates, (3-methacryloxypropyl) trichlorosilane (AB109004, ABCR, Karlsruhe, Germany) was immobilized to the surface prior to replication. The glass substrates were rinsed in isopropanol and subsequently activated by oxygen plasma for 3 min (PICO plasma system, Diener electronic, Ebhausen, Germany). The substrates were

placed together with 50 μl of silane in a vacuum chamber for about 60 min at a reduced pressure of about 50 mbar. The treated glass slides were stored in darkness and were used within two weeks.

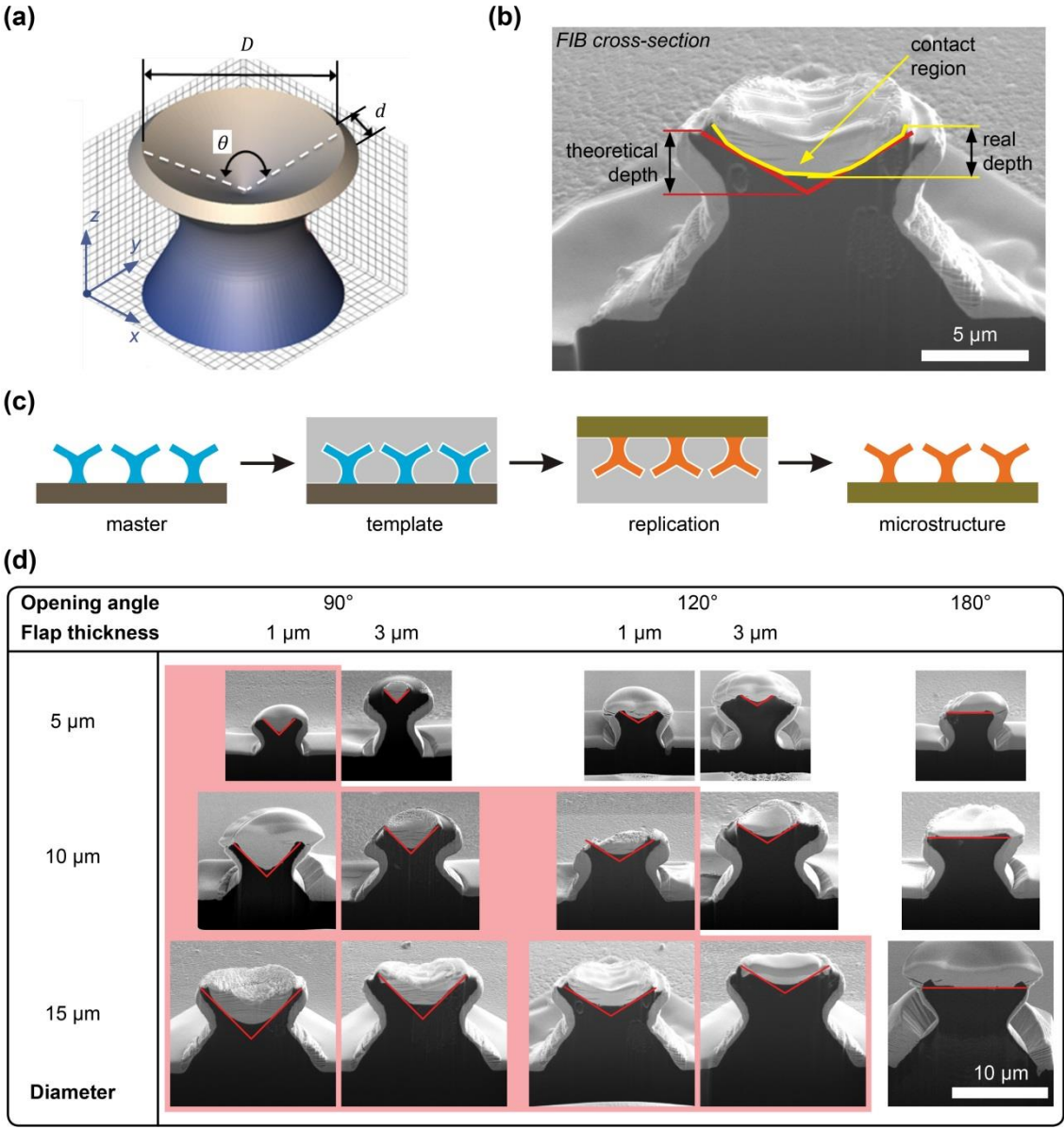


Figure 7.1. Funnel-shaped microstructures. **(a)** 3D-CAD model for two-photon lithography. The diameter, D , the flap thickness, d , and the opening angle, θ , of the funnels were systematically varied. **(b)** Scanning electron micrograph of a FIB cross-section ($D = 15 \mu\text{m}$, $d = 1 \mu\text{m}$, $\theta = 120^\circ$). Bright: platinum deposit. The depicted real structures (yellow contour line) differed from the CAD model (red contour line) due to material shrinkage. **(c)** Schematic of the double molding steps. Master structures (blue) were fabricated using two-photon-lithography on a glass substrate and replicated into PDMS (grey). This template was then used to fabricate the funnel-shaped structures out of PEGdms (orange). **(d)** Secondary electron micrographs of FIB cross-sections. The structures exhibiting pull-off stresses higher than 1 MPa (see Figure 7.3b) are highlighted in light red. The red lines are intended to guide the eye and show the theoretical opening angle.

7.3.2 Adhesion measurements.

Single microstructures were adhesion-tested in ambient conditions (room temperature and 55-60% relative humidity) using a Hysitron triboindenter (TI 950, Minneapolis, MN, USA). The system consisted of a force/displacement-controlled transducer coupled with an optical camera. This allowed for accurate positioning of the sample and recording of force-displacement data. All measurements were carried out with a flat diamond punch (Synton-MDP, Nidau, Switzerland) with a diameter of 50 μm . Each measurement was performed as follows. Flat punch and microstructure were brought into contact and, after a stabilization period of 45 s, the microstructure was compressed. The force was recorded while the punch was attached to the microstructure with a velocity of 240 nm/s until a pre-set compression depth was reached. Then, the position was held for 1 s, and the punch was pulled with the same velocity of 240 nm/s until it detached from the microstructure (**Figure 7.2a**). The maximum force necessary for detachment is the pull-off force, F_p . The pull-off stress, σ_p , was calculated by dividing the pull-off force by the apparent contact area of the structures obtained from SEM characterization. To evaluate pull-off stresses after comparable compressive loading, the indentation depth for each structure was chosen to correspond to the theoretical depth of the cavity as defined by the CAD model. The real depth, however, was slightly smaller due to proximity effects in the two-photon process that led to rounded corners (**Figure 7.1b**). For the structures with 180° opening angle, the indentation depth was chosen to yield similar preload stress compared to the 120° funnel structures.

For *in situ* observation, selected experiments were performed inside a DualBeam scanning electron microscope (SEM) and focused ion beam (FIB, Versa 3D DualBeam, FEI, Hillsboro, Oregon, US) equipped with a picoindenter (PI-87, Hysitron, Minneapolis, MN, USA). These tests were performed under reduced air pressure of approximately $1.5 \cdot 10^{-3}$ Pa.

7.3.3 SEM imaging.

SEM images were taken using the SEM capabilities of the DualBeam. All samples were coated with approximately 3 nm gold layer to eliminate surface charging effects. Focused ion beam cross sections were prepared using the focused gallium ion beam at an accelerating voltage of 30 kV and a current of 3 nA. To protect the microstructures from undesired FIB damage, an approx. 2 μm platinum protective stripe was first deposited on top of each microstructure. This was done using the ion beam induced deposition technique inside the DualBeam at 30 kV and 300 pA.

7.3.4 Numerical simulations.

Finite element simulations were performed using axisymmetric models (Comsol 5.1, COMSOL Inc., Burlington, MA, USA). The geometric parameters of the three selected models in our study were based on real dimensions obtained from the FIB cross sections and digitally rebuilt with Solid Works 2013 (Dassault Systèmes, Vélizy-Villacoublay, France). For the simulations of the attachment, an elastic half-space (substrate) with a Poisson's ratio of 0.33 was compressed along a frictionless contact against the microstructures, which were assigned a Poisson's ratio of 0.44 and an elastic modulus of 175 MPa. The ratio of the elastic moduli between the substrate and the microstructure was 120. The microstructures

were assigned hyperelastic properties based on Neo-Hookean equations. For the mesh generation of the microstructures and the substrate, triangular and square elements were used, respectively. The contact was formulated as a Lagrangian contact and the substrate was defined as the receiving part of contact. The stresses within the structures as well as the stresses induced in the substrate were extracted from simulations and qualitatively analyzed with regard to the deformation behavior of the microstructures and the evolution of stress distributions along the microstructure-substrate interface.

7.4 Results and discussion

Funnel-shaped microstructures were successfully manufactured in a two-step process as shown in **Figure 7.1c**. A master template containing all 16 different microstructures was generated using two-photon lithography. By placing all structures on each sample, inhomogeneities and deviations induced by the manufacturing process and errors in the adhesion measurements induced by misalignment could be reduced. Cross-sections of all replicated microstructures were prepared to determine the real dimensions and the contact areas, which were further used to calculate pull-off stresses (**Figure 7.1b** and **7.1d**).

A typical force-displacement curve obtained for a funnel-shaped microstructure is pictured in **Figure 7.2a** and can be divided into three characteristic regimes:

- Regime 1: During attachment, the compressive loading curve first exhibits a small slope that relates to elastic deformation and bending of the flaps. This slope ($15.7 \mu\text{N}/\mu\text{m}$) corresponds to an initially high compliance of the microstructures.
- Regime 2: With increasing load, the stiffness of the microstructures drastically increases, which is represented by a steeper slope ($101.3 \mu\text{N}/\mu\text{m}$). In addition to the deformation of the flaps, the stem of the microstructure was elastically deformed.
- Regime 3 corresponds to the unloading of the structures, which finally leads to detachment. ($156.8 \mu\text{N}/\mu\text{m}$)

Adhesion measurements were repeated on each structure without significant damage or plastic deformation as shown in the **Supplemental Video**. In contrast to mushroom-shaped microstructures, the pull-off stress of funnel-shaped microstructures depended on the indentation depth as exemplarily shown in **Figure 7.2b**. A similar behavior has already been reported for micropillars with concave faces by del Campo *et al.*⁴⁵ In fact, the initial contact of the flaps to the substrate led to an insignificant contact area with negligible adhesion. Only upon bending and stretching of the flaps did the whole structure form intimate contact with the substrate and were high pull-off forces obtained as reported in **Figure 7.2b**.

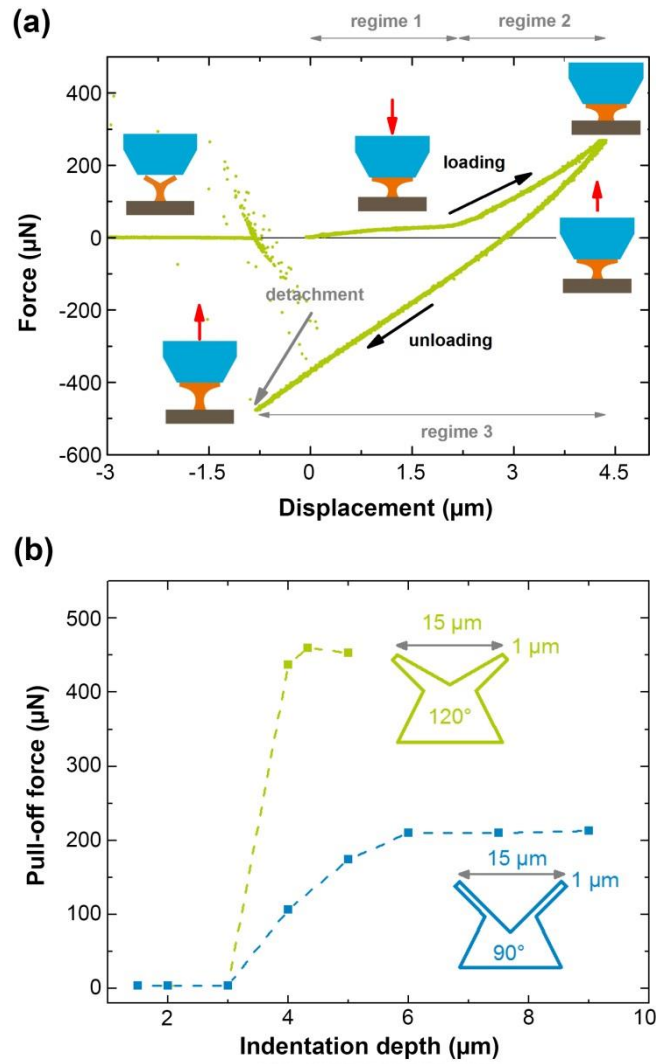


Figure 7.2. Typical force-displacement curve and pull-off force as function of indentation depth. **(a)** The compressive loading curve (positive force) often comprises two parts with different slopes corresponding to bending of the flaps (regime 1) transitioning into compression of the whole structure (regime 2). The unloading curve (negative force values, regime 3) terminates in a maximal tensile force indicating the pull-off force. The scattered data upon detachment are artifacts due to vibrations of the indenter. **(b)** Pull-off force as a function of the indentation depth for two PEGdma600 microstructures with 15 μm diameter, 1 μm flap thickness and opening angles of 120° (green) and 90° (blue).

Figure 7.3a shows the force-displacement curves for structures with different opening angles but similar diameter ($D = 15 \mu\text{m}$) and flap thickness ($d = 1 \mu\text{m}$). Both the 120° and 90° structure exhibited the three characteristic regimes described above, while for the 180° structure, i.e., the mushroom structure, regime 1 could not be detected, as expected. For regime 3, a very similar behavior of all microstructures was obtained, characterized by an almost linear initial decrease in stress (2.39 MPa/μm for the structures with 15 μm diameter) and similar initial slopes of the unloading curves irrespective of their opening angles. This observation indicates that the contact stiffness of the attached microstructures was similar. For the structures with an opening angle of 120°, the unloading curve until detachment is almost linear; this indicates that the contact area remained constant because partial detachment or crack propagation would result in a decrease of stiffness. For the structures with

90° opening angle, we observed a gradual decrease of stiffness during unloading, which most likely reflects a continuous detachment.

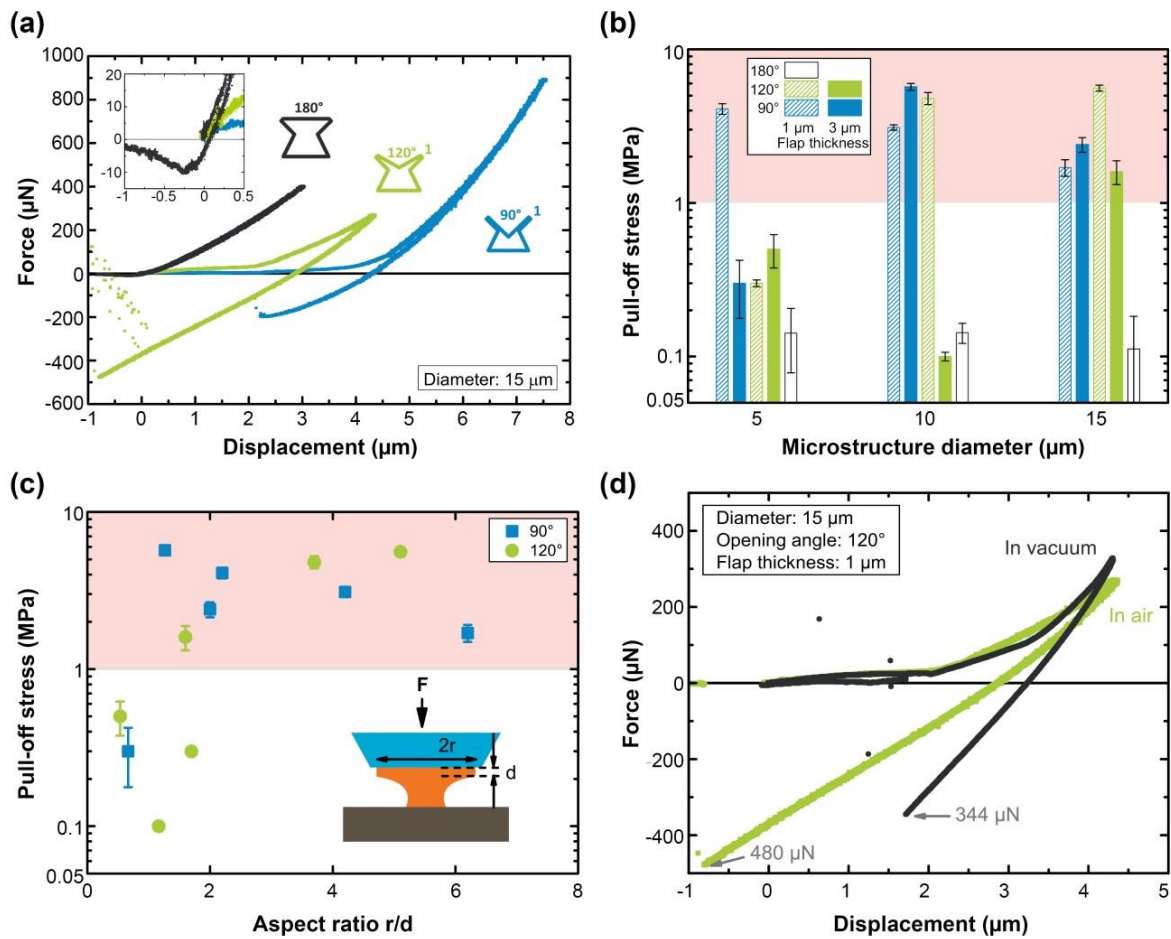


Figure 7.3. Detachment behavior measured for the different microstructures. **(a)** Force-displacement curves for microstructures with diameter of $15\ \mu\text{m}$ and flap thickness of $1\ \mu\text{m}$ and different opening angles of 180° (black), 120° (green) and 90° (blue). The insert shows the force-displacement curve of the mushroom-shaped structure (opening angle 180°) in detail. **(b)** Pull-off stresses as a function of diameter, flap thickness and opening angle. Results for $1\ \mu\text{m}$ and $3\ \mu\text{m}$ flap thickness are shown in shaded and full color, respectively. **(c)** Pull-off stresses as a function of aspect ratio, i.e. contact radius divided by flap thickness, for opening angles of 120° (green, circles) and 90° (blue, squares). The light red area highlights the pull-off stress ranging above $1\ \text{MPa}$ in both (b) and (c). **(d)** Force-displacement curve under ambient conditions (green) and under reduced pressure at about $1.5 \cdot 10^{-3}\ \text{Pa}$ (dark green), both performed in situ with the picoindenter. Reported values represent the pull-off forces.

The determined pull-off stresses are shown as a function of size and shape of the microstructures in **Figure 7.3b**. For example, microstructures with $15\ \mu\text{m}$ diameter and $1\ \mu\text{m}$ flap thickness and opening angles of 90° and 120° exhibited pull-off stress values of $1.7 \pm 0.2\ \text{MPa}$ and $5.6 \pm 0.2\ \text{MPa}$, respectively. That is one order of magnitude larger compared to $112 \pm 7\ \text{kPa}$ for the mushroom-shaped structure with 180° opening angle as a control. To provide an overview of the geometric variations, cross-sections of all structures are shown in **Figure 7.1d**. Funnel-shaped structures with comparable compact tip shape, for example, diameter of $5\ \mu\text{m}$ and flap thickness of $3\ \mu\text{m}$, resulted in low pull-off

stresses most probably due to insufficient flexibility of the flaps. The flexibility of the flaps increased with higher flap length to thickness ratio, which, in turn, enabled intimate contact and, therefore, high pull-off stresses. **Figure 7.3c** illustrates the relationship between the pull-off stresses obtained and the aspect ratio, defined as the radius of contact divided by the flap thickness, for all geometries. For aspect ratio of two and more, the structures exhibited pull-off stress values higher than 1 MPa as highlighted by the light red boxes in **Figures 7.1d, 7.3b** and **7.3c**.

The shape of the microstructures might lead to the conclusion that the main contribution to adhesion is based on suction. However, the adhesive stress induced by suction, σ_{suc} , is limited by the atmospheric pressure of $p_{atm} \approx 100$ kPa. Hence, its maximal contribution to the pull-off stress is more than one order of magnitude smaller than the values obtained. In addition, experiments comparing adhesion under normal and reduced pressure of about $1.5 \cdot 10^{-3}$ Pa were performed *in situ* with the nanoindenter. The pull-off stress obtained was only 30% lower than under ambient conditions as shown in **Figure 7.3d**, which demonstrates that suction plays an insignificant role.

Due to the hydrophilic nature of the polymer material, capillary forces might contribute to the adhesion.²⁵⁹ The adhesive stress induced by capillarity, σ_{cap} , can be estimated as follows: $\sigma_{cap} \approx \frac{2L\gamma\cos\theta}{2A} + \frac{2\gamma}{R}$, where L is the length of the three-phase contact line, γ is the surface tension of water, θ is the contact angle, A is the contact area and R is the radius of the fluid meniscus. We assume ideal wetting ($\theta = 0^\circ$), a thickness of the fluid film, h , that is much smaller than the radius of the meniscus ($h \approx R/100$) and use values from FIB cross sections to determine the contact area. The resulting estimate of a capillary contribution is about 50 kPa, which is significantly smaller than the measured pull-off stresses.

Interestingly, the pull-off stresses obtained exceed by far the values of mushroom-shaped microstructures reported here and in the literature.^{260,261} Such a result is unexpected because deformation of the flaps stores elastic energy, which could act against interfacial adhesion. The following possible explanations can be put forward:

1. Increase of real contact area: The highly compliant flaps may lead to better adaptation of the structures to slight irregularities on the substrate surface or to small misalignments. Particularly, the gradual contact formation from the edge of the flaps towards the center of the structure most likely ensures intimate contact over the whole contact area. This can possibly increase the real contact area over the case of mushroom structures with the same diameter in contact. In the unloading regime, the prior deformation of the flaps might induce frictional components that further increase adhesion as known from insects⁷, geckoes²⁶² and artificial systems.²⁶³
2. Stress distribution: Funnel-shaped microstructures exhibit compressive stresses at the edge of the structure. As will be shown below, the magnitude of stress singularities at the edge is most probably reduced, which can have a beneficial impact on the pull-off stress.⁴¹

Figure 7.4a shows the normal stresses in vertical direction at selected deformation steps for different opening angles. For the mushroom structures (opening angle of 180°), normal stresses were highest at the center and reduced at the corner of the structure immediately upon contact (indentation depth 1000 nm), in agreement with literature.^{41,256,257} For the funnel-shaped microstructures, the results demonstrate the elastic flap deformation in accordance to the previously described regime 1 (**Figure 7.2a**). At the beginning of the compressive loading, the structure exhibited only a small contact area. With increasing indentation depth, the flaps deformed and induced two opposing stress regions,

i.e., a tensile stress field on the substrate-facing side of the flaps (red region) and a compressive stress field on the opposite side (blue region). Between both regions, a stress-free zone formed. The compressive stresses in the stem were lower compared to the mushroom structure. In addition to the stresses inside the structures, the interfacial stresses varied characteristically between the funnel-shaped structures and the mushroom structures (**Figure 7.4b**). For the mushroom structure, the maximum interfacial stress was always located close to the center (I). In contrast, the flaps of the funnel-shaped structures induced an interfacial compressive stress concentration (II) that shifted radially from the edge (i.e., the location of initial contact) towards the center (III), while the contact area increased simultaneously. For similar indentation depths, the stress distributions of the 120° and 90° structures differ in magnitude and lateral position of the stress minima. For the 90° structures, small normal stresses reflect the high compliance of the structure during attachment in regime 1 in accordance to the experiments (**Figure 7.3a**). In addition, shear stresses resulting from the radial elongation of the flaps might also play an important role in adhesion, but could not be captured with our calculations.

Gao *et al.*⁴⁶ reported on concave tip curvatures as a structural concept for uniform interfacial stress distribution by reducing corner singularities in particular. In their theoretical work, adhesion of pillars with concave faces and varying pillar size was calculated. For small pillar diameters (< 100 nm), the pillars formed complete contact with the substrate immediately upon contact without preload. For larger pillar diameters (> 100 nm), in contrast, complete contact could be only established upon exceeding a certain threshold of preload (or indentation depth), which is in accordance with our experimental findings and previous reports.^{45,264} In addition to the concave curvature, the funnel-shaped microstructures exhibit flaps similar to that known from mushroom-shaped structures. We believe that the funnel-shaped microstructures combine the structural concept of concave-shaped pillars with that of mushroom structures to result in high pull-off stresses. However, the attachment process to the substrates including the transition from a non-adhesive to a highly adhesive state is of fundamental importance in understanding these structures.

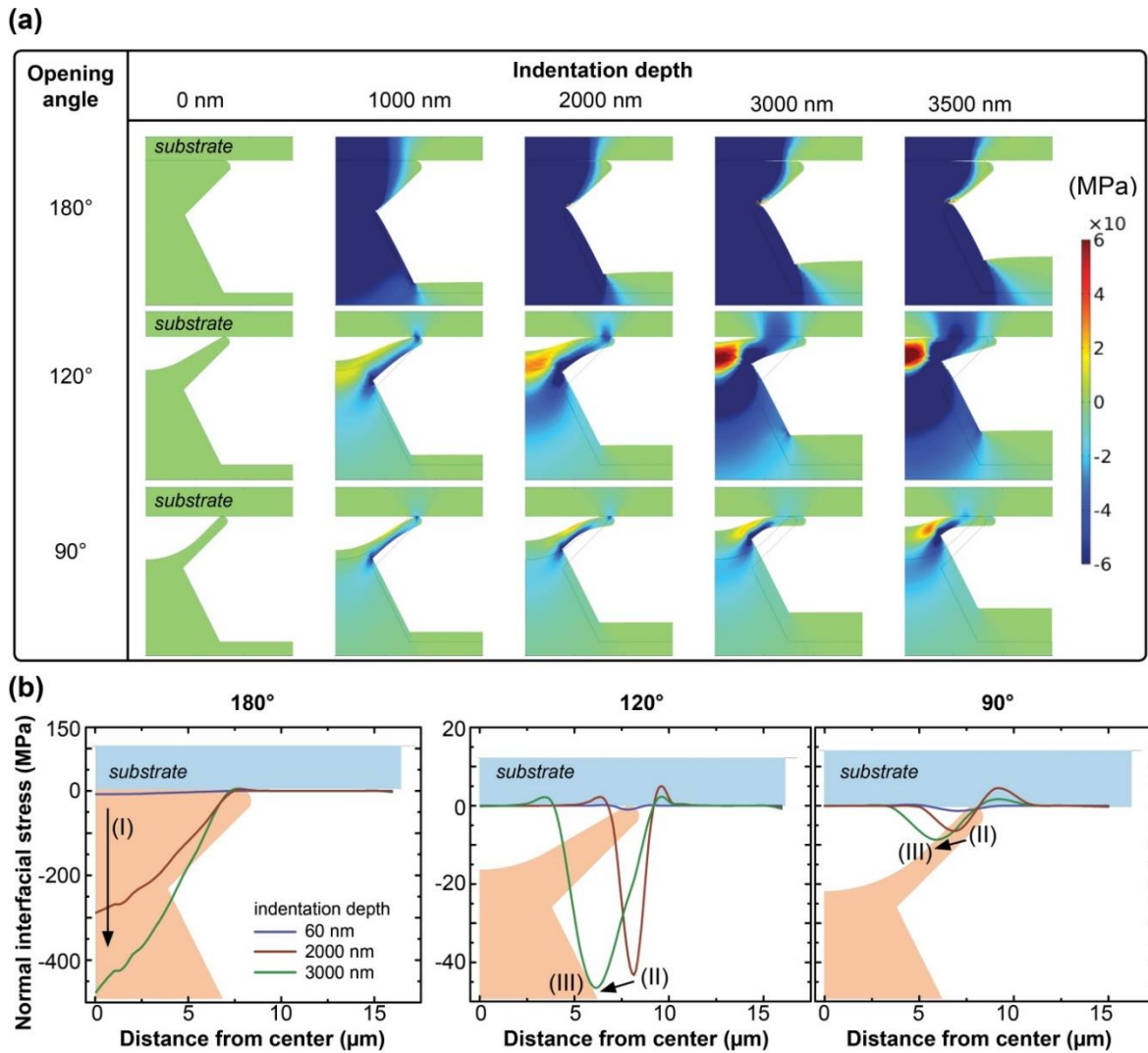


Figure 7.4. Results of finite element simulations. **(a)** Normal stresses inside the microstructures, with different opening angles, and the substrates at different indentation depths. During attachment (compressive pre-loading), the images represent a half cross-section of the axisymmetric FE model. Maximal compressive and tensile stresses are shown in blue (negative) and red (positive), respectively. Neutral stress regions are shown in green. **(b)** Normal interfacial stress as function of indentation depth: 60 nm (blue), 2000 nm (red) and 3000 nm (green). The characteristic features and trends of the stress distributions are marked with arrows.

7.5 Conclusion

In the present work, we introduced funnel-shaped microstructures as a novel structural concept for strong and reversible patterned adhesives. We successfully demonstrated the generation of such structures using two-photon lithography and nanoimprint technique.

In summary, we can conclude:

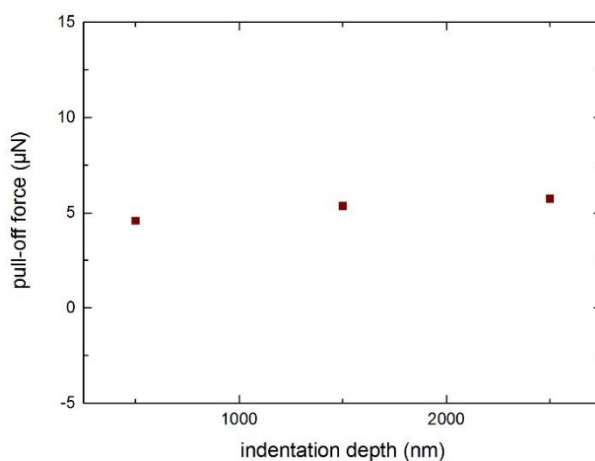
- The pull-off stresses obtained reached values up to 5.6 MPa for single microstructures, which is, to the best of our knowledge, higher than any values reported in literature for artificial dry adhesives. It is expected that also arrays of funnel-shaped structures will surpass arrays with other geometries although arrays generally tend to show lower adhesion than single microstructures.²⁵⁴
- Tests under reduced pressure revealed that most probably van-der-Waals interactions contribute to the adhesion, while contribution of suction and capillarity play only a minor role.
- The flexibility of the flaps provides high compliance during contact formation that helps to accommodate surface irregularities and even small misalignments between the structure and the substrate.
- The exceptionally high adhesion is very likely based on an enhanced real contact area due to gradual attachment from the edge toward the center of the structure. We also argue that the interfacial stress distribution is more conducive to adhesion in these structures.
- Our funnel-shaped microstructures resemble a synthesis of concave tip curvature as theoretically advanced by Gao⁴⁶ and mushroom-shaped structures including highly compliant flaps for intimate contact formation and strong adhesion.

The paper shows that substantial improvement of dry micropatterned adhesive can still be expected from structure designs with optimized shapes.

7.6 Supplemental information

7.6.1 Indentation depth dependent adhesion of mushroom structures.

The influence of the indentation depth on the pull-off stress for mushroom structures (i.e. 180° structures) is shown in **Supplemental Figure S 7.1**. In contrast to funnel shaped structures, no dependency on the indentation depth was observed upon first contact. Thus, we chose the indentation depth for each diameter in order for the preload stress to be comparable with the preload reached for the 120° funnel structures.

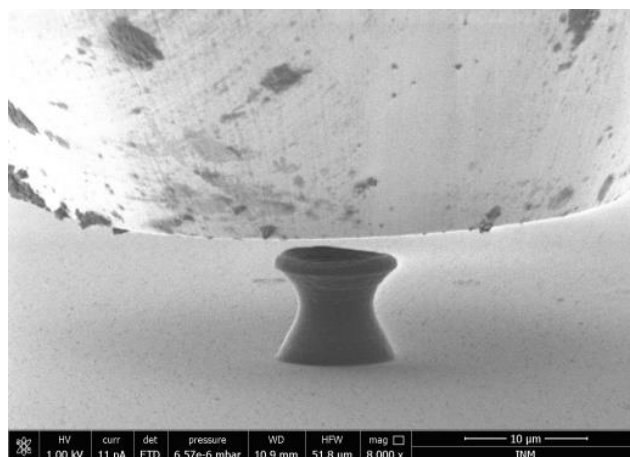


Supplemental Figure S 7.1. Pull-off force as a function of the indentation depth for PEGdma600 mushroom structures (i.e. 180° structures) with 10 µm diameter are shown.

7.6.2 In-situ compression of funnel-shaped structures

The video demonstrating the reversible attachment of the funnel-structures can be found online under:

<http://onlinelibrary.wiley.com/store/10.1002/admi.201700292/asset/supinfo/admi201700292-sup-0002-S2.avi?v=1&s=4b6ee556b8de4d706dc5abaa7d6c6d5c7ea3a2f2>



Supplemental Figure S 7.2. Still image of the video demonstrating the reversible attachment and detachment of a funnel-shaped structure inside an SEM.

Discussion

8 Discussion

While, a few decades ago almost all assemblies were held together by fasteners like screws and bolts, the importance of adhesives has grown with the evolution and miniaturization of technology. Structural adhesives and pressure sensitive adhesives are at present indispensable in, for example, electrical devices, and in a variety of other applications where lightweight design is critical. Bioinspired structural adhesives are, however, not yet widely used in applications. Their fields of application will be based on their primary asset, namely reusability with damage neither to the adhesive nor to the substrate. Robotics, biomedical innovations, and wearable electronics are amongst the fields that could greatly benefit of the further research in this area. Potential applications include innovative pick-and-place technology, functional implants, or wound dressings. Furthermore, adhesives containing electronics could be worn on the skin without impeding the haptic perception and enabling, for instance, the remote control of mobile phones by touch interaction. Many limitations still have to be overcome, one being the substrate roughness.

Inspired by the blueprints found in nature, different strategies to create new functional adhesives were investigated in this work (**Figure 8.1**). While **Part I** and **Part II** focused on the mechanical properties of materials to tune adhesion, the change of the shape is used to tune adhesion in **Part III**.

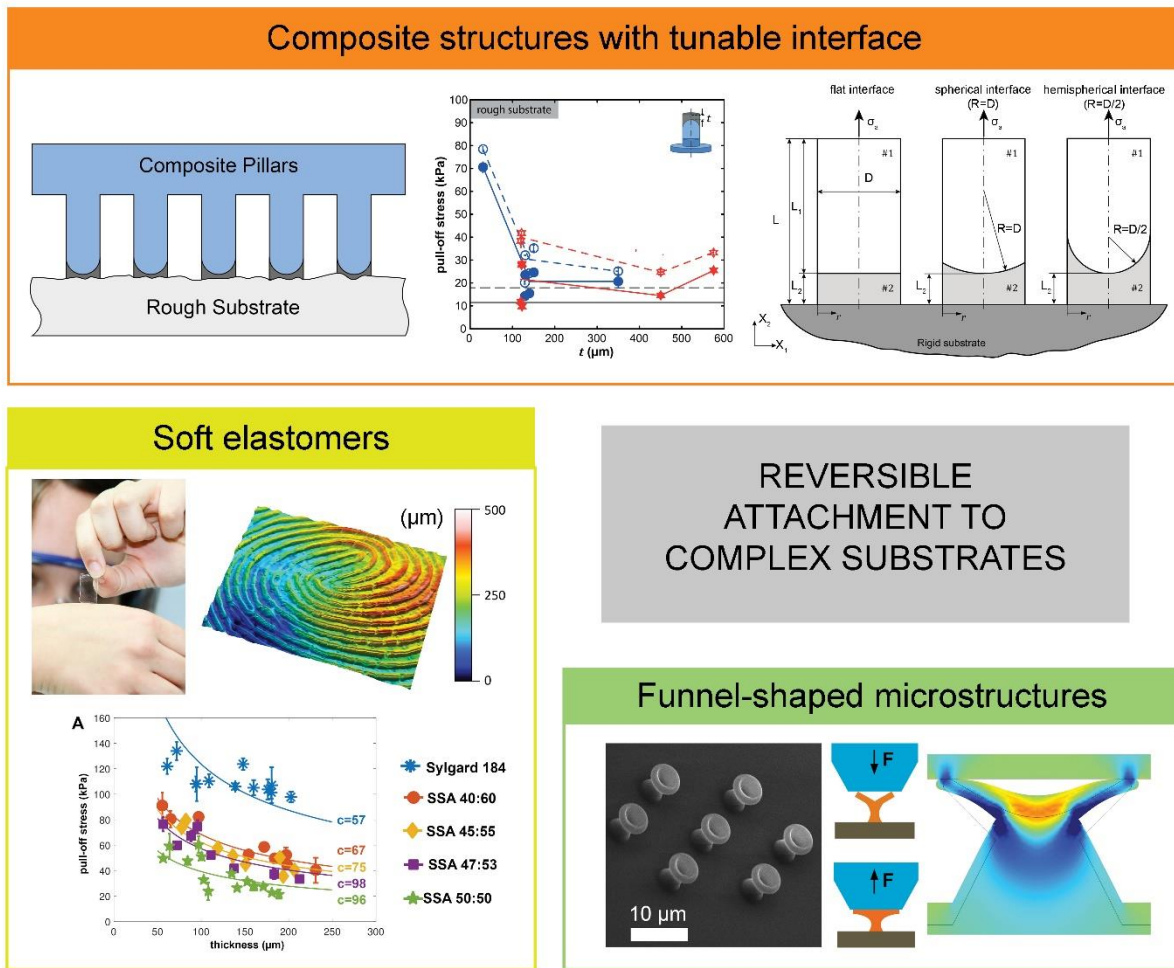


Figure 8.1. Graphical summary of the present work. **Part I (Chapter 4)** focuses on composite structures with tunable interface. Normal adhesion measurements as well as finite element simulations revealed increased pull-off strength with decreasing tip thickness, increasing elastic modulus ratio and a strong influence of the interface curvature. **Part II (Chapter 5 and 6)** concentrates on characterization and evaluation of soft elastomeric materials for application as skin adhesive. A systematic investigation of the influence of mixing ratio and film thickness on the pull-off stress was performed followed by a study on the influence of substrates with skin-like roughness. **Part III (Chapter 7)** presents a tip shape concept, funnel-shaped microstructures, to enhance compliance of currently used mushroom-shaped structures. Master structures were fabricated using two-photon-lithography, replicated in PEGdma and their adhesion tested using a nanoindentation setup. Additionally, finite element simulations were performed to visualize the deformation of the structures with different geometrical variations. Images reprinted with permission from ^{1-3,173}.

8.1 Discussion and Outlook

The macroscopic composites presented in **Chapter 4** display an example of dry adhesives where the tip shape does not govern adhesion strength. In contrast, at its origin is the combination of a soft and a stiff **material**. The soft material is responsible for adaptation to surface roughness. The stiffer material provides stability and is also responsible for the translation of the applied preload to the soft terminal layer, where the deformation is highest. Pull-off stresses of up to 80 kPa on smooth and rough glass were observed following detachment by propagation of a center crack. The increased pull-off stresses and different detachment mechanisms can partly be explained by the modified **stress distribution** between adhesive structure and substrate. Preliminary simulations showed that the composite structures with thin terminal layer reduced the magnitude of the stress singularity at the edge of the contact zone. Additionally, the stress in the center dramatically increased for composite structures with curved interface and thin tips, which yielded a stress concentration and a circular crack front initiating at the center of the contact zone. A detailed numerical study on the effect of elastic modulus ratio, curvature of the interface and tip thickness on the stress distributions emphasizing on the analysis of the magnitude of the edge stresses was performed by Balijepalli et al.¹⁷³

Composite structures were shown as a promising concept to circumvent current limitations of mushroom shaped structures on rough surfaces. Manufacturing multi-material structures with a simple overall geometrical shape opens up new designs for dry adhesives. The limitations of single-material systems include a trade-off between stability of the structures and mechanical properties, as collapse limits the use of very soft materials.^{145,265,266}

In the wake of our publications (Fischer et al.¹ and Balijepalli et al.¹⁷³), two more concepts for multi-material composite structures were published by Gorumlu et al.²⁶⁷ and Drotlef et al.²⁶⁸. Gorumlu et al.²⁶⁷ proposed to introduce a thin soft layer of polyurethane with an elastic modulus of about 172 kPa on polyurethane mushroom structures with an elastic modulus of about 8.9 MPa at the micron-scale to result in a stiffness gradient, the so called “functionally graded structures”, similarly to the work by Bae et al.⁴⁹. They were able to demonstrate that the pull-off stress of their composite structures was not dramatically affected by surface roughness of glass substrates (RMS in the range of 54 to 408 nm), and was over three times higher compared to the monolithic control samples on the roughest substrate. They found that a thicker soft layer ($t \approx 7 \mu\text{m}$) yielded better adaptation to the rough surface and higher pull-off stresses compared to thinner tips ($t \approx 4 \mu\text{m}$), proposing as an explanation partial contact formation and lower stored elastic energy.

Drotlef et al.²⁶⁸ proposed a concept for very similar composite mushrooms for application as wearable sensor on skin. Their approach is based on a soft, medical grade vinylsiloxane as tip material, applied by inking, but then cured directly against the skin to achieve optimal conformation to the roughness. After optimization of the structure geometry and manufacturing process, their structures exhibited high adhesion strength of up to 18 kPa to human skin. Furthermore, the authors demonstrated that strain sensors could be integrated in the adhesive to measure signals such as breathing with a very low signal-to-noise ratio. Multiple use of the structures is however only possible after a new inking and curing step, as the roughness of the skin is transferred on the microstructures, and thus prevents reuse.

Although several concepts for macro- and microscale composite structures exist at this point, the present work is to the best of our knowledge the only approach using the interface geometry to

enforce specific crack mechanisms to enhance adhesion. Therefore, it would be of great interest to downscale the structures to the micron-scale so as to increase the overall array size. This would allow for composite structures to be employed in large-scale applications requiring adhesion to rough surfaces. In the papers, design guidelines for downscaling were identified through experiments¹ and numerical simulations¹⁷³, however no manufacturing process has yet been established.

While the composite pillars with tunable interface presented in **Chapter 4** as well as the regular mushroom-shaped structures have a tip parallel to the substrate, and thus a relatively constant contact area, the funnel-shaped structures presented in **Chapter 7** utilize their **flexible tip** to achieve high adhesion strength. The tip contributed to the adaptation to substrates and lead to an increase of the contact area with increasing preload up to a plateau. Compared to other single-material dry adhesives in literature, the funnel-shaped structures show over an order of magnitude higher adhesion stresses on smooth substrates in air. These structures have been shown to maintain function in vacuum when suction-based attachment structures will not.

Future investigations will need to show whether the concept of funnel-shaped structures can be **upscaled** and what **application fields** it can be tailored to. Further optimization of the geometry and material will possibly yield even higher adhesion stresses. This optimization will not only necessitate trying out new structure parameters, but will also aid addressing several outstanding questions. For example, it is not intuitive that the high strain induced in the tips is conducive to the high adhesion strength. Additionally, the shape is expected to yield an inbuilt defect in the center of the contact area. The simulations presented in **Chapter 7** suggested that a frictional component might play a role in the adhesion process, but further simulations will be necessary to confirm this hypothesis.

Through **Chapter 4** and **Chapter 7**, the importance of the **combination of experiments and numerical simulations** in the design process of dry adhesives was shown. The possibility to evaluate a wide range of parameters and thus assess promising parameter combinations for experiments is unprecedented. However, the analysis of simulations can be ambiguous. In **Chapter 4**, the stress distributions were only analyzed qualitatively. In the more detailed study by Balijepalli et al.¹⁷³, the simulations were evaluated mainly regarding the magnitude of the stress at the edge of the contact, and do not provide a full explanation for the different detachment mechanisms. Firstly, the model was axisymmetric, and can thus not describe non-axisymmetric crack propagation such as finger-like cracks. Secondly, the simulations are based on small strains and focus on the stress distribution before crack initiation. The physical foundation of the model utilized to estimate adhesion strength is based on crack initiation at the edge, and thus does not cover the case of center cracks. In **Chapter 7**, the stress distribution was analyzed at different indentation depths, i.e. time points, but is restricted to the approach of structure and substrate. Here, a more complex simulation with several steps would be interesting to gain information about the stress distribution during the retraction, considering the stress states induced during approach.

Due to the possible occurrence of countless different **failure mechanisms**, it is difficult to predict adhesion strength and crack type solely based on numerical simulations. Even with the many models in existence, it is still not entirely clear what an “optimal stress distribution” looks like and how to achieve it, especially taking into account roughness. Thus, it is extremely important to combine

experimental work and numerical simulation with suitable analytical models to further the knowledge regarding this topic and contribute towards the field of adhesives.

In **Part II**, comprising **Chapter 5** and **Chapter 6**, the normal adhesion measurements of unstructured elastomeric films were analyzed. The results take into account numerous material, substrate and experimental parameters as well as surface treatments. One of the motivations for **Part II** of the thesis was to contribute to the fundamentals and material selection for future adhesives which are gentle in their interaction with the body, for instance for wound management or wearable interfaces, by furthering the knowledge about the underlying mechanisms. Biomedical adhesives are, however, very challenging due to the multitude of functions the adhesives have to fulfil. It was therefore not possible to address all those in the present thesis, especially concerning the upscaling and in-vivo testing. Some insights into further efforts in this area will be elaborated in the next paragraphs, thus integrating the research in a broader context.

As it is not yet possible to manufacture microstructured composite patches with all necessary requirements, a **simplified model system** consisting of two layers without microstructure, the backing layer and the adhesive layer, was used for preliminary experiments.²⁶⁹ The composite film was manufactured via two consecutive doctor blade applications based on the process described in **Chapter 5** and **Chapter 6**. An example of an adhesive is shown in **Figure 8.2a**. With this process, the film thicknesses of adhesive layer and backing layer can be varied independently. To illustrate the **adaptation to skin** of different layer thicknesses, three different patches with similar backing layer thickness of about 30 μm and three different adhesive layer thicknesses were manufactured and applied to skin (**Figure 8.2b**). Due to the overall low thickness of the patches, all conform and adhere well to skin. However, it is visible that the thickest patch does not fully adapt to the wrinkles while the two thin patches seem to adapt very accurately to the surface roughness profiles.

Such silicone patches were recently successfully used in animal experiments as **artificial grafts for tympanoplasty** in a collaborative experiment between INM (Dr. K. Kruttwig) and the University Clinic of Saarland University (Dr. G. Wenzel). The soft layer thickness was chosen in line with the experiments presented in **Chapter 6**. On the basis of the findings from **Chapter 5** and the requirements for the application as tympanic membrane patch, more comprehensive studies of the **biocompatibility** of the SSA material and how it can be influenced by either **plasma treatment or protein adsorption** were carried out by M. Danner^{270,271} and S. Boyadzhieva²⁷² in the framework of their Bachelor thesis and student internship report. Both works show that surface modification of the elastomer can significantly increase biocompatibility, but the influence on the adhesion behavior must always be regarded at the same time.

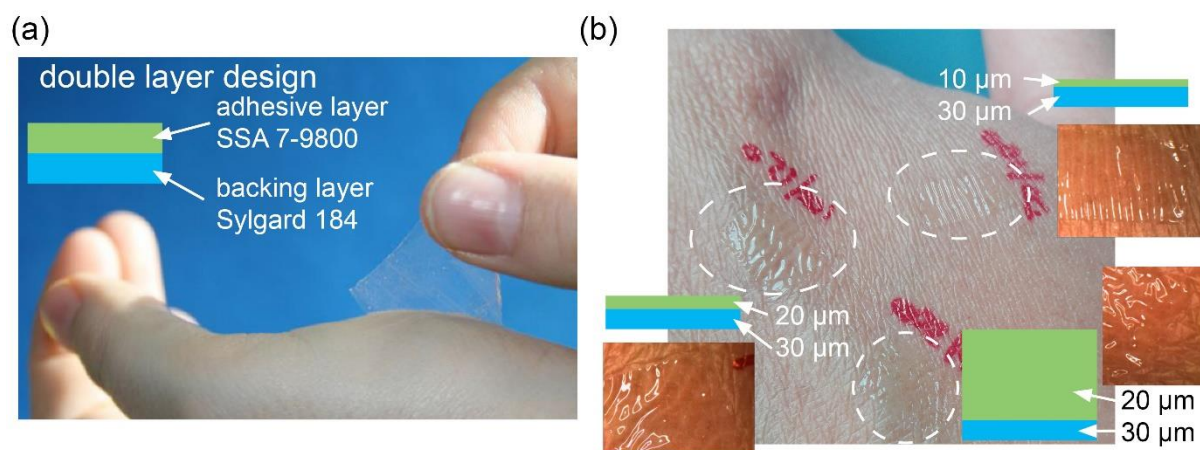


Figure 8.2. Model-system for adhesive patches. (a) Schematic and picture of the double-layer dry adhesive with a backing layer made of Sylgard 184 and adhesive layer made of Soft Skin Adhesive MG 7-9800 (both from Dow Corning, Auburn, MI, USA). (b) Patches with different layer thicknesses resulting in varying bending stiffness applied on a human hand. The three patches were manufactured with similar backing layer thickness of about $30\ \mu\text{m}$ Sylgard 184 and different thickness of the adhesive layer of about $10\ \mu\text{m}$ (top right), $20\ \mu\text{m}$ (left) and $80\ \mu\text{m}$ (bottom right). The patches with thicker layer cannot replicate the surface topography of the skin while the thinner patches are able to follow very intimately the topography of the wrinkles.

In **Chapter 4**, **Chapter 5** and **Chapter 6** we studied the detachment behavior and adhesion strength of soft elastic materials from surfaces with a wide range of **roughness**. Generally, roughness is known to negatively influence adhesion strength, but adhesion can sometimes actually benefit from roughness. In the case of the composite structures presented in **Chapter 4**, material properties and interface geometry determine the crack type. Center cracks seemed particularly conducive for high adhesion strength on both the smooth and rough surface, and could be initiated by composites with thin tip layer and high elastic modulus ratio, where adhesion strength reached on the smooth and rough substrate was similar. The substrate roughness did not inhibit center crack formation, and higher roughness even yield increased pull-off stresses at elongated hold times compared to the smooth substrate. In the case of the center crack, a void forms in the center of the contact area and expands towards the edge of the contact zone. Reduced pressure inside the cavities and a resulting suction effect might contribute to the adhesion strength. This would however require good sealing in the outer contact zone to reduce diffusion of gas. On rough substrates, a perfect sealing and contact is unlikely. Despite this, it may even contribute to the high adhesion strength by inducing local stress concentrations thus favoring crack propagation in a desirable region or reducing the propagation velocity locally.²³³

In **Chapter 6**, pull-off stress on substrates with small roughness was higher than on the smoothest substrate for elastomeric films of different thickness. When the roughness asperities are very large compared to the film thickness, the asperities locally create defects, reduced contact area and high stored elastic energy, yielding a drastic reduction in contact area or high elastic deformation.²⁶⁷ However, when the roughness is small compared to the film thickness, it can also positively influence adhesion by generating local gradients in strain energy having a dissipative effect in crack growth and

thus acting contributing to crack trapping. Similar observations have been reported by many authors.^{120,233,273,274}

Making **versatile adhesives** that are at the same time strong and yet easy to detach on a variety of surfaces is still a big challenge. However, in many approaches to design fibrillar adhesives, a key aspect is left out of consideration: The substrate roughness does not always have to be a challenge, but can also be part of the solution. As fibrillar adhesives use the principle of contact splitting, asperities on rough surfaces could potentially be used to trap cracks and guide detachment. This gives rise to new possibilities, but also necessitates even more understanding of the underlying mechanics and the interfacial processes between adhesive and rough substrates during detachment. In optimizing these designs, many variables can be tuned and finding the sweet spots of this multivariate problem is a real challenge.

A **complex optimization problem** arises with two very different approaches to solve it:

- Make a system with sufficient adhesion on a multitude of substrates and avoid sweet spots as this does not make adhesives versatile
- Optimize system for highest performance on a specific surface and find the sweet spots

While making universal adhesives might be a good option for some applications, industrial and high-tech applications will certainly rely on optimized, specialized solutions that fulfil several functions at the same time. Especially adhesives with integrated switchability to reverse the adhesion will grow in importance. Future research will need to prove whether solutions exist that provide the required properties while being inexpensive to manufacture and intuitive to use.

8.2 Summary and Conclusions

With this work, new bioinspired concepts to optimize dry adhesives for various surfaces were explored. These will hopefully contribute to the improvement in the field of reversible adhesives. The main aspects of the work are summarized in the following:

- Macroscopic composite structures consisting of a thin, soft layer atop a stiffer stalk yield higher pull-off strength on smooth and rough surfaces compared to single-material reference structures. Their detachment can be tuned by changing the interface geometry between both materials, the tip layer thickness and the elastic modulus ratio between tip and stalk, initiating edge cracks, finger cracks or center cracks. Composite structures with curved interface and very thin soft layer showed highest and notably comparable adhesion on the smooth and rough substrate.
- Finite element simulations revealed that the enhanced adhesion strength of composite structures with decreasing tip thickness and increasing elastic modulus ratio is likely to be caused by a reduced magnitude of the corner stress singularity and increased center stress.
- Unstructured silicone elastomer films made of SSA MG 7-9800 showed mixing ratio, film thickness and surface treatment dependent mechanical and adhesion properties. Roughness has a stronger effect on the adhesion of the stiffer polymers, especially after plasma treatment. For the softest material, SSA mixed with equal weight parts of both components, the adhesion strength on the rough and smooth substrate were comparable. Additionally, the biocompatibility of the materials was investigated.
- Focusing on SSA MG 7-9800 films prepared with equal weight amounts of the two components, two regimes of adhesion were observed. Films with a thickness much higher than a characteristic material-defined length scale are insensitive to roughness as well as hold time and yield a relatively constant pull-off stress. The pull-off stress of thin films strongly varies depending on substrate roughness. It was observed to increase compared to thick films as long as the film thickness is larger than twice the peak-to-valley amplitude. Below this value, high elastic energies are stored in the film.
- Funnel-shaped microstructures represent a new tip-shape concept reaching pull-off strengths of up to 5.6 MPa for smooth substrates. Their thin, bendable flaps yield a high compliance of the overall structure. Numerical simulations highlighted differences in stress distributions comparing funnel-shaped structures to mushroom structures. Based on *in-situ* experiments under reduced pressure, we conjecture that the suction and capillary component contributing are small, and van der Waals forces dominate the adhesion, but further experiments and simulations will be necessary to fully understand the mechanisms.

The most important conclusions from this work are:

- The loss of adhesion on surfaces with roughness can be overcome by engineering of structures to control the detachment mechanisms.
- Composite structures with curved interface and very thin soft top layer can yield similar or even higher adhesion strength on rough compared to smooth substrates. Increasing the elastic modulus ratio between both materials is conducive for high adhesion and the most benefit can be obtained for elastic modulus ratios of 1000 and higher, where a saturation is expected.
- The stress distribution can indicate differences in delamination mechanisms.
- Adhesion of silicone elastomers to rough substrates can decrease after plasma treatment due to stiffening of the surface layer. Silicones with lower elastic modulus were less sensitive to this effect.
- Adhesion strength to substrates with roughness can be tuned using the film thickness and hold time. While thick films tend to be insensitive to roughness and hold time, thinner films are sensitive to those parameters. To maximize adhesion strength of thin films, the film thickness must fulfil $h_{film} > R_z^2 \cdot E/G_c$, where E is the Young's modulus and G_c the critical energy release rate.
- Funnel-shaped microstructures yield high adhesion on smooth substrates based on van der Waals forces due to their compliant tip. Future experiments will need to show whether funnel-shaped structures enable better tolerance against misalignment and are applicable for rough surfaces.

There are many challenges associated with designing and manufacturing bioinspired dry adhesives for functional adhesion on rough substrates. Natural role models are usually adapted to a wide variety of conditions, such as surface material, topography and environmental factors such as humidity. In addition, they are able to take advantage of muscular action to actuate their attachment pads, both to enhance adhesion and to switch to the non-adhesive state. Integrating such an adaptive, intelligent system in artificial structures will remain difficult to realize and will benefit from advances in the field of active materials. In the future, it will be interesting to combine current concepts of dry adhesives with ideas from these emerging fields to explore new paths for bioinspired adhesives.

Appendix

9 List of figures

Figures

Figure 2.1. Concepts for attachment in nature.	6
Figure 2.2. Adhesion to rough surfaces in nature: smooth adhesive pads and fibrillary adhesives.	7
Figure 2.3. Biomimetic concepts to increase adhesion by varying tip shape or material properties.	8
Figure 2.4. Representation of the origin of suction force.	11
Figure 2.5. Wide span of the roughness “spectrum” from ideal atomically smooth surfaces to structures with asperities in the range of nm, μm , mm and beyond.	12
Figure 2.6. Schematic of a surface profile to illustrate the important factors to determine roughness parameters.	13
Figure 2.7. Comparison of three surfaces with same average peak-to-valley distance, R_z , but different topographies.	14
Figure 2.8. Normal tack test measurement data and their analysis.	16
Figure 2.9. Normal stress distributions at the interface between fibril and substrate.	18
Figure 3.1. Microstructures with functional regions.	26
Figure 4.1. Two-step molding process for composite pillar fabrication.	31
Figure 4.2. Experimental setup for adhesion measurements on smooth and rough substrates.	33
Figure 4.3. Pull-off stress of conventional pillars (controls) made entirely from polyurethane on smooth (filled symbols) and rough substrates (open symbols) as a function of preload and for different hold times.	34
Figure 4.4. Pull-off stress of composite pillars as a function of the soft layer thickness, t	35
Figure 4.5. Detachment mechanisms of composite pillars.	36
Figure 4.6. Hold time effects on pull-off stress of composite pillars with varying soft layer thickness.	38
Figure 4.7. Hold time-related relative increase in adhesion σ_∞/σ_0 and rate of adhesion enhancement $\Delta\sigma/\tau_0$ of composite pillars adhered to rough substrates.	39
Figure 5.1. Experimental setup for adhesion testing.	50
Figure 5.2. Determined material properties of the polymer materials from rheometer measurements.	53

Figure 5.3. Adhesion measurements on the smooth substrate as a function of film thickness and pull-off velocity.	55
Figure 5.4. Cellular morphology after 24 h culture on polymeric surface.	57
Figure 5.5. Comparison of the characteristic adhesion parameters obtained from smooth and rough substrates for Sylgard 184, SSA 40:60 and SSA 50:50 with and without plasma treatment.	59
Figure 6.1. Topography of substrates used for adhesion testing, as characterized by stylus profilometry.	67
Figure 6.2. Roughness power spectra of the substrates used for adhesion testing.	68
Figure 6.3. Adhesion measurement results as function of film thickness and substrate roughness....	69
Figure 6.4. Exemplary pictures of the detachment mechanisms.	70
Figure 6.5. Stress relaxation behaviour of the films on the different substrates.	71
Figure 6.6. Hold time effect on adhesion.	72
Figure 7.1. Funnel-shaped microstructures.	84
Figure 7.2. Typical force-displacement curve and pull-off force as function of indentation depth.	87
Figure 7.3. Detachment behavior measured for the different microstructures.	88
Figure 7.4. Results of finite element simulations.	91
Figure 8.1. Graphical summary of the present work.	98
Figure 8.2. Model-system for adhesive patches.	102

Supplemental Figures

Supplemental Figure S 4.1. Stress distributions along the substrate-pillar interface obtained from FEM simulations (plain strain).....	43
Supplemental Figure S 5.1. Determination of protein adsorption.....	61
Supplemental Figure S 5.2. Comparison of the characteristic stress displacement curve of Sylgard 184 and SSA 50:50 on both substrates and detachment mechanisms.....	62
Supplemental Figure S 6.1. Adhesion measurements on glass substrates (GS 1 and GS 2), original VitroSkin (VS 1 and VS 2) and their respective epoxy replica (ES 1 to ES 4).	76
Supplemental Figure S 6.2. Analysis of the stress relaxation behaviour of the films on different substrates.	77
Supplemental Figure S 7.1. Pull-off force as a function of the indentation depth for PEGdma600 mushroom structures (i.e. 180° structures) with 10 µm diameter are shown.	93
Supplemental Figure S 7.2. Still image of the video demonstrating the reversible attachment and detachment of a funnel-shaped structure inside an SEM.....	93

10 List of tables

Tables

Table 5.1. Water contact angle measurements. 56

Supplemental Tables

Supplemental Table S 4.1. Complete overview of fit parameters from Eq. 4.1 (see main manuscript) for the hold time dependent pull-off stress of composite pillars on the smooth substrate. 42

Supplemental Table S 4.2. Complete overview of fit parameters from Eq. 4.1 (see main manuscript) for the hold time dependent pull-off stress of composite pillars on the rough substrate. 42

Supplemental Table S 6.1. Fitting parameters from the relaxation analysis. 78

11 List of publications

Peer-reviewed publications

- **Fischer, S. C. L.**, Groß, K., Torrents Abad, O., Becker, M. M., Park, E., Hensel, R., & Arzt, E. (2017). Funnel-Shaped Microstructures for Strong Reversible Adhesion. *Advanced Materials Interfaces*.
- **Fischer, S. C. L.**, Kruttwig, K., Bandmann, V., Hensel, R., & Arzt, E. (2017). Adhesion and Cellular Compatibility of Silicone-Based Skin Adhesives. *Macromolecular Materials and Engineering*, 302(5).
- **Fischer, S. C. L.**, Arzt, E., & Hensel, R. (2016). Composite pillars with a tunable interface for adhesion to rough substrates. *ACS applied materials & interfaces*, 9(1), 1036-1044.
- Balijepalli, R. G., **Fischer, S. C. L.**, Hensel, R., McMeeking, R. M., & Arzt, E. (2017). Numerical study of adhesion enhancement by composite fibrils with soft tip layers. *Journal of the Mechanics and Physics of Solids*, 99, 357-378.
- **Fischer, S. C. L.**, Levy, O., Kroner, E., Hensel, R., Karp, J. M., & Arzt, E. (2016). Bioinspired polydimethylsiloxane-based composites with high shear resistance against wet tissue. *Journal of the mechanical behavior of biomedical materials*, 61, 87-95.

Non-peer-reviewed publications

- **S. C. L. Fischer**, K. Groß, O. Torrents Abad, M. M. Becker, R. Hensel, E. Arzt *Funnel-shaped microstructures for high adhesion on the microscale*, Proc. 40th Annu. Meet. Adhes. Soc. 2017
- R. Hensel, **S. C. L. Fischer**, R. Balijepalli, R. McMeeking, E. Arzt *Adhesion of composite pillars to rough surfaces*, Proc. 40th Annu. Meet. Adhes. Soc. 2017

Patent applications

- R. Hensel, **S. C. L. Fischer**, E. Arzt, „Komposit-Pillarstrukturen“, Aktenzeichen: DE10 2015 103 965.6, Prioritätsdatum 17.03.2015
- E. Arzt, **S. C. L. Fischer**, K. Kruttwig, R. Hensel, B. Schick, G. Wenzel, „Vorrichtung mit einer strukturierten Beschichtung“, Aktenzeichen: DE102016113956.4, Prioritätsdatum 28.07.2016

12 References

- (1) Fischer, S. C. L.; Arzt, E.; Hensel, R. Composite Pillars with a Tunable Interface for Adhesion to Rough Substrates. *ACS Appl. Mater. Interfaces* **2017**, *9* (1), 1036–1044.
- (2) Fischer, S. C. L.; Kruttwig, K.; Bandmann, V.; Hensel, R.; Arzt, E. Adhesion and Cellular Compatibility of Silicone-Based Skin Adhesives. *Macromol. Mater. Eng.* **2017**, 1600526.
- (3) Fischer, S. C. L.; Groß, K.; Torrents Abad, O.; Becker, M. M.; Park, E.; Hensel, R.; Arzt, E. Funnel-Shaped Microstructures for Strong Reversible Adhesion. *Adv. Mater. Interfaces* **2017**, 1700292.
- (4) Scholz, I.; Barnes, W. J. P.; Smith, J. M.; Baumgartner, W. Ultrastructure and Physical Properties of an Adhesive Surface, the Toe Pad Epithelium of the Tree Frog, *Litoria Caerulea* White. *J. Exp. Biol.* **2008**, *212* (2).
- (5) Gao, H.; Wang, X.; Yao, H.; Gorb, S.; Arzt, E. Mechanics of Hierarchical Adhesion Structures of Geckos. In *Mechanics of Materials*; 2005; Vol. 37, pp 275–285.
- (6) Labonte, D.; Clemente, C. J.; Dittrich, A.; Kuo, C.-Y.; Crosby, A. J.; Irschick, D. J.; Federle, W. Extreme Positive Allometry of Animal Adhesive Pads and the Size Limits of Adhesion-Based Climbing. *Proc. Natl. Acad. Sci. U. S. A.* **2016**, *113* (5), 1297–1302.
- (7) Labonte, D.; Federle, W. Scaling and Biomechanics of Surface Attachment in Climbing Animals. *Philos. Trans. R. Soc. Lond. B. Biol. Sci.* **2015**, *370* (1661), 20140027.
- (8) Gorb, S. N. Biological Attachment Devices: Exploring Nature’s Diversity for Biomimetics. *Philos. Trans. R. Soc. London A Math. Phys. Eng. Sci.* **2008**, *366* (1870).
- (9) Nachtigall, W. *Biological Mechanisms of Attachment*; Springer Berlin Heidelberg: Berlin, Heidelberg, 1974.
- (10) Meyers, M. A.; Chen, P.-Y.; Lin, A. Y.-M.; Seki, Y. Biological Materials: Structure and Mechanical Properties. *Prog. Mater. Sci.* **2008**, *53* (1), 1–206.
- (11) Gorb, S. N. *Attachment Devices of Insect Cuticle*; Kluwer Academic Publishers: Dordrecht, 2007.
- (12) Autumn, K.; Gravish, N. Gecko Adhesion: Evolutionary Nanotechnology. *Philos. Trans. R. Soc., A* **2008**, *366* (1870), 1575–1590.
- (13) Hiller, U. Untersuchungen Zum Feinbau Und Zur Funktion Der Haftborsten von Reptilien. *Zeitschrift für Morphol. der Tiere* **1968**, *62* (4), 307–362.
- (14) Varenberg, M.; Pugno, N. M.; Gorb, S. N. Spatulate Structures in Biological Fibrillar Adhesion. *Soft Matter* **2010**, *6* (14), 3269.
- (15) Huber, G.; Gorb, S. N.; Spolenak, R.; Arzt, E. Resolving the Nanoscale Adhesion of Individual Gecko Spatulae by Atomic Force Microscopy. *Biol. Lett.* **2005**, *1* (1), 2–4.
- (16) Peisker, H.; Michels, J.; Gorb, S. N. Evidence for a Material Gradient in the Adhesive Tarsal Setae of the Ladybird Beetle *Coccinella Septempunctata*. *Nat. Commun.* **2013**, *4*, 1661.
- (17) Gorb, S. N.; Filippov, A. E. Fibrillar Adhesion with No Clusterisation: Functional Significance of Material Gradient along Adhesive Setae of Insects. *Beilstein J. Nanotechnol.* **2014**, *5* (1), 837–845.

- (18) Arzt, E.; Gorb, S.; Spolenak, R. From Micro to Nano Contacts in Biological Attachment Devices. *Proc. Natl. Acad. Sci. U. S. A.* **2003**, *100* (19), 10603–10606.
- (19) Gao, H.; Ji, B.; Jager, I. L.; Arzt, E.; Fratzl, P. Materials Become Insensitive to Flaws at Nanoscale: Lessons from Nature. *Proc. Natl. Acad. Sci.* **2003**, *100* (10), 5597–5600.
- (20) Kamperman, M.; Kroner, E.; Del Campo, A.; McMeeking, R. M.; Arzt, E. Functional Adhesive Surfaces with “Gecko” Effect: The Concept of Contact Splitting. *Adv. Eng. Mater.* **2010**, *12* (5), 335–348.
- (21) Lee, H.; Scherer, N. F.; Messersmith, P. B. Single-Molecule Mechanics of Mussel Adhesion. *Proc. Natl. Acad. Sci.* **2006**, *103* (35), 12999–13003.
- (22) Melzer, B.; Steinbrecher, T.; Seidel, R.; Kraft, O.; Schwaiger, R.; Speck, T. The Attachment Strategy of English Ivy: A Complex Mechanism Acting on Several Hierarchical Levels. *J. R. Soc. Interface* **2010**, *7* (50).
- (23) Clemente, C. J.; Federle, W. Pushing versus Pulling: Division of Labour between Tarsal Attachment Pads in Cockroaches. *Proc. R. Soc. B Biol. Sci.* **2008**, *275* (1640), 1329–1336.
- (24) Cho, W. K.; Ankrum, J. a; Guo, D.; Chester, S. a; Yang, S. Y.; Kashyap, A.; Campbell, G. a; Wood, R. J.; Rijal, R. K.; Karnik, R.; Langer, R.; Karp, J. M. Microstructured Barbs on the North American Porcupine Quill Enable Easy Tissue Penetration and Difficult Removal. *Proc. Natl. Acad. Sci. U. S. A.* **2012**, *109*, 21289–21294.
- (25) Yang, S. Y.; O’Cearbhaill, E. D.; Sisk, G. C.; Park, K. M.; Cho, W. K.; Villiger, M.; Bouma, B. E.; Pomahac, B.; Karp, J. M. A Bio-Inspired Swellable Microneedle Adhesive for Mechanical Interlocking with Tissue. *Nat. Commun.* **2013**, *4*, 1702.
- (26) Scherge, M.; Gorb, S. S. *Biological Micro- and Nanotribology*; NanoScience and Technology; Springer Berlin Heidelberg: Berlin, Heidelberg, 2001.
- (27) Gorb, S. N. Frictional Surfaces of the Elytra-to-Body Arresting Mechanism in Tenebrionid Beetles (Coleoptera : Tenebrionidae): Design of Co-Opted Fields of Microtrichia and Cuticle Ultrastructure. *Int. J. Insect Morphol. Embryol.* **1998**, *27*, 205–225.
- (28) Gorb, S. N. Evolution of the Dragonfly Head-Arresting System. *Proc. R. Soc. B Biol. Sci.* **1999**, *266* (1418), 525–535.
- (29) Tramacere, F.; Kovalev, A.; Kleinteich, T.; Gorb, S. N.; Mazzolai, B. Structure and Mechanical Properties of Octopus *Vulgaris* Suckers. *J. R. Soc. Interface* **2014**, *11*, 20130816.
- (30) Pixabay - Photos are licensed under the Creative Commons Licence CC0 www.pixabay.com.
- (31) Dahlquist, C. A. An Investigation into the Nature of Tack. *Adhes. Age* **1959**, *2* (25).
- (32) Autumn, K.; Majidi, C.; Groff, R. E.; Dittmore, a; Fearing, R. Effective Elastic Modulus of Isolated Gecko Setal Arrays. *J. Exp. Biol.* **2006**, *209* (Pt 18), 3558–3568.
- (33) Pattantyus-Abraham, A.; Krahn, J.; Menon, C. Recent Advances in Nanostructured Biomimetic Dry Adhesives. *Front. Bioeng. Biotechnol.* **2013**, *1*, 22.
- (34) Jeong, H. E.; Suh, K. Y. Nanohairs and Nanotubes: Efficient Structural Elements for Gecko-Inspired Artificial Dry Adhesives. *Nano Today*. 2009, pp 335–346.
- (35) Zhou, M.; Tian, Y.; Sameoto, D.; Zhang, X.; Meng, Y.; Wen, S. Controllable Interfacial Adhesion Applied to Transfer Light and Fragile Objects by Using Gecko Inspired Mushroom-Shaped Pillar Surface. *ACS Appl. Mater. Interfaces* **2013**, *5* (20), 10137–10144.

- (36) Purto, J.; Frensemeier, M.; Kroner, E. Switchable Adhesion in Vacuum Using Bio-Inspired Dry Adhesives. *ACS Appl. Mater. Interfaces* **2015**, *7* (43), 24127–24135.
- (37) Yu, J.; Chary, S.; Das, S.; Tamelier, J.; Turner, K. L.; Israelachvili, J. N. Friction and Adhesion of Gecko-Inspired PDMS Flaps on Rough Surfaces. *Langmuir* **2012**, *28* (31), 11527–11534.
- (38) Lee, H.; Lee, B. P.; Messersmith, P. B. A Reversible Wet/dry Adhesive Inspired by Mussels and Geckos. *Nature* **2007**, *448* (7151), 338–341.
- (39) Shafiq, Z.; Cui, J.; Pastor-Pérez, L.; San Miguel, V.; Gropeanu, R. A.; Serrano, C.; del Campo, A. Bioinspired Underwater Bonding and Debonding on Demand. *Angew. Chemie* **2012**, *124* (18), 4408–4411.
- (40) Fischer, S. C. L.; Levy, O.; Kroner, E.; Hensel, R.; Karp, J. M.; Arzt, E. Bioinspired Polydimethylsiloxane-Based Composites with High Shear Resistance against Wet Tissue. *J. Mech. Behav. Biomed. Mater.* **2016**, *61*, 87–95.
- (41) Balijepalli, R. G.; Begley, M. R.; Fleck, N. A.; McMeeking, R. M.; Arzt, E. Numerical Simulation of the Edge Stress Singularity and the Adhesion Strength for Compliant Mushroom Fibrils Adhered to Rigid Substrates. *Int. J. Solids Struct.* **2016**, *85–86*, 160–171.
- (42) Greiner, C.; Spolenak, R.; Arzt, E. Adhesion Design Maps for Fibrillar Adhesives: The Effect of Shape. *Acta Biomater.* **2009**, *5* (2), 597–606.
- (43) Heepe, L.; Gorb, S. N. Biologically Inspired Mushroom-Shaped Adhesive Microstructures. *Annu. Rev. Mater. Res.* **2014**, *44* (1), 173–203.
- (44) Aksak, B.; Sahin, K.; Sitti, M. The Optimal Shape of Elastomer Mushroom-like Fibers for High and Robust Adhesion. *Beilstein J. Nanotechnol.* **2014**, *5*, 630–638.
- (45) Del Campo, A.; Greiner, C.; Arzt, E. Contact Shape Controls Adhesion of Bioinspired Fibrillar Surfaces. *Langmuir* **2007**, *23* (20), 10235–10243.
- (46) Gao, H.; Yao, H. Shape Insensitive Optimal Adhesion of Nanoscale Fibrillar Structures. *Proc. Natl. Acad. Sci.* **2004**, *101* (21), 7851–7856.
- (47) Minsky, H. K.; Turner, K. T. Achieving Enhanced and Tunable Adhesion via Composite Posts. *Appl. Phys. Lett.* **2015**, *106* (20), 201604.
- (48) Bae, W. G.; Kwak, M. K.; Jeong, H. H. E.; Pang, C.; Jeong, H. H. E.; Suh, K.-Y. Fabrication and Analysis of Enforced Dry Adhesives with Core-shell Micropillars. *Soft Matter* **2013**, *9* (5), 1422.
- (49) Bae, W. G.; Kim, D.; Kwak, M. K.; Ha, L.; Kang, S. M.; Suh, K. Y. Enhanced Skin Adhesive Patch with Modulus-Tunable Composite Micropillars. *Adv. Healthcare Mater.* **2013**, *2* (1), 109–113.
- (50) Kroner, E.; Kaiser, J. S.; Fischer, S. C. L.; Arzt, E. Bioinspired Polymeric Surface Patterns for Medical Applications. *J. Appl. Biomater. Funct. Mater.* **2012**, *10* (3), 287–292.
- (51) Kim, S.; Sitti, M. Biologically Inspired Polymer Microfibers with Spatulate Tips as Repeatable Fibrillar Adhesives. *Appl. Phys. Lett.* **2006**, *89* (26), 261911.
- (52) Greiner, C.; Del Campo, A.; Arzt, E. Adhesion of Bioinspired Micropatterned Surfaces: Effects of Pillar Radius, Aspect Ratio, and Preload. *Langmuir* **2007**, *23*, 3495–3502.
- (53) Hui, C.-Y.; Jagota, A.; Shen, L.; Rajan, A.; Glassmaker, N.; Tang, T. Design of Bio-Inspired Fibrillar Interfaces for Contact and Adhesion — Theory and Experiments. *J. Adhes. Sci. Technol.* **2007**, *21*, 1259–1280.
- (54) Gorb, S. N.; Varenberg, M. Mushroom-Shaped Geometry of Contact Elements in Biological

- Adhesive Systems. *J. Adhes. Sci. Technol.* **2007**, *21* (12–13), 1175–1183.
- (55) Brodoceanu, D.; Bauer, C. T.; Kroner, E.; Arzt, E.; Kraus, T. Hierarchical Bioinspired Adhesive Surfaces—a Review. *Bioinspir. Biomim.* **2016**, *11* (5), 51001.
- (56) Spolenak, R.; Gorb, S.; Arzt, E. Adhesion Design Maps for Bio-Inspired Attachment Systems. *Acta Biomater.* **2005**, *1* (1), 5–13.
- (57) Bauer, C. T.; Kroner, E.; Fleck, N. A.; Arzt, E. Hierarchical Macroscopic Fibrillar Adhesives: In Situ Study of Buckling and Adhesion Mechanisms on Wavy Substrates. *Bioinspiration Biomimetics* **2015**, *10* (6), 66002.
- (58) Gorb, S. N.; Varenberg, M.; Peressadko, A.; Tuma, J. Biomimetic Mushroom-Shaped Fibrillar Adhesive Microstructure. *J. R. Soc. Interface* **2007**, *4* (October 2006), 271–275.
- (59) Khaderi, S. N.; Fleck, N. A.; Arzt, E.; McMeeking, R. M. Detachment of an Adhered Micropillar from a Dissimilar Substrate. *J. Mech. Phys. Solids* **2015**, *75*, 159–183.
- (60) Heepe, L.; Kovalev, A. E.; Varenberg, M.; Tuma, J.; Gorb, S. N. First Mushroom-Shaped Adhesive Microstructure: A Review. *Theor. Appl. Mech. Lett.* **2012**, *2* (1), 14008.
- (61) Kroner, E.; Arzt, E. Single Macropillars as Model Systems for Tilt Angle Dependent Adhesion Measurements. *Int. J. Adhes. Adhes.* **2012**, *36*, 32–38.
- (62) Heepe, L.; Kovalev, A. E.; Filippov, A. E.; Gorb, S. N. Adhesion Failure at 180 000 Frames per Second: Direct Observation of the Detachment Process of a Mushroom-Shaped Adhesive. *Phys. Rev. Lett.* **2013**, *111* (10).
- (63) Kwak, M. K.; Jeong, H. E.; Bae, W. G.; Jung, H. S.; Suh, K. Y. Anisotropic Adhesion Properties of Triangular-Tip-Shaped Micropillars. *Small* **2011**, *7*, 2296–2300.
- (64) Jeong, H. E.; Lee, J. K.; Kwak, M. K.; Moon, S. H.; Suh, K. Y. Effect of Leaning Angle of Gecko-Inspired Slanted Polymer Nanohairs on Dry Adhesion. *Appl. Phys. Lett.* **2010**, *96*.
- (65) Jeong, H. E.; Lee, J.-K.; Kim, H. N.; Moon, S. H.; Suh, K. Y. A Nontransferring Dry Adhesive with Hierarchical Polymer Nanohairs. *Proc. Natl. Acad. Sci. U. S. A.* **2009**, *106* (14), 5639–5644.
- (66) Khaled, W. Bin; Sameoto, D. Anisotropic Dry Adhesive via Cap Defects. *Bioinspir. Biomim.* **2013**, *8* (4), 44002.
- (67) Scholz, I.; Baumgartner, W.; Federle, W. Micromechanics of Smooth Adhesive Organs in Stick Insects: Pads Are Mechanically Anisotropic and Softer towards the Adhesive Surface. *J. Comp. Physiol. A* **2008**, *194* (4), 373–384.
- (68) Webber, R. E.; Shull, K. R.; Roos, A.; Creton, C. Effects of Geometric Confinement on the Adhesive Debonding of Soft Elastic Solids. *Phys. Rev. E* **2003**, *68* (2), 21805.
- (69) Minsky, H. K.; Turner, K. T. Composite Micro-Posts with High Dry Adhesion Strength. *ACS Appl. Mater. Interfaces* **2017**, acsami.7b01491.
- (70) Tramacere, F.; Appel, E.; Mazzolai, B.; Gorb, S. N. Hairy Suckers: The Surface Microstructure and Its Possible Functional Significance in the Octopus *Vulgaris* Sucker. *Beilstein J. Nanotechnol.* **2014**, *5*, 561–565.
- (71) Kessens, C. C.; Thomas, J.; Desai, J. P.; Kumar, V. Versatile Aerial Grasping Using Self-Sealing Suction. In *2016 IEEE International Conference on Robotics and Automation (ICRA)*; IEEE, 2016; pp 3249–3254.
- (72) Manabe, R.; Suzumori, K.; Wakimoto, S. A Functional Adhesive Robot Skin with Integrated

- Micro Rubber Suction Cups. In *2012 IEEE International Conference on Robotics and Automation*; IEEE, 2012; pp 904–909.
- (73) Bandyopadhyay, P. R.; Hrubes, J. D.; Leinhos, H. A. Biorobotic Adhesion in Water Using Suction Cups. *Bioinspir. Biomim.* **2008**, *3* (1), 16003.
- (74) Tramacere, F.; Beccai, L.; Mattioli, F.; Sinibaldi, E.; Mazzolai, B. Artificial Adhesion Mechanisms Inspired by Octopus Suckers. In *Proceedings - IEEE International Conference on Robotics and Automation*; 2012; pp 3846–3851.
- (75) Briones, L.; Bustamante, P.; Serna, M. A. Wall-Climbing Robot for Inspection in Nuclear Power Plants. In *Proceedings of the 1994 IEEE International Conference on Robotics and Automation*; IEEE Comput. Soc. Press, 1994; pp 1409–1414.
- (76) Zhao, Y.; Fu, Z.; Cao, Q.; Wang, Y. Development and Applications of Wall-Climbing Robots with a Single Suction Cup. *Robotica* **2004**, *22* (6), 643–648.
- (77) Sekhar, P. Duct Fan Based Wall Climbing Robot for Concrete Surface Crack Inspection. In *2014 Annual IEEE India Conference (INDICON)*; IEEE, 2014; pp 1–6.
- (78) Kawasaki, S.; Kikuchi, K. Development of a Small Legged Wall Climbing Robot with Passive Suction Cups. In *ICDES2014*; 2014; pp 112–116.
- (79) Yoshida, Y.; Ma, S. Design of a Wall-Climbing Robot with Passive Suction Cups. In *2010 IEEE International Conference on Robotics and Biomimetics*; IEEE, 2010; pp 1513–1518.
- (80) Baik, S.; Kim, D. W.; Park, Y.; Lee, T.-J.; Ho Bhang, S.; Pang, C. A Wet-Tolerant Adhesive Patch Inspired by Protuberances in Suction Cups of Octopi. *Nature* **2017**, *546* (7658), 396–400.
- (81) Chen, Y.-C.; Yang, H. Octopus-Inspired Assembly of Nanosucker Arrays for Dry/Wet Adhesion. *ACS Nano* **2017**, *11* (6), 5332–5338.
- (82) Martina, D.; Creton, C.; Damman, P.; Jeusette, M.; Lindner, A. Adhesion of Soft Viscoelastic Adhesives on Periodic Rough Surfaces. *Soft Matter* **2012**, *8* (19), 5350.
- (83) Pastewka, L.; Robbins, M. O. Contact between Rough Surfaces and a Criterion for Macroscopic Adhesion. *Proc. Natl. Acad. Sci. U. S. A.* **2014**, *111* (9), 3298–3303.
- (84) Fuller, K. N. G.; Tabor, D. The Effect of Surface Roughness on the Adhesion of Elastic Solids. *Proc. R. Soc. A Math. Phys. Eng. Sci.* **1975**, *345* (1642), 327–342.
- (85) Greenwood, J. A.; Williamson, J. B. P. Contact of Nominally Flat Surfaces. *Proc. R. Soc. A Math. Phys. Eng. Sci.* **1966**, *295* (1442), 300–319.
- (86) Kovalev, A. E.; Dening, K.; Persson, B. N. J.; Gorb, S. N. Surface Topography and Contact Mechanics of Dry and Wet Human Skin. *Beilstein J. Nanotechnol.* **2014**, *5*, 1341–1348.
- (87) Bhushan, B. Nanotribological and Nanomechanical Properties of Skin with and without Cream Treatment Using Atomic Force Microscopy and Nanoindentation. *J. Colloid Interface Sci.* **2012**, *367* (1), 1–33.
- (88) van Kuilenburg, J.; Masen, M. A.; van der Heide, E. A Review of Fingerpad Contact Mechanics and Friction and How This Affects Tactile Perception. *Proc. Inst. Mech. Eng. Part J J. Eng. Tribol.* **2013**, *229* (3), 243–258.
- (89) Barreau, V.; Hensel, R.; Guimard, N. K.; Ghatak, A.; McMeeking, R. M.; Arzt, E. Fibrillar Elastomeric Micropatterns Create Tunable Adhesion Even to Rough Surfaces. *Adv. Funct. Mater.* **2016**, *26* (26), 4687–4694.

- (90) Persson, B. N. J. Contact Mechanics for Randomly Rough Surfaces. *Surf. Sci. Rep.* **2006**, *61* (4), 201–227.
- (91) Persson, B. N. J.; Albohr, O.; Tartaglino, U.; Volokitin, A. I.; Tosatti, E. On the Nature of Surface Roughness with Application to Contact Mechanics, Sealing, Rubber Friction and Adhesion. *J. Phys. Condens. Matter* **2005**, *17* (1), R1–R62.
- (92) Creton, C.; Hooker, J.; Shull, K. R. Bulk and Interfacial Contributions to the Debonding Mechanisms of Soft Adhesives: Extension to Large Strains. *Langmuir* **2001**, *17* (16), 4948–4954.
- (93) Shull, K. R. Contact Mechanics and the Adhesion of Soft Solids. *Mater. Sci. Eng. R Reports* **2002**, *36* (1), 1–45.
- (94) Creton, C.; Lakrout, H. Micromechanics of Flat-Probe Adhesion Tests of Soft Viscoelastic Polymer Films. *J. Polym. Sci. Part B Polym. Phys.* **2000**, *38* (7), 965–979.
- (95) Chung, J. Y.; Chaudhury, M. K. Soft and Hard Adhesion. *J. Adhes.* **2005**, *81* (10–11), 1119–1145.
- (96) Lakrout, H.; Sergot, P.; Creton, C. Direct Observation of Cavitation and Fibrillation in a Probe Tack Experiment on Model Acrylic Pressure-Sensitive-Adhesives. *J. Adhes.* **1999**, *69* (3–4), 307–359.
- (97) Creton, C.; Ciccotti, M. F. Rapture and Adhesion of Soft Materials : A Review. *Reports Prog. Phys.* **2016**, *79* (4), 46601.
- (98) Tobolsky, A. V. *Mechanische Eigenschaften Und Struktur von Polymeren*; Berliner Union, 1967.
- (99) Flügge, W. *Viscoelasticity*; Springer Berlin Heidelberg: Berlin, Heidelberg, 1975.
- (100) Schwarzl, F. R. *Polymermechanik*; Springer Berlin Heidelberg: Berlin, Heidelberg, 1990.
- (101) Oyen, M. L. Analytical Techniques for Indentation of Viscoelastic Materials. *Philos. Mag.* **2006**, *86* (33–35), 5625–5641.
- (102) Tirella, A.; Mattei, G.; Ahluwalia, A. Strain Rate Viscoelastic Analysis of Soft and Highly Hydrated Biomaterials. *J. Biomed. Mater. Res. - Part A* **2014**, *102* (10), 3352–3360.
- (103) Davis, C. S.; Lemoine, F.; Darnige, T.; Martina, D.; Creton, C.; Lindner, A. Debonding Mechanisms of Soft Materials at Short Contact Times. *Langmuir* **2014**, *30* (35), 10626–10636.
- (104) Akisanya, A. R.; Fleck, N. A. Interfacial Cracking from the Freeedge of a Long Bi-Material Strip. *Int. J. Solids Struct.* **1997**, *34* (13), 1645–1665.
- (105) Afferrante, L.; Carbone, G. The Mechanisms of Detachment of Mushroom-Shaped Micro-Pillars: From Defect Propagation to Membrane Peeling. *Macromol. React. Eng.* **2013**, *7* (11), 609–615.
- (106) Carbone, G.; Pierro, E. A Review of Adhesion Mechanisms of Mushroom-Shaped Microstructured Adhesives. *Meccanica* **2013**, *48* (8), 1819–1833.
- (107) Micciché, M.; Arzt, E.; Kroner, E. Single Macroscopic Pillars as Model System for Bioinspired Adhesives: Influence of Tip Dimension, Aspect Ratio, and Tilt Angle. *ACS Appl. Mater. Interfaces* **2014**, *6* (10), 7076–7083.
- (108) Heepe, L.; Varenberg, M.; Itovich, Y.; Gorb, S. N. Suction Component in Adhesion of Mushroom-Shaped Microstructure. *J. R. Soc. Interface* **2011**, *8* (57), 585–589.
- (109) Henrey, M.; Díaz Téllez, J. P.; Wormnes, K.; Pambaguian, L.; Menon, C. Towards the Use of

- Mushroom-Capped Dry Adhesives in Outer Space: Effects of Low Pressure and Temperature on Adhesion Strength. *Aerosp. Sci. Technol.* **2013**, *29* (1), 185–190.
- (110) Sameoto, D.; Sharif, H.; Menon, C. Investigation of Low-Pressure Adhesion Performance of Mushroom Shaped Biomimetic Dry Adhesives. *J. Adhes. Sci. Technol.* **2012**, *26* (23), 2641–2652.
- (111) Maugis, D. On the Contact and Adhesion of Rough Surfaces. *J. Adhes. Sci. Technol.* **1996**, *10* (2), 161–175.
- (112) Persson, B. N. J.; Tosatti, E. The Effect of Surface Roughness on the Adhesion of Elastic Solids. *J. Chem. Phys.* **2001**, *115* (12), 5597–5610.
- (113) Persson, B. N. J.; Scaraggi, M. Theory of Adhesion: Role of Surface Roughness. *J. Chem. Phys.* **2014**, *141* (12), 124701.
- (114) Persson, B. N. J.; Albohr, O.; Creton, C.; Peveri, V. Contact Area between a Viscoelastic Solid and a Hard, Randomly Rough, Substrate. *J. Chem. Phys.* **2004**, *120* (18), 8779–8793.
- (115) Dapp, W. B.; Lücke, A.; Persson, B. N. J.; Müser, M. H. Self-Affine Elastic Contacts: Percolation and Leakage. *Phys. Rev. Lett.* **2012**, *108* (June), 1–4.
- (116) Creton, C.; Leibler, L. How Does Tack Depend on Time of Contact and Contact Pressure? *J. Polym. Sci. Part B Polym. Phys.* **1996**, *34* (3), 545–554.
- (117) Chiche, A.; Pareige, P.; Creton, C. Role of Surface Roughness in Controlling the Adhesion of a Soft Adhesive on a Hard Surface. *Comptes Rendus l'Académie des Sci. - Ser. IV - Phys.* **2000**, *1* (9), 1197–1204.
- (118) Briggs, G. A. D.; Briscoe, B. J. The Effect of Surface Topography on the Adhesion of Elastic Solids. *J. Phys. D. Appl. Phys.* **1977**, *10* (18), 2453–2466.
- (119) Purtov, J.; Gorb, E. V.; Steinhart, M.; Gorb, S. N. Measuring of the Hardly Measurable: Adhesion Properties of Anti-Adhesive Surfaces. *Appl. Phys. A Mater. Sci. Process.* **2013**, *111* (1), 183–189.
- (120) Davis, C. S.; Martina, D.; Creton, C.; Lindner, A.; Crosby, A. J. Enhanced Adhesion of Elastic Materials to Small-Scale Wrinkles. *Langmuir* **2012**, *28* (42), 14899–14908.
- (121) Hui, C. Y.; Lin, Y. Y.; Baney, J. M. The Mechanics of Tack: Viscoelastic Contact on a Rough Surface. *J. Polym. Sci. Part B Polym. Phys.* **2000**, *38* (11), 1485–1495.
- (122) McNichol, L.; Lund, C.; Rosen, T.; Gray, M. Medical Adhesives and Patient Safety. *J. Wound, Ostomy Cont. Nurs.* **2013**, *40* (4), 365–380.
- (123) Matsumura, H.; Imai, R.; Ahmatjan, N.; Ida, Y.; Gondo, M.; Shibata, D.; Wanatabe, K. Removal of Adhesive Wound Dressing and Its Effects on the Stratum Corneum of the Skin: Comparison of Eight Different Adhesive Wound Dressings. *Int. Wound J.* **2014**, *11* (1), 50–54.
- (124) Trojahn, C.; Dobos, G.; Schario, M.; Ludriksone, L.; Blume-Peytavi, U.; Kottner, J. Relation between Skin Micro-Topography, Roughness, and Skin Age. *Ski. Res. Technol.* **2015**, *21* (1), 69–75.
- (125) Jacobi, U.; Chen, M.; Frankowski, G.; Sinkgraven, R.; Hund, M.; Rzany, B.; Sterry, W.; Lademann, J. In Vivo Determination of Skin Surface Topography Using an Optical 3D Device. *Ski. Res. Technol.* **2004**, *10* (4), 207–214.
- (126) Krueger, N.; Luebberding, S.; Oltmer, M.; Streker, M.; Kerscher, M. Age-Related Changes in Skin Mechanical Properties: A Quantitative Evaluation of 120 Female Subjects. *Ski. Res.*

- Technol.* **2011**, *17* (2), 141–148.
- (127) Wu, K. S.; van Osdol, W. W.; Dauskardt, R. H. Mechanical Properties of Human Stratum Corneum: Effects of Temperature, Hydration, and Chemical Treatment. *Biomaterials* **2006**, *27* (5), 785–795.
- (128) Biniak, K.; Kaczvinsky, J.; Matts, P.; Dauskardt, R. H. Understanding Age-Induced Alterations to the Biomechanical Barrier Function of Human Stratum Corneum. *J. Dermatol. Sci.* **2015**, *80* (2), 94–101.
- (129) Netzlaff, F.; Lehr, C.-M.; Wertz, P. W.; Schaefer, U. F. The Human Epidermis Models EpiSkin[®], SkinEthic[®] and EpiDerm[®]: An Evaluation of Morphology and Their Suitability for Testing Phototoxicity, Irritancy, Corrosivity, and Substance Transport. *Eur. J. Pharm. Biopharm.* **2005**, *60* (2), 167–178.
- (130) Lir, I.; Haber, M.; Dodiuk-Kenig, H. Skin Surface Model Material as a Substrate for Adhesion-to-Skin Testing. *J. Adhes. Sci. Technol.* **2007**, *21* (15), 1497–1512.
- (131) Lang, N.; Pereira, M. J.; Lee, Y.; Friehs, I.; Vasilyev, N. V.; Feins, E. N.; Ablasser, K.; O’Cearbhaill, E. D.; Xu, C.; Fabozzo, A.; Padera, R.; Wasserman, S.; Freudenthal, F.; Ferreira, L. S.; Langer, R.; Karp, J. M.; del Nido, P. J. A Blood-Resistant Surgical Glue for Minimally Invasive Repair of Vessels and Heart Defects. *Sci. Transl. Med.* **2014**, *6* (218), 218ra6-218ra6.
- (132) Kheyfets, V. O.; Thornton, R. C.; Kowal, M.; Finol, E. A. A Protocol for Measuring Pull-Off Stress of Wound-Treatment Polymers. *J. Biomech. Eng.* **2014**, *136* (7), 74501.
- (133) Gurtner, G. C.; Dauskardt, R. H.; Wong, V. W.; Bhatt, K. A.; Wu, K.; Vial, I. N.; Padois, K.; Korman, J. M.; Longaker, M. T. Improving Cutaneous Scar Formation by Controlling the Mechanical Environment. *Ann. Surg.* **2011**, *254* (2), 217–225.
- (134) Laulicht, B.; Langer, R.; Karp, J. M. Quick-Release Medical Tape. *Proc. Natl. Acad. Sci.* **2012**, *109* (46), 18803–18808.
- (135) Hammock, M. L.; Chortos, A.; Tee, B. C.-K.; Tok, J. B.-H.; Bao, Z. 25th Anniversary Article: The Evolution of Electronic Skin (E-Skin): A Brief History, Design Considerations, and Recent Progress. *Adv. Mater.* **2013**, *25* (42), 5997–6038.
- (136) Rim, Y. S.; Bae, S.-H.; Chen, H.; De Marco, N.; Yang, Y. Recent Progress in Materials and Devices toward Printable and Flexible Sensors. *Adv. Mater.* **2016**, *28* (22), 4415–4440.
- (137) Kim, D.-H.; Rogers, J. A. Stretchable Electronics: Materials Strategies and Devices. *Adv. Mater.* **2008**, *20* (24), 4887–4892.
- (138) Weigel, M.; Nittala, A. S.; Olwal, A.; Steimle, J. SkinMarks: Enabling Interactions on Body Landmarks Using Conformal Skin Electronics. In *Proceedings of the 2017 CHI Conference on Human Factors in Computing Systems - CHI '17*; ACM Press: New York, New York, USA, 2017; pp 3095–3105.
- (139) Kao, H.-L. (Cindy); Holz, C.; Roseway, A.; Calvo, A.; Schmandt, C. DuoSkin: Rapidly Prototyping On-Skin User Interfaces Using Skin-Friendly Materials. In *Proceedings of the 2016 ACM International Symposium on Wearable Computers - ISWC '16*; ACM Press: New York, New York, USA, 2016; pp 16–23.
- (140) Weigel, M.; Lu, T.; Bailly, G.; Oulasvirta, A.; Majidi, C.; Steimle, J. iSkin: Flexible, Stretchable and Visually Customizable on-Body Touch Sensors for Mobile Computing. In *Proceedings of the 33rd Annual ACM Conference on Human Factors in Computing Systems - CHI '15*; ACM Press: New York, New York, USA, 2015; pp 2991–3000.

- (141) Amjadi, M.; Yoon, Y. J.; Park, I. Ultra-Stretchable and Skin-Mountable Strain Sensors Using Carbon nanotubes–Ecoflex Nanocomposites. *Nanotechnology* **2015**, *26* (37), 375501.
- (142) Tee, B. C.-K.; Wang, C.; Allen, R.; Bao, Z. An Electrically and Mechanically Self-Healing Composite with Pressure- and Flexion-Sensitive Properties for Electronic Skin Applications. *Nat. Nanotechnol.* **2012**, *7* (12), 825–832.
- (143) Lei, T.; Guan, M.; Liu, J.; Lin, H.-C.; Pfattner, R.; Shaw, L.; McGuire, A. F.; Huang, T.-C.; Shao, L.; Cheng, K.-T.; Tok, J. B.-H.; Bao, Z. Biocompatible and Totally Disintegrable Semiconducting Polymer for Ultrathin and Ultralightweight Transient Electronics. *Proc. Natl. Acad. Sci.* **2017**, 201701478.
- (144) Chortos, A.; Liu, J.; Bao, Z. Pursuing Prosthetic Electronic Skin. *Nat. Mater.* **2016**, *15* (9), 937–950.
- (145) Parness, A.; Soto, D.; Esparza, N.; Gravish, N.; Wilkinson, M.; Autumn, K.; Cutkosky, M. A Microfabricated Wedge-Shaped Adhesive Array Displaying Gecko-like Dynamic Adhesion, Directionality and Long Lifetime. *J. R. Soc. Interface* **2009**, *6* (41), 1223–1232.
- (146) Kwak, M. K.; Jeong, H.-E.; Suh, K. Y. Rational Design and Enhanced Biocompatibility of a Dry Adhesive Medical Skin Patch. *Adv. Mater.* **2011**, *23* (34), 3949–3953.
- (147) Villar-Fernandez, M. A.; Lopez-Escamez, J. A. Outlook for Tissue Engineering of the Tympanic Membrane. *Audiol. Res.* **2015**, *5* (1).
- (148) Amoils, C. P.; Jackler, R. K.; Lustig, L. R. Repair of Chronic Tympanic Membrane Perforations Using Epidermal Growth Factor. *Otolaryngol. Head. Neck Surg.* **1992**, *107* (5), 669–683.
- (149) Gerber, M. J.; Mason, J. C.; Lambert, P. R. Hearing Results After Primary Cartilage Tympanoplasty. *Laryngoscope* **2000**, *110* (12), 1994–1999.
- (150) Hong, P.; Bance, M.; Gratzner, P. F. Repair of Tympanic Membrane Perforation Using Novel Adjuvant Therapies: A Contemporary Review of Experimental and Tissue Engineering Studies. *Int. J. Pediatr. Otorhinolaryngol.* **2013**, *77* (1), 3–12.
- (151) Ghassemifar, R.; Redmond, S.; Zainuddin; Chirila, T. V. Advancing Towards a Tissue-Engineered Tympanic Membrane: Silk Fibroin as a Substratum for Growing Human Eardrum Keratinocytes. *J. Biomater. Appl.* **2010**, *24* (7), 591–606.
- (152) Hakuba, N.; Tabata, Y.; Hato, N.; Fujiwara, T.; Gyo, K. Gelatin Hydrogel with Basic Fibroblast Growth Factor for Tympanic Membrane Regeneration. *Otol. Neurotol.* **2014**, *35* (6), 540–544.
- (153) Kim, J.; Kim, C. H.; Park, C. H.; Seo, J.-N.; Kweon, H.; Kang, S. W.; Lee, K. G. Comparison of Methods for the Repair of Acute Tympanic Membrane Perforations: Silk Patch vs. Paper Patch. *Wound Repair Regen.* **2010**, *18* (1), 132–138.
- (154) Muerbe, D.; Zahnert, T.; Bornitz, M.; Huettenbrink, K.-B. Acoustic Properties of Different Cartilage Reconstruction Techniques of the Tympanic Membrane. *Laryngoscope* **2002**, *112* (10), 1769–1776.
- (155) Flück, M.; Giraud, M. N.; Tunç, V.; Chiquet, M. Tensile Stress-Dependent Collagen XII and Fibronectin Production by Fibroblasts Requires Separate Pathways. *Biochim. Biophys. Acta - Mol. Cell Res.* **2003**, *1593* (2–3), 239–248.
- (156) Kaiser, J. S.; Kamperman, M.; de Souza, E. J.; Schick, B.; Arzt, E. Adhesion of Biocompatible and Biodegradable Micropatterned Surfaces. *Int. J. Artif. Organs* **2011**, *34* (2), 180–184.
- (157) De Souza, E. J.; Kamperman, M.; Castellanos, G.; Kroner, E.; Armbruester, V.; Romann, M. S.; Schick, B.; Arzt, E. In Vitro Adhesion Measurements between Skin and Micropatterned

- Poly(dimethylsiloxane) Surfaces. In *Proceedings of the 31st Annual International Conference of the IEEE Engineering in Medicine and Biology Society: Engineering the Future of Biomedicine, EMBC 2009*; 2009; pp 6018–6021.
- (158) King, D. R.; Bartlett, M. D.; Gilman, C. A.; Irschick, D. J.; Crosby, A. J. Creating Gecko-Like Adhesives for “Real World” Surfaces. *Adv. Mater.* **2014**, *26* (25), 4345–4351.
- (159) Persson, B. N. J. On the Mechanism of Adhesion in Biological Systems. *J. Chem. Phys.* **2003**, *118* (16), 7614–7621.
- (160) Huber, G.; Gorb, S. N.; Hosoda, N.; Spolenak, R.; Arzt, E. Influence of Surface Roughness on Gecko Adhesion. *Acta Biomater.* **2007**, *3*, 607–610.
- (161) Kasem, H.; Varenberg, M. Effect of Counterface Roughness on Adhesion of Mushroom-Shaped Microstructure. *J. R. Soc. Interface* **2013**, *10* (87), 20130620–20130620.
- (162) Vajpayee, S.; Jagota, A.; Hui, C.-Y. Adhesion of a Fibrillar Interface on Wet and Rough Surfaces. *J. Adhes.* **2010**, *86* (1), 39–61.
- (163) Gorb, S.; Gorb, E.; Kastner, V. Scale Effects on the Attachment Pads and Friction Forces in Syrphid Flies (Diptera, Syrphidae). *J. Exp. Biol.* **2001**, *204* (Pt 8), 1421–1431.
- (164) Zhou, M.; Pesika, N.; Zeng, H.; Tian, Y.; Israelachvili, J. Recent Advances in Gecko Adhesion and Friction Mechanisms and Development of Gecko-Inspired Dry Adhesive Surfaces. *Friction* **2013**, *1* (2), 114–129.
- (165) Kroner, E.; Blau, J.; Arzt, E. Note: An Adhesion Measurement Setup for Bioinspired Fibrillar Surfaces Using Flat Probes. *Rev. Sci. Instrum.* **2012**, *83* (1), 16101.
- (166) Jacobs, T. D. B.; Junge, T.; Pastewka, L. Quantitative Characterization of Surface Topography Using Spectral Analysis. *Surf. Topogr. Metrol. Prop.* **2017**, *5* (1), 13001.
- (167) Marquardt, D. W. An Algorithm for Least-Squares Estimation of Nonlinear Parameters. *J. Soc. Ind. Appl. Math.* **1963**, *11* (2), 431–441.
- (168) More, J. J. The Levenberg-Marquardt Algorithm: Implementation and Theory. In *Numerical Analysis*; Watson, G. A., Ed.; Lecture Notes in Mathematics; Springer Berlin Heidelberg: Berlin, Heidelberg, 1978; Vol. 630, pp 105–116.
- (169) Nase, J.; Lindner, A.; Creton, C. Pattern Formation during Deformation of a Confined Viscoelastic Layer: From a Viscous Liquid to a Soft Elastic Solid. *Phys. Rev. Lett.* **2008**, *101* (7), 74503.
- (170) Ghatak, A.; Chaudhury, M. K.; Shenoy, V.; Sharma, A. Meniscus Instability in a Thin Elastic Film. *Phys. Rev. Lett.* **2000**, *85* (20), 4329–4332.
- (171) Shull, K. R.; Flanigan, C. M.; Crosby, A. J. Fingering Instabilities of Confined Elastic Layers in Tension. *Phys. Rev. Lett.* **2000**, *84* (14), 3057–3060.
- (172) Mönch, W.; Herminghaus, S. Elastic Instability of Rubber Films between Solid Bodies. *Europhys. Lett.* **2001**, *53* (4), 525–531.
- (173) Balijepalli, R. G.; Fischer, S. C. L.; Hensel, R.; McMeeking, R. M.; Arzt, E. Numerical Study of Adhesion Enhancement by Composite Fibrils with Soft Tip Layers. *J. Mech. Phys. Solids* **2017**, *99*, 357–378.
- (174) Kwak, M. K.; Pang, C.; Jeong, H. E.; Kim, H. N.; Yoon, H.; Jung, H. S.; Suh, K. Y. Towards the next Level of Bioinspired Dry Adhesives: New Designs and Applications. *Adv. Funct. Mater.* **2011**, *21*, 3606–3616.

- (175) Creton, C. Pressure-Sensitive Adhesives: An Introductory Course. *MRS Bull.* **2011**, *28* (6), 434–439.
- (176) Maassen, W.; Meier, M. A. R.; Willenbacher, N. Unique Adhesive Properties of Pressure Sensitive Adhesives from Plant Oils. *Int. J. Adhes. Adhes.* **2016**, *64*, 65–71.
- (177) Udagama, R.; Degrandi-Contraires, E.; Creton, C.; Graillat, C.; McKenna, T. F. L.; Bourgeat-Lami, E. Synthesis of Acrylic–Polyurethane Hybrid Latexes by Miniemulsion Polymerization and Their Pressure-Sensitive Adhesive Applications. *Macromolecules* **2011**, *44* (8), 2632–2642.
- (178) Czech, Z. Development of Solvent-Free Pressure-Sensitive Adhesive Acrylics. *Int. J. Adhes. Adhes.* **2004**, *24* (2), 119–125.
- (179) Sun, S.; Li, M.; Liu, A. A Review on Mechanical Properties of Pressure Sensitive Adhesives. *Int. J. Adhes. Adhes.* **2013**, *41*, 98–106.
- (180) Dimas, D. A.; Dallas, P. P.; Rekkas, D. M.; Choulis, N. H. Effect of Several Factors on the Mechanical Properties of Pressure-Sensitive Adhesives Used in Transdermal Therapeutic Systems. *AAPS PharmSciTech* **2000**, *1* (2), 80–87.
- (181) Tan, H. S.; Pfister, W. R. Pressure-Sensitive Adhesives for Transdermal Drug Delivery Systems. *Pharm. Sci. Technol. Today* **1999**, *2* (2), 60–69.
- (182) Tokumura, F.; Homma, T.; Tomiya, T.; Kobayashi, Y.; Matsuda, T. Properties of Pressure-Sensitive Adhesive Tapes with Soft Adhesives to Human Skin and Their Mechanism. *Ski. Res. Technol.* **2007**, *13* (2), 211–216.
- (183) Renvoise, J.; Burlot, D.; Marin, G.; Derail, C. Adherence Performances of Pressure Sensitive Adhesives on a Model Viscoelastic Synthetic Film: A Tool for the Understanding of Adhesion on the Human Skin. *Int. J. Pharm.* **2009**, *368*, 83–88.
- (184) Chang, E. P. Viscoelastic Windows of Pressure-Sensitive Adhesives. *The Journal of Adhesion*. 1991, pp 189–200.
- (185) Toddywala, R.; Chien, Y. W. Evaluation of Silicone-Based Pressure-Sensitive Adhesives for Transdermal Drug Delivery. I. Effect of Penetrant Hydrophilicity. *J. Control. Release* **1990**, *14* (1), 29–41.
- (186) Venkatraman, S.; Gale, R. Skin Adhesives and Skin Adhesion. 1. Transdermal Drug Delivery Systems. *Biomaterials* **1998**, *19*, 1119–1136.
- (187) Mason, S. R. Type of Soap and the Incidence of Skin Tears among Residents of a Long-Term Care Facility. *Ostomy. Wound. Manage.* **1997**, *43* (8), 26–30.
- (188) Karp, J. M.; Langer, R. Materials Science: Dry Solution to a Sticky Problem. *Nature* **2011**, *477* (7362), 42–43.
- (189) Fisher, G. J.; Wang, Z.; Datta, S. C.; Varani, J.; Kang, S.; Voorhees, J. J. Pathophysiology of Premature Skin Aging Induced by Ultraviolet Light. *N. Engl. J. Med.* **1997**, *337* (20), 1419–1429.
- (190) Thanawala, S. K.; Chaudhury, M. K. Surface Modification of Silicone Elastomer Using Perfluorinated Ether. *Langmuir* **2000**, *16* (3), 1256–1260.
- (191) Lloyd, A. W.; Faragher, R. G. A.; Denyer, S. P. Ocular Biomaterials and Implants. *Biomaterials* **2001**, *22* (8), 769–785.
- (192) Roth, J.; Albrecht, V.; Nitschke, M.; Bellmann, C.; Simons, F.; Zschoche, S.; Michel, S.; Luhmann, C.; Grundke, K.; Voit, B. Surface Functionalization of Silicone Rubber for Permanent Adhesion Improvement. *Langmuir* **2008**, *24* (21), 12603–12611.

- (193) Tan, S. H.; Nguyen, N.-T.; Chua, Y. C.; Kang, T. G. Oxygen Plasma Treatment for Reducing Hydrophobicity of a Sealed Polydimethylsiloxane Microchannel. *Biomicrofluidics* **2010**, *4* (3), 32204.
- (194) Fuard, D.; Tzvetkova-Chevolleau, T.; Decossas, S.; Tracqui, P.; Schiavone, P. Optimization of Poly-Di-Methyl-Siloxane (PDMS) Substrates for Studying Cellular Adhesion and Motility. *Microelectron. Eng.* **2008**, *85* (5–6), 1289–1293.
- (195) Wang, Z.; Volinsky, A. A.; Gallant, N. D. Crosslinking Effect on Polydimethylsiloxane Elastic Modulus Measured by Custom-Built Compression Instrument. *J. Appl. Polym. Sci.* **2014**, *131* (22), n/a-n/a.
- (196) Brown, X. Q.; Ookawa, K.; Wong, J. Y. Evaluation of Polydimethylsiloxane Scaffolds with Physiologically-Relevant Elastic Moduli: Interplay of Substrate Mechanics and Surface Chemistry Effects on Vascular Smooth Muscle Cell Response. *Biomaterials* **2005**, *26* (16), 3123–3129.
- (197) Van Midwoud, P. M.; Janse, A.; Merema, M. T.; Groothuis, G. M. M.; Verpoorte, E. Comparison of Biocompatibility and Adsorption Properties of Different Plastics for Advanced Microfluidic Cell and Tissue Culture Models. *Anal. Chem.* **2012**, *84* (9), 3938–3944.
- (198) Meitl, M. a.; Zhu, Z.-T.; Kumar, V.; Lee, K. J.; Feng, X.; Huang, Y. Y.; Adesida, I.; Nuzzo, R. G.; Rogers, J. a. Transfer Printing by Kinetic Control of Adhesion to an Elastomeric Stamp. *Nat. Mater.* **2006**, *5* (1), 33–38.
- (199) Kendall, K. The Adhesion and Surface Energy of Elastic Solids. *J. Phys. D. Appl. Phys.* **1971**, *4* (8), 320.
- (200) Gent, A. N. Fracture Mechanics of Adhesive Bonds. *Rubber Chem. Technol.* **1974**, *47* (1), 202–212.
- (201) Crosby, A. J.; Shull, K. R.; Lakrout, H.; Creton, C. Deformation and Failure Modes of Adhesively Bonded Elastic Layers. *J. Appl. Phys.* **2000**, *88* (5), 2956.
- (202) Creton, C.; Ciccotti, M. Fracture and Adhesion of Soft Materials: A Review. *Reports Prog. Phys.* **2016**, *79* (4), 46601.
- (203) Nase, J.; Ramos, O.; Creton, C.; Lindner, A. Debonding Energy of PDMS. *Eur. Phys. J. E* **2013**, *36* (9), 103.
- (204) Toworfe, G.; Composto, R.; Adams, C.; Shapiro, I.; Ducheyne, P. Effect of Surface Activated Poly(dimethylsiloxane) on Fibronectin Adsorption and Cell Function. *Departmental Papers (MSE)*. 2003.
- (205) Dimilla, P. A.; Albelda, S. M.; Quinn, J. A. Adsorption and Elution of Extracellular Matrix Proteins on Non-Tissue Culture Polystyrene Petri Dishes. *J. Colloid Interface Sci.* **1992**, *153* (1), 212–225.
- (206) Lhoest, J. B.; Detrait, E.; van den Bosch de Aguilar, P.; Bertrand, P. Fibronectin Adsorption, Conformation, and Orientation on Polystyrene Substrates Studied by Radiolabeling, XPS, and ToF SIMS. *J. Biomed. Mater. Res.* **1998**, *41* (1), 95–103.
- (207) Rezanian, A.; Healy, K. E. Biomimetic Peptide Surfaces That Regulate Adhesion, Spreading, Cytoskeletal Organization, and Mineralization of the Matrix Deposited by Osteoblast-like Cells. *Biotechnol. Prog.* **1999**, *15* (1), 19–32.
- (208) Marchand, A.; Das, S.; Snoeijer, J. H.; Andreotti, B. Contact Angles on a Soft Solid: From Young's Law to Neumann's Law. *Phys. Rev. Lett.* **2012**, *109* (23), 236101.

- (209) Wu, Y.; Zhao, Q.; Anderson, J. M.; Hiltner, A.; Lodoen, G. A.; Payet, C. R. Effect of Some Additives on the Biostability of a Poly(etherurethane) Elastomer. *J. Biomed. Mater. Res.* **1991**, *25* (6), 725–739.
- (210) Briganti, E.; Losi, P.; Raffi, A.; Scoccianti, M.; Munaò, A.; Soldani, G. Silicone Based Polyurethane Materials: A Promising Biocompatible Elastomeric Formulation for Cardiovascular Applications. *J. Mater. Sci. Mater. Med.* **2006**, *17* (3), 259–266.
- (211) Persson, B. N. J.; Gorb, S. The Effect of Surface Roughness on the Adhesion of Elastic Plates with Application to Biological Systems. *J. Chem. Phys.* **2003**, *119*, 11437.
- (212) Owen, M. J.; Smith, P. J. Plasma Treatment of Polydimethylsiloxane. *J. Adhes. Sci. Technol.* **1994**, *8* (10), 1063–1075.
- (213) Amstein, C. F.; Hartman, P. A. Adaptation of Plastic Surfaces for Tissue Culture by Glow Discharge. *J. Clin. Microbiol.* **1975**, *2* (1), 46–54.
- (214) Oehr, C. Plasma Surface Modification of Polymers for Biomedical Use. *Nucl. Instruments Methods Phys. Res. Sect. B Beam Interact. with Mater. Atoms* **2003**, *208*, 40–47.
- (215) Peterson, S. L.; McDonald, A.; Gourley, P. L.; Sasaki, D. Y. Poly(dimethylsiloxane) Thin Films as Biocompatible Coatings for Microfluidic Devices: Cell Culture and Flow Studies with Glial Cells. *J. Biomed. Mater. Res. A* **2005**, *72* (1), 10–18.
- (216) Jo, B.-H.; Van Lerberghe, L. M.; Motsegood, K. M.; Beebe, D. J. Three-Dimensional Micro-Channel Fabrication in Polydimethylsiloxane (PDMS) Elastomer. *J. Microelectromechanical Syst.* **2000**, *9* (1), 76–81.
- (217) Mills, K. L.; Zhu, X.; Takayama, S.; Thouless, M. D. The Mechanical Properties of a Surface-Modified Layer on Poly(dimethylsiloxane). *J. Mater. Res.* **2008**, *23* (1), 37–48.
- (218) Pinto, S.; Alves, P.; Matos, C. M.; Santos, A. C.; Rodrigues, L. R.; Teixeira, J. A.; Gil, M. H. Poly(dimethyl Siloxane) Surface Modification by Low Pressure Plasma to Improve Its Characteristics towards Biomedical Applications. *Colloids Surf. B. Biointerfaces* **2010**, *81* (1), 20–26.
- (219) Fakes, D. W.; Newton, J. M.; Watts, J. F.; Edgell, M. J. Surface Modification of a Contact Lens Co-Polymer by Plasma-Discharge Treatments. *Surf. Interface Anal.* **1987**, *10* (8), 416–423.
- (220) Putignano, C.; Carbone, G.; Dini, D. Mechanics of Rough Contacts in Elastic and Viscoelastic Thin Layers. *Int. J. Solids Struct.* **2015**, *69–70*, 507–517.
- (221) Tang, W.; Zhang, J.; Chen, S.; Chen, N.; Zhu, H.; Ge, S.; Zhang, S. Tactile Perception of Skin and Skin Cream. *Tribol. Lett.* **2015**, *59* (1), 24.
- (222) Tobin, D. J. Biochemistry of Human Skin—our Brain on the Outside. *Chem. Soc. Rev.* **2006**, *35* (1), 52–67.
- (223) Kim, T.; Park, J.; Sohn, J.; Cho, D.; Jeon, S. Bioinspired, Highly Stretchable, and Conductive Dry Adhesives Based on 1D–2D Hybrid Carbon Nanocomposites for All-in-One ECG Electrodes. *ACS Nano* **2016**, *10* (4), 4770–4778.
- (224) Krueger, E. M.; Cullum, M. E.; Nichols, T. R.; Taylor, M. G.; Sexton, W. L.; Murahata, R. I. Novel Instrumentation to Determine Peel Force in Vivo and Preliminary Studies with Adhesive Skin Barriers. *Ski. Res. Technol.* **2013**, n/a-n/a.
- (225) Wokovich, A. M.; Brown, S. A.; McMaster, F. J.; Doub, W. H.; Cai, B.; Sadrieh, N.; Chen, M. L.; Machado, S.; Shen, M.; Buhse, L. F. Evaluation of Substrates for 90 Degrees Peel Adhesion - A Collaborative Study. I. Medical Tapes. *J. Biomed. Mater. Res. PART B-APPLIED Biomater.* **2008**,

87B (1), 105–113.

- (226) Quan, M. B.; Edwards, C.; Marks, R. Non-Invasive in Vivo Techniques to Differentiate Photodamage and Ageing in Human Skin. *Acta Derm. Venereol.* **1997**, *77* (6), 416–419.
- (227) Jones, I.; Currie, L.; Martin, R. A Guide to Biological Skin Substitutes. *Br. J. Plast. Surg.* **2002**, *55* (3), 185–193.
- (228) Chen, S.; Bhushan, B. Nanomechanical and Nanotribological Characterization of Two Synthetic Skins with and without Skin Cream Treatment Using Atomic Force Microscopy. *J. Colloid Interface Sci.* **2013**, *398*, 247–254.
- (229) Findley, W. N.; Lai, J. S.; Onaran, K. *Creep and Relaxation of Nonlinear Viscoelastic Materials*; Dover Publications; Revised ed. edition (January 15, 2013), 2013.
- (230) Ferry, J. D. *Viscoelastic Properties of Polymers*; 1980.
- (231) Ganghoffer, J. F.; Gent, A. N. Adhesion of a Rigid Punch to a Thin Elastic Layer. *J. Adhes.* **1995**, *48* (1–4), 75–84.
- (232) Hensel, R.; McMeeking, R. M.; Kossa, A. Adhesion of a Rigid Punch to a Confined Elastic Layer Revisited. *J. Adhes.* **2017**, *accepted*.
- (233) Guduru, P. R. R.; Bull, C. Detachment of a Rigid Solid from an Elastic Wavy Surface: Experiments. *J. Mech. Phys. Solids* **2007**, *55* (3), 473–488.
- (234) Hui, C.-Y.; Glassmaker, N. J.; Tang, T.; Jagota, A. Design of Biomimetic Fibrillar Interfaces: 2. Mechanics of Enhanced Adhesion. *J. R. Soc. Interface* **2004**, *1* (1), 35–48.
- (235) Jermann, R.; Toumiat, M.; Imfeld, D. Development of an in Vitro Efficacy Test for Self-Tanning Formulations. *Int. J. Cosmet. Sci.* **2002**, *24* (1), 35–42.
- (236) Full, R. J.; Autumn, K.; Liang, Y. A.; Hsieh, S. T.; Zesch, W.; Chan, W. P.; Kenny, T. W.; Fearing, R. Adhesive Force of a Single Gecko Foot-Hair. *Nature* **2000**, *405* (6787), 681–685.
- (237) Persson, B. N. J. Biological Adhesion for Locomotion on Rough Surfaces: Basic Principles and A Theorist's View. *MRS Bulletin.* 2007, pp 486–490.
- (238) Gorb, S. N. *Functional Surfaces in Biology*; Gorb, S. N., Ed.; Springer Netherlands: Dordrecht, 2009; Vol. 2.
- (239) Chary, S.; Tamelier, J.; Turner, K. A Microfabricated Gecko-Inspired Controllable and Reusable Dry Adhesive. *Smart Mater. Struct.* **2013**, *22* (2), 25013.
- (240) Paretkar, D.; Kamperman, M.; Schneider, A. S.; Martina, D.; Creton, C.; Arzt, E. Bioinspired Pressure Actuated Adhesive System. *Mater. Sci. Eng. C* **2011**, *31* (6), 1152–1159.
- (241) del Campo, A.; Arzt, E. Design Parameters and Current Fabrication Approaches for Developing Bioinspired Dry Adhesives. *Macromol. Biosci.* **2007**, *7* (2), 118–127.
- (242) Hawkes, E. W.; Christensen, D. L.; Jiang, H.; Cutkosky, M. R. Grasping without Squeezing: Shear Adhesion Gripper with Fibrillar Thin Film. In *2015 IEEE International Conference on Robotics and Automation (ICRA)*; IEEE, 2015; pp 2305–2312.
- (243) Mengüç, Y.; Sitti, M. Gecko-Inspired Polymer Adhesives. In *Polymer Adhesion, Friction, and Lubrication*; John Wiley & Sons, Inc.: Hoboken, NJ, USA, 2013; pp 351–389.
- (244) del Campo, A.; Arzt, E. *Generating Micro- and Nanopatterns on Polymeric Materials*; 2011.
- (245) Hensel, R.; Helbig, R.; Aland, S.; Voigt, A.; Neinhuis, C.; Werner, C. Tunable Nano-Replication

- to Explore the Omniphobic Characteristics of Springtail Skin. *NPG Asia Mater.* **2013**, 5 (2), e37.
- (246) Hensel, R.; Finn, A.; Helbig, R.; Braun, H. G.; Neinhuis, C.; Fischer, W. J.; Werner, C. Biologically Inspired Omniphobic Surfaces by Reverse Imprint Lithography. *Adv. Mater.* **2014**, 26 (13), 2029–2033.
- (247) Hensel, R.; Neinhuis, C.; Werner, C. The Springtail Cuticle as a Blueprint for Omniphobic Surfaces. *Chem. Soc. Rev.* **2016**, 45 (2), 323–341.
- (248) Huber, G.; Mantz, H.; Spolenak, R.; Mecke, K.; Jacobs, K.; Gorb, S. N.; Arzt, E. Evidence for Capillarity Contributions to Gecko Adhesion from Single Spatula Nanomechanical Measurements. *Proc. Natl. Acad. Sci. U. S. A.* **2005**, 102, 16293–16296.
- (249) Israelachvili, J. *Intermolecular and Surface Forces, 3rd Edition*; 2010.
- (250) Popov, V. *Kontaktmechanik Und Reibung: Ein Lehr-Und Anwendungsbuch von Der Nanotribologie Bis Zur Numerischen Simulation*; Springer-Verlag, 2009.
- (251) Kroner, E.; Paretkar, D. R.; McMeeking, R. M.; Arzt, E. Adhesion of Flat and Structured PDMS Samples to Spherical and Flat Probes: A Comparative Study. *J. Adhes.* **2011**, 87 (5), 447–465.
- (252) Boesel, L. F.; Cremer, C.; Arzt, E.; Campo, A. Del; Greiner, C.; Arzt, E.; del Campo, A.; Cremer, C.; Arzt, E.; Campo, A. Del. *Gecko-Inspired Surfaces: A Path to Strong and Reversible Dry Adhesives*; 2010; Vol. 22, pp 2125–2137.
- (253) Aksak, B.; Murphy, M. P.; Sitti, M. Adhesion of Biologically Inspired Vertical and Angled Polymer Microfiber Arrays. *Langmuir* **2007**, 23 (6), 3322–3332.
- (254) Bacca, M.; Booth, J. A.; Turner, K. L.; McMeeking, R. M. Load Sharing in Bioinspired Fibrillar Adhesives with Backing Layer Interactions and Interfacial Misalignment. *J. Mech. Phys. Solids* **2016**, 96, 428–444.
- (255) McMeeking, R. M.; Arzt, E.; Evans, A. G. Defect Dependent Adhesion of Fibrillar Surfaces. *J. Adhes.* **2008**, 84 (7), 675–681.
- (256) Spuskanyuk, A. V.; McMeeking, R. M.; Deshpande, V. S.; Arzt, E. The Effect of Shape on the Adhesion of Fibrillar Surfaces. *Acta Biomater.* **2008**, 4 (6), 1669–1676.
- (257) Carbone, G.; Pierro, E. Sticky Bio-Inspired Micropillars: Finding the Best Shape. *Small* **2012**, 8 (9), 1449–1454.
- (258) Spolenak, R.; Gorb, S.; Gao, H.; Arzt, E. Effects of Contact Shape on the Scaling of Biological Attachments. *Proc. R. Soc. A Math. Phys. Eng. Sci.* **2005**, 461 (2054), 305–319.
- (259) Cheng, S.; Robbins, M. O. Capillary Adhesion at the Nanometer Scale. *Phys. Rev. E - Stat. Nonlinear, Soft Matter Phys.* **2014**, 89 (6).
- (260) Yi, H.; Hwang, I.; Lee, J. H.; Lee, D.; Lim, H.; Tahk, D.; Sung, M.; Bae, W.-G.; Choi, S.-J.; Kwak, M. K.; Jeong, H. E. Continuous and Scalable Fabrication of Bioinspired Dry Adhesives via a Roll-to-Roll Process with Modulated Ultraviolet-Curable Resin. *ACS Appl. Mater. Interfaces* **2014**, 6 (16), 14590–14599.
- (261) Sameoto, D.; Ferguson, B. Robust Large-Area Synthetic Dry Adhesives. *J. Adhes. Sci. Technol.* **2014**, 28 (3–4), 337–353.
- (262) Autumn, K.; Dittmore, A.; Santos, D.; Spenko, M.; Cutkosky, M. Frictional Adhesion: A New Angle on Gecko Attachment. *J. Exp. Biol.* **2006**, 209, 3569–3579.
- (263) Zeng, H.; Pesika, N.; Tian, Y.; Zhao, B.; Chen, Y.; Tirrell, M.; Turner, K. L.; Israelachvili, J. N.

- Frictional Adhesion of Patterned Surfaces and Implications for Gecko and Biomimetic Systems. *Langmuir* **2009**, *25* (13), 7486–7495.
- (264) McMeeking, R. M.; Ma, L.; Arzt, E. Bi-Stable Adhesion of a Surface with a Dimple. *Adv. Eng. Mater.* **2010**, *12* (5), 389–397.
- (265) Majidi, C.; Groff, R. E.; Maeno, Y.; Schubert, B.; Baek, S.; Bush, B.; Maboudian, R.; Gravish, N.; Wilkinson, M.; Autumn, K.; Fearing, R. S. High Friction from a Stiff Polymer Using Microfiber Arrays. *Phys. Rev. Lett.* **2006**, *97* (7).
- (266) Roca-Cusachs, P.; Rico, F.; Martínez, E.; Toset, J.; Farré, R.; Navajas, D. Stability of Microfabricated High Aspect Ratio Structures in Poly(dimethylsiloxane). *Langmuir* **2005**, *21* (12), 5542–5548.
- (267) Gorumlu, S.; Aksak, B. Sticking to Rough Surfaces Using Functionally Graded Bio-Inspired Microfibres. *R. Soc. Open Sci.* **2017**, *4* (6), 161105.
- (268) Drotlef, D.-M.; Amjadi, M.; Yunusa, M.; Sitti, M. Bioinspired Composite Microfibers for Skin Adhesion and Signal Amplification of Wearable Sensors. *Adv. Mater.* **2017**, *29* (28), 1701353.
- (269) Boyadzhieva, S.; Fischer, S. C. L.; Lösch, S.; Rutz, A.; Arzt, E.; Kruttwig, K. Thin Film Composite Silicone Elastomers for Cell Culture and Skin Applications: Manufacturing and Characterization. *submitted*.
- (270) Danner, M. Investigation of the Influence of Oxygen Plasma Treatment to the Long-Term Biocompatibility and the Mechanical Properties of Silicone Elastomers, Kaiserslautern University of Applied Sciences, 2016.
- (271) Danner, M. Investigation of the Adhesion Properties and Biocompatibility of the Silicone Elastomer SSA MG 7-9800 in Consideration of Oxygen Plasma Treatment, Kaiserslautern University of Applied Sciences, 2017.
- (272) Boyadzhieva, S. Influence of Protein Adsorption, Substrate Roughness, Film Thickness and Hold Time on the Adhesion Behaviour of the Silicone Elastomer SSA MG 7-9800, Saarland University, 2017.
- (273) Glassmaker, N. J.; Jagota, A.; Hui, C.-Y.; Noderer, W. L.; Chaudhury, M. K. Biologically Inspired Crack Trapping for Enhanced Adhesion. *Proc. Natl. Acad. Sci.* **2007**, *104* (26), 10786–10791.
- (274) Vajpayee, S.; Long, R.; Shen, L.; Jagota, A.; Hui, C.-Y. Effect of Rate on Adhesion and Static Friction of a Film-Terminated Fibrillar Interface. *Langmuir* **2009**, *25* (5), 2765–2771.